Searching for Transiting Extra-solar Planets at Optical and Radio Wavelengths

Alexis Michael Sheridan Smith

Submitted for the degree of Doctor of Philosophy

9th October 2009

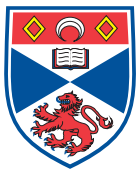

University
of
St Andrews

Declaration

I, Alexis Smith, hereby certify that this thesis, which is approximately 25,000 words in length, has been written by me, that it is the record of work carried out by me and that it has not been submitted in any previous application for a higher degree.

I was admitted as a research student in September 2005 and as a candidate for the degree of PhD in September 2005; the higher study for which this is a record was carried out in the University of St Andrews between 2005 and 2009.

Date Signature of candidate

I hereby certify that the candidate has fulfilled the conditions of the Resolution and Regulations appropriate for the degree of PhD in the University of St Andrews and that the candidate is qualified to submit this thesis in application for that degree.

Date Signature of supervisor

Copyright Agreement

In submitting this thesis to the University of St Andrews we understand that we are giving permission for it to be made available for use in accordance with the regulations of the University Library for the time being in force, subject to any copyright vested in the work not being affected thereby. We also understand that the title and the abstract will be published, and that a copy of the work may be made and supplied to any bona fide library or research worker, that my thesis will be electronically accessible for personal or research use unless exempt by award of an embargo as requested below, and that the library has the right to migrate my thesis into new electronic forms as required to ensure continued access to the thesis. We have obtained any third-party copyright permissions that may be required in order to allow such access and migration, or have requested the appropriate embargo below.

The following is an agreed request by candidate and supervisor regarding the electronic publication of this thesis: Access to Printed copy and electronic publication of thesis through the University of St Andrews.

Date Signature of candidate

Date Signature of supervisor

For my parents, Liz and Peter.

Abstract

This thesis is concerned with various aspects of the detection and characterisation of transiting extra-solar planets. The noise properties of photometric data from SuperWASP, a wide-field survey instrument designed to detect exoplanets, are investigated. There has been a large shortfall in the number of planets such transit surveys have detected, compared to previous predictions of the planet catch. It has been suggested that correlated, or red, noise in the photometry is responsible for this; here it is confirmed that red noise is present in the SuperWASP photometry, and its effects on planet discovery are quantified.

Examples are given of follow-up photometry of candidate transiting planets, confirming that modestly-sized telescopes can rule out some candidates photometrically. A Markov-chain Monte Carlo code is developed to fit transit lightcurves and determine the depth of such lightcurves in different passbands. Tests of this code with transit data of WASP-3 b are reported.

The results of a search for additional transiting planets in known transiting planetary systems are presented. SuperWASP photometry of 24 such systems is searched for additional transits. No further planets are discovered, but a strong periodic signal is detected in the photometry of WASP-10. This is ascribed to stellar rotational variation, the period of which is determined to be 11.91 ± 0.05 days. Monte Carlo modelling is performed to quantify the ability of SuperWASP to detect additional transiting planets; it is determined that there is a good (> 50 per cent) chance of detecting additional, Saturn-sized planets in $P \sim 10$ day orbits.

Finally, the first-ever attempt to detect the secondary eclipse of a transiting extra-solar planet at radio wavelengths is made. Although no eclipse is conclusively detected, upper limits to the flux density from HD 189733 b are established, and compared to theoretical predictions of the flux due to electron-cyclotron maser emission.

Acknowledgements

There are a number of people without whom it would not have been possible for me to complete this thesis. First of all, I would like to thank my supervisor, Andrew Cameron for his patience, advice and wisdom over the last four years.

Three other people have also helped me greatly with my work and supervised me while observing; I owe them a huge debt of gratitude. They are Tim Lister, Jane Greaves and Leslie Hebb. I would also like to thank all the other members of SuperWASP, the staff of the National Radio Astronomy Observatory, the staff of the Observatorio del Teide and Roger Stapleton for their work which enabled me to have some data to work on, and also to Ian Taylor for ensuring I had the necessary hardware and software to do something with that data! Thanks must also go to Tom Robitaille for all his technical help over the years, particularly with the style files used to produce this thesis.

Working as part of the Astronomy Group in St. Andrews for the last four years has been a hugely enjoyable, as well as educational, experience. I would like to thank all the group members who made it such an open and friendly place to work in, particularly my fellow PhD students.

Next, I would like to thank the three fantastic flat mates it has been my immense privilege to live with - Nick Dunstone, Máire Ní Mhórdha and Noé Kains, who has also endured the misfortune of sharing an office with me for the past three years!

I doubt I would have managed to remain as sane as I have without the distraction offered by the University of St Andrews Staff and Postgraduate Cricket Club. Thank you to all those who have played cricket with me over the past four seasons, allowing me to forget about work for a while, discover some of the most beautiful spots in Fife and the surrounding area, and occasionally take a wicket or two. Special thanks go to Stan, David and Patrick for captaining, organising and always sharing a commiserative pint or two in the Whey Pat after yet another defeat!

Finally, I wish to thank everyone without whom I would not have started at St. Andrews in the first place. I am grateful to my teachers and the good friends I made at Caistor Grammar School and at the University of Durham. Most importantly, I would like to express my gratitude to my family, particularly my grandparents and sisters, Imogen and Verity, but most of all my parents. For all your love, support, encouragement, and for always believing in me, thank you.

Contents

List of Figures

List of Tables

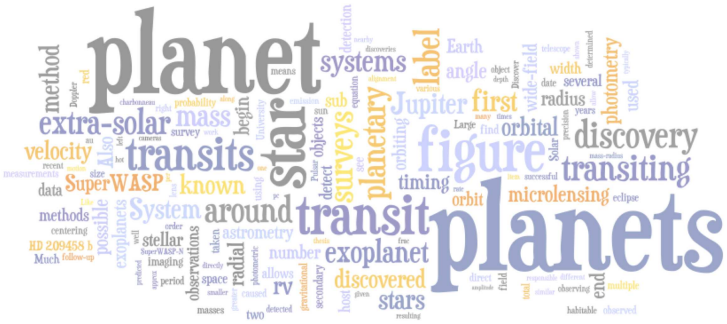

1 Introduction

1.1 Planets

1.1.1 Worlds beyond our own

There has been speculation about the possible existence of planets outside our Solar System for many years. Famously, Giordano Bruno, later burned at the stake for heresy, postulated the existence of extra-solar planets as part of his 'infinite universe' philosophy. In his *De L'Infinito Universo et Mondi* (*On the Infinite Universe and Worlds*) of 1584, he declares his belief (translation from Singer 1950) that,

> "There are then innumerable suns, and an infinite number of earths revolve around those suns, just as the seven we can observe revolve around this sun which is close to us."

It took more than four centuries before the first of Bruno's 'infinite number of earths' were discovered orbiting some of the 'innumerable suns' in our Galaxy. First, planets were discovered orbiting pulsars Wolszczan & Frail (1992), and then, a few years later, main-sequence stars Mayor & Queloz (1995).

In the 14 years since Mayor & Queloz's discovery of 51 Peg b, the pace of exoplanet discovery has increased rapidly (Fig. 1.1).

1.1.2 The definition of a 'planet'

Before going any further, it is useful to discuss exactly what is meant by the term 'planet'. To the ancient Greeks, the planets (meaning 'wandering stars') were the seven bodies thought to orbit the Earth in the Ptolemaic system, namely the Moon, Mercury, Venus, the Sun, Mars, Jupiter, and Saturn. After the heliocentric model of Copernicus became generally accepted, the Moon and Sun were removed from the list of planets and the Earth added to the five planets visible to the naked eye.

Although several of the larger main-belt asteroids were briefly classed as planets, the list of known planets expanded slowly with the discoveries of Uranus in 1781 by Herschel (Herschel & Watson, 1781), Neptune in 1846 by LeVerrier and Adams (Adams 1846; Le Verrier 1847), and Pluto by Tombaugh in 1930 (Lowell Putnam & Slipher, 1932). The discovery of several objects of similar size to Pluto orbiting the Sun beyond Neptune in recent years, combined with the discovery of numerous planets orbiting stars beyond the Solar System, led to the need for formal definitions of what constitutes a planet.

In 2003 the International Astronomical Union (IAU) adopted the following working definition of what constitutes an *extra-solar* planet (Boss, 2003),

> "1. Objects with true masses below the limiting mass for thermonuclear fusion of deuterium (currently calculated to be 13 times the mass of Jupiter for objects with the same isotopic abundance as the Sun) that orbit stars or stellar remnants are "planets" (no matter how they formed). The minimum mass and size required for an extrasolar object to be considered a planet should be the same as that used in the Solar System.
>
> 2. Substellar objects with true masses above the limiting mass for thermonuclear fusion of deuterium are "brown dwarfs", no matter how they formed or where they are located.
>
> 3. Free-floating objects in young star clusters with masses below the limiting mass for thermonuclear fusion of deuterium are not "planets", but are "sub-brown dwarfs" (or whatever name is most appropriate)."

For the purposes of this thesis, and indeed any current work in the field of extra-solar planets, the above definition is sufficient; there is no need for a lower limit to the mass. The minimum mass required to constitute a planet is under debate within the context of our own Solar System, but we are unable to discovery such low-mass objects around other stars at present. Henceforth then, a 'planet', 'exoplanet', or 'extra-solar planet' will be used interchangeably to mean an object less massive than 13 Jupiter masses (M_J), which is in orbit around a star.

1.2 Discovering extra-solar planets

In this section, I outline briefly the history of exoplanet discovery and the different methods used to detect such planets. The two most successful methods to date are the radial velocity and transit methods; these methods are discussed in sections 1.2.2 and 1.2.3, respectively. Pulsar timing (Sec. 1.2.1) was used to discover the first exoplanets, and gravitational microlensing (Sec. 1.2.4) and direct imaging (Sec. 1.2.5) have both been used successfully to detect a number of planets. The less-successful methods of astrometry and transit timing are also briefly discussed in Sec. 1.2.6 and Sec. 1.2.7, respectively.

1.2.1 Pulsar timing

The first extra-solar planets to be discovered were the low-mass planets orbiting the pulsar PSR1257+12 (Wolszczan & Frail, 1992). They were discovered by measuring, with high precision, the timing of this millisecond pulsar over several months. Because such objects ordinarily have extremely stable rotation periods, it was possible for Wolszczan and Frail to detect the variations in timing caused by the varying light travel time due to the reflex orbit of the pulsar.

Although responsible for the first exoplanet discoveries, this method has only allowed the discovery of a total of seven planets in four systems, and constitutes a separate line of study to that of planets around main-sequence stars.

1.2.2 Radial velocity

By far the most successful of all planet-finding techniques to date is the radial velocity (RV), or Doppler spectroscopy, method, which was responsible for all the planets discovered around main-sequence stars from the 1995 discovery of 51 Peg b (Mayor & Queloz, 1995) until the

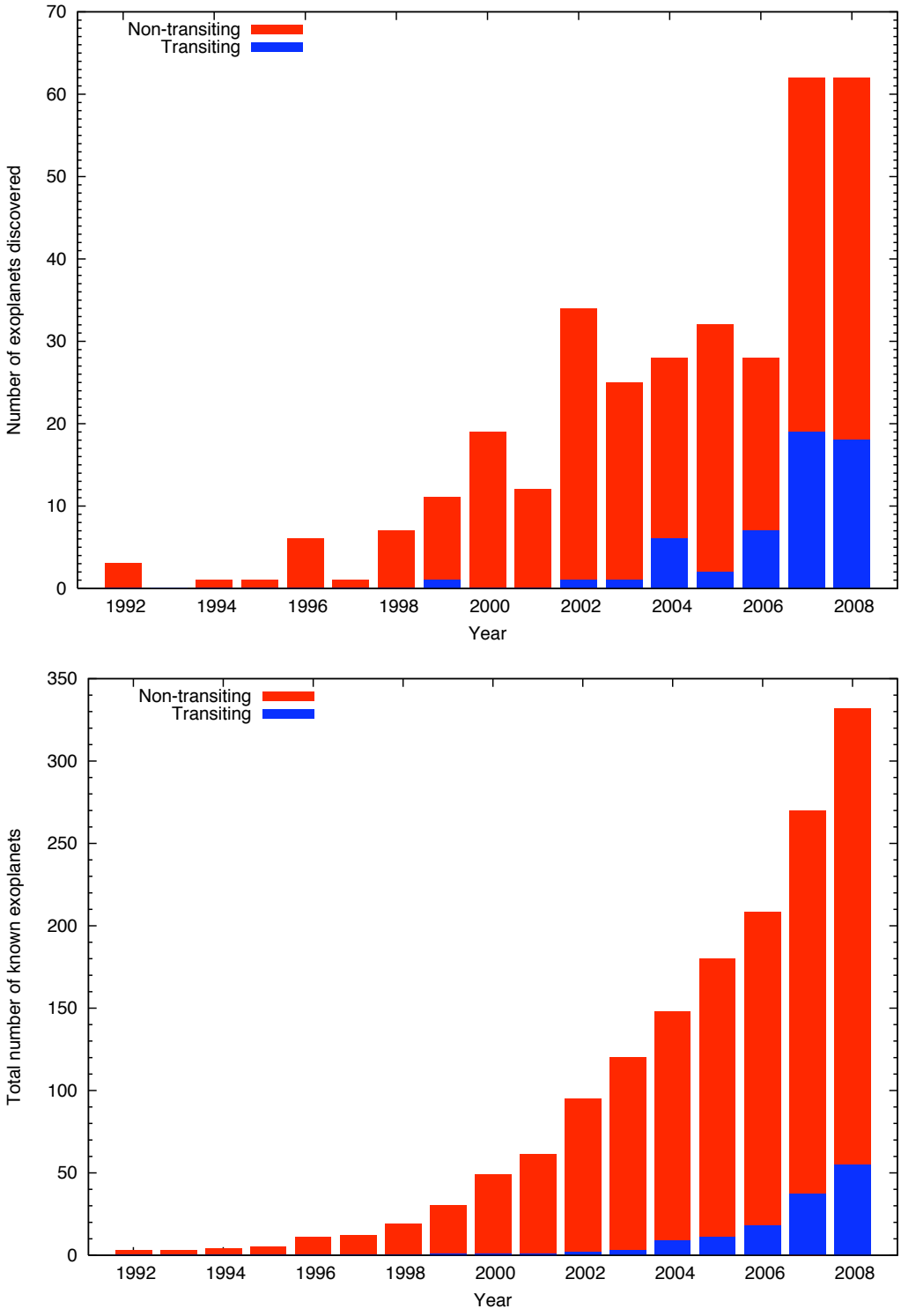

Figure 1.1: Discovery rate of extra-solar planets. *Upper panel*: number of discoveries each year 1992 - 2008. *Lower panel*: cumulative extra-solar planet discoveries. In each panel, transiting planets are indicated by blue bars, and non-transiting planets by red bars. Data taken from *The Extrasolar Planets Encyclopaedia* – http://www.exoplanet.eu

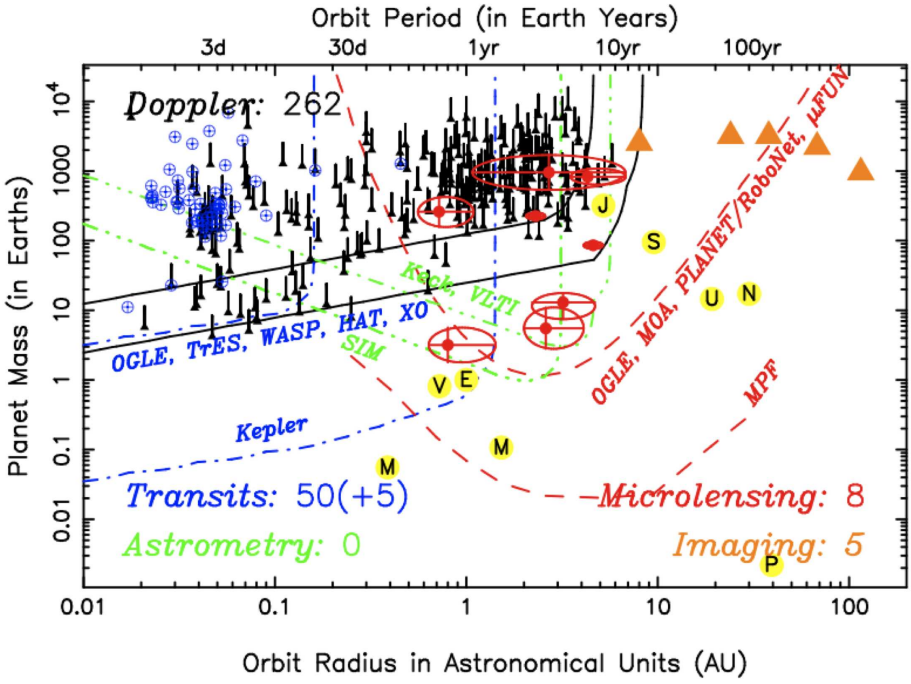

Figure 1.2: Exoplanet discovery space. Planet mass is plotted against orbital radius / orbital period for the 325 exoplanets known at 2009 March. Transiting planets (55 total) are shown in blue, planets discovered by means of radial velocity in black (262), those discovered by means of gravitational microlensing (8) in red, and those discovered by means of direct imaging (5) in orange. Also shown are the planets of the Solar System (indicated by the planet's initial letter in a yellow circle). The detection thresholds of various experiments are shown in the colours corresponding to the method they employ. Selected thresholds are discussed in further detail in the text. Figure courtesy of Keith Horne.

discovery of the first planet (OGLE-TR-56 b) by means of transits, in 2002 (Konacki et al., 2003). Like the astrometric method (Sec. 1.2.6), the radial velocity method relies on detecting the motion of a star around the barycentre of a planetary system. The RV technique allows the velocity of the star along the line-of-sight to be determined, by measuring small changes in the wavelength of stellar spectral lines caused by the Doppler effect. The amplitude of this RV signal is proportional to the mass of the planet and inversely proportional to the square of the orbital separation. This results in massive planets in close orbits being favoured by this detection technique (see Fig. 1.2). Furthermore, because only the line-of-sight velocity can be detected, systems that are inclined at close to 90°, where the RV amplitude is maximal, are favoured. This also means that systems inclined at 0° cannot be detected as there is no component of the orbital reflex motion along the line-of-sight. In general, the orbital inclination angle, i, is not known (unless $i \approx 90°$, and the planet is observed to transit the disc of its host star, see Sec. 1.2.3) and so the planetary mass, M_p, cannot be determined directly, only $M_p \sin i$.

The orbital period, P, is determined directly from the radial velocity curve and the eccentricity, e, of the orbit from the shape of this curve. $M_p \sin i$ is then calculated according to the following equation (see e.g. de Pater & Lissauer 2001),

$$M_p \sin i = K \left(\frac{P}{2\pi G} \right)^{\frac{1}{3}} \left(M_* + M_p \right)^{\frac{2}{3}} \sqrt{1 - e^2} \,, \tag{1.1}$$

where K is the semi-amplitude of the radial velocity signal and G the gravitational constant. Since the stellar mass is several orders of magnitude larger than the planetary mass, the approximation $(M_* + M_p) \approx M_*$ can be used. The stellar mass is usually estimated from the effective stellar temperature, $T_{\rm eff}$.

The amplitude of the radial velocity signal which revealed the presence of 51 Peg b is 59 ms^{-1}, caused by a planet with $M_p \sin i = 0.47\ M_J$ orbiting a G5 dwarf in 4.23 d (Mayor & Queloz 1995; Fig. 1.3). For comparison, Jupiter induces a reflex motion of 12.5 ms^{-1} of the Sun, whereas the Earth produces only a 0.1 ms^{-1} shift. Sensitivity (rms) limits of 5 ms^{-1} for 10 yr and 1 ms^{-1} for 20 yr are indicated by black lines in Fig. 1.2. Current high-resolution spectrographs such as SOPHIE, which is in use on the 1.93-m telescope at the Observatoire de Haute-Provence, can achieve Doppler spectroscopy with a stability of around 1–2 ms^{-1} (Bouchy & The Sophie Team, 2006).

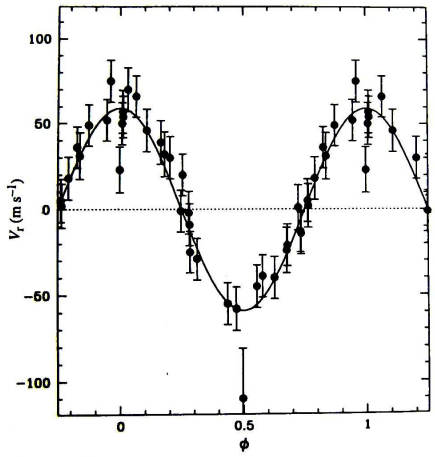

Figure 1.3: Radial velocity curve of 51 Peg. The radial velocity of the star is plotted against the orbital phase of the planetary system. Figure taken from Mayor & Queloz (1995)

1.2.3 Transits

It was seen in Sec. 1.2.2 that the information it is possible to obtain with the radial velocity technique alone is limited. The orbital inclination angle remains unknown, and so only a lower limit to the planetary mass is established. Detecting the reduction in stellar flux when a planet passes directly in front of, or transits, its star allows the inclination angle to be determined ($i = 90°$ for a star transiting the centre of its star). This, when combined with radial velocity measurements, allows the mass of the planet to be determined. Transits also enable the radius of the planet to be measured, allowing the mass-radius relation for these objects to be investigated (Fig. 1.7). The amount of stellar light that is blocked by the passage of the planet across the stellar disc is approximately equal to the square of the ratio of the planetary and the stellar radii (see equation 1.5). Combining this with an estimate of the stellar radius (e.g. from main-sequence stellar theory) allows a reasonably accurate determination of the planet's size. Transiting planets also allow all kinds of follow-up observations which mean they can be characterised in ways not possible for non-transiting systems, as will be seen in Sec. 1.5.

The obvious disadvantage of transits as a method of planet detection is that it requires a fortuitous alignment of the system in order for a transit to be exhibited. For each extra-solar planetary system that does exhibit transits, there will be many more that do not. The probability, $\mathscr{P}$(alignment), that a particular planet transits its host star can be calculated from consideration of the geometry of the system (assuming orbits that are randomly inclined to the line-of-sight).

In order for a system to exhibit transits, the following condition must be satisfied (Sackett, 1999),

$$\cos i \leq \frac{R_* + R_\mathrm{p}}{a}, \tag{1.2}$$

where R_* is the stellar radius, R_p the planetary radius, and a the orbital semi-major axis. The probability that a given system transits can be calculated by integrating over the values of cos i that result in a transit and normalising by the integral of all possible values of cos i, which are equally likely if planetary orbits are randomly inclined to the line-of-sight,

$$\mathscr{P}(\text{alignment}) = \frac{\int_0^{(R_*+R_p)/a} d(\cos i)}{\int_0^1 d(\cos i)} = \frac{R_* + R_\mathrm{p}}{a} \approx \frac{R_*}{a} \tag{1.3}$$

Thus the probability of a Solar System analogue being aligned such that Earth transits the Sun is 0.0046, and for Jupiter this probability is 0.0001. Also, several transits of a particular object must be observed in order to confirm the existence of a planet, requiring that observations be made over a time-scale equal to several times the orbital period. The gap between observations must be less than the duration of the transit, in order not to miss such an event. The duration of transit, t_tr is a function of R_*, a and the orbital period, P,

$$t_\mathrm{tr} = \frac{R_* P}{\pi a}, \tag{1.4}$$

assuming a circular orbit and an equatorial transit. The duration of a Jupiter transit is therefore around 1.2 d, and an Earth transit would last for around 13 h.

The reduction in brightness (depth) of the host star during transit, Δm, is proportional to the ratio of the squares of the radii of planet and star. Tingley & Sackett (2005) determine the depth to be given by,

$$\Delta m \approx 1.3 \left(\frac{R_\mathrm{p}}{R_*}\right)^2 \tag{1.5}$$

The factor of 1.3 in this equation arises from modelling the limb-darkening of the star, i.e. it accounts for the fact that the stellar disc is not uniformly bright, but is darker around the edges (limbs). The transit depths for Earth and Jupiter transiting the Sun are 0.01 and 1.3 per cent, respectively. Fig. 1.4 shows an image of Venus transiting the Sun as seen from Earth

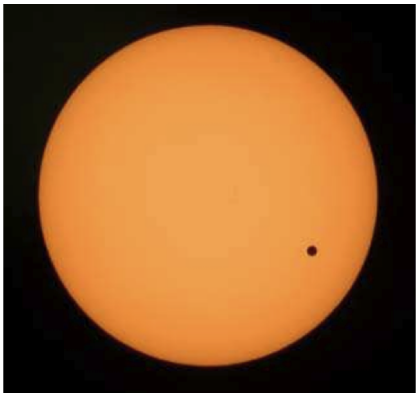

Figure 1.4: The 2004 June 08 transit of Venus across the Sun. Photograph taken from JBAA (2005)

in 2004, producing a transit with a depth fractionally shallower than that produced by an Earth-sized planet.

All of the above results in the requirements that, even if every star had an Earth analogue, we would have to observe around 200 such systems to detect a single Earth. The observations would have to made with the precision of the order of tens of micro magnitudes, continuously for several years. Current ground based photometric precision is of the order of 1 mmag.

Much easier to find, however, are transiting hot Jupiters (HJs). These typically have periods of just a few days; separations of a few hundredths of an astronomical unit; and transit durations of a few hours[1]. Additionally, the probability of alignment such that transits will occur is much greater for a HJ system than for planets that orbit at several au. For a typical HJ, $\mathscr{P}(\text{alignment}) \approx 0.1$; that is about 1 in 10 HJs will exhibit transits.

HD 209458 b: the first transiting planet

Although transits were proposed as a means for detecting planets similar to hot Jupiters by Struve (1952) (who also suggested the use of high-precision radial velocity measurements to detect planets), the first exoplanet detected by means of transits was HD 209458 b, which had already been discovered by radial velocity observations. Transits of this system were observed by Charbonneau et al. (2000) and by Henry et al. (2000). The transits observed by Charbonneau et al. (2000) using STARE, a small (0.1-m), wide-field survey telescope are compared in Fig. 1.5 to the high-precision photometry later obtained by Brown et al. (2001) using the *Hubble Space Telescope*.

Because of the proximity to Earth of HD 209458 and its consequent brightness (it remains

[1]Take, for instance, the first known transiting exoplanet HD 209458 b, which has $P = 3.52$ days; $a = 0.045$ au; and $t_{\text{tr}} = 3.2$ hours.

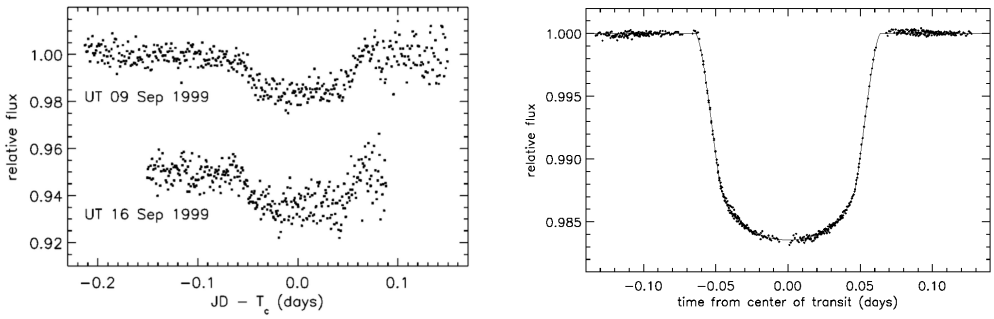

Figure 1.5: Transit photometry of HD 209458 b. Left: The first ever exoplanet transit lightcurve, taken with the *STARE* telescope. Figure taken from Charbonneau et al. (2000). Right: A *Hubble Space Telescope* lightcurve taken from Brown et al. (2001).

the brightest transiting planet host star, with $V = 7.65$), HD 209458 b remains a popular target for various follow-up observations and characterisation studies (see Sec. 1.5 for some examples).

Transit surveys

The discovery of the transits of HD 209458 b inspired a plethora of surveys to detect planets using transits in the first instance. These surveys have become increasingly successful over the past few years, and are responsible for all but six of the known transiting planets to date[2].

Fig. 1.1(a) shows the increasing proportion of known planets that transit their host stars. As a further illustration of the recent rate of exoplanet discovery, when the work for this thesis commenced in 2005 September, only 10 transiting planets were known, this number now stands at 59. In the same time, the total number of known exoplanets has doubled to 348 (as at 2009 May).

The transit surveys employed to date fall into one of three categories of survey, (i) wide-field surveys using similar types of camera to that Charbonneau et al. (2000) used to detect the transits of HD 209458 b; (ii) deep surveys using larger (typically ~ 2 m in diameter), more conventional telescopes; and (iii) space-based endeavours such as *CoRoT* (Barge et al., 2008) and *Kepler* (Borucki et al., 2009), which represent the next generation of transit surveys.

The Optical Gravitational Lensing Experiment (OGLE), a deep field survey, was initially the most successful, with five discoveries between 2002 and 2004 (as well as a further three in 2007). However, the faint nature of stars in such a deep survey (the OGLE planet host stars

[2]HD 149026 b, HD 17156 b, HD 189733 b, HD 80606 b and GJ 436 b were, like HD 209458 b, initially detected by Doppler spectroscopy and only subsequently discovered to transit their host stars.

all have I-band magnitudes between 14 and 16) make spectroscopic confirmation difficult, and preclude much follow-up work as well. They do, rather like gravitational microlensing, however, offer insight into the frequency of planets around stars beyond the immediate Solar neighbourhood in the Galaxy.

The wide-field surveys have been the most successful, not only in quantitative terms (responsible for 35 of the 59 known transiting exoplanets), but also in providing targets for characterisation work (see Sec. 1.5). Several similar wide-field surveys are in successful operation, namely HATNet (Hungarian Automated Telescope Network) (Bakos et al., 2002); Super-WASP (Wide Angle Search for Planets) (Pollacco et al. 2006; Sec. 1.3); TrES (Trans-Atlantic Exoplanet Survey), which incorporates the aforementioned STARE telescope (O'Donovan et al., 2006b) and XO (McCullough et al., 2005).

These wide-field survey instruments typically consist of a battery of small lenses, each equipped with a CCD camera which images tens of square degrees, operated robotically. Large numbers of stars are imaged many times per night, and the resulting lightcurves are searched for transit signatures. Once these transiting planet candidates are identified, follow-up observations, in the form of Doppler spectroscopy measurements, are required to confirm the planetary nature of the transiting body. Higher-precision transit photometry is usually obtained as well, in order to better constrain observational parameters such as the transit depth and duration, leading to more accurate measures of parameters such as the planetary radius. The operation of wide-field transit surveys will be discussed in greater detail in Sec. 1.3, with specific reference to the SuperWASP survey, and the subject of follow-up photometry is discussed further in Chapter 3.

Although the wide-field surveys have reached maturity over the last few years and are now operating in what Charbonneau (2009) describes as 'production-line mode', the exoplanet discovery space that they can explore remains limited (Fig. 1.2). The factors limiting the ability to find longer-period planets are, of course, the length of the observing baseline, and the transit probability (Eqn. 1.3). The ability to find longer-period planets will increase with time if such surveys continue to observe the same fields (see chapter 2), although data sharing between survey instruments at different longitudes may be required to maximise the planet haul in the presence of the problem of observing windows (Fleming et al., 2008). That is, the problem of being able to observe only during the hours of darkness, which means that

planets with certain ephemerides will never be observed to transit from a particular terrestrial longitude.

Pushing down the limit to the size of planets that wide-field transit surveys can find perhaps represents a bigger problem, determined as it is by the precision of the photometry. It may prove possible to achieve higher-precision photometry, however, as the sources of systematic noise inherent in all these surveys becomes better understood and strategies are developed to reduce it. As is demonstrated in chapter 2, observing a given system for longer (and thus observing a greater number of individual transits) acts to increase the signal-to-noise ratio and so make smaller transits detectable.

The potential improvements in wide-field surveys described in the previous paragraph will still prove insufficient to enable these surveys to detect Earth-like planets around Solar-type stars, which is regarded by many as one of the major goals of exoplanet discovery. Wide-field surveys may, however, discover planets at orbital distances at which liquid water may exist on the planetary surface. The range of orbital distances for which this is the case is known as the 'habitable zone' of a star (Kasting et al., 1993), the location of which varies with the spectral type of the star. Because M-dwarfs have much smaller luminosities than G-dwarfs such as the Sun, the habitable zone is located much closer to the star, reducing the orbital period of planets in the habitable zone, as well as increasing the geometric probability of transit. Furthermore, because of the much smaller radius of these stars, much smaller planets can be discovered for a given photometric precision.

Charbonneau (2009) considers the case of a planet with a radius twice that of Earth orbiting in the habitable zone of both a G2-dwarf and an M5-dwarf. The planet orbits the G2-dwarf with a period of 1 yr and a transit probability of around 0.5 per cent, compared to just 15 d in the case of the M5-dwarf with a transit probability of 1.6 per cent. The depths of the two transits would be 0.03 and 0.5 per cent respectively. The radial velocity signal is also more favourable in the M-dwarf scenario; the peak-to-peak amplitude is 10ms^{-1} compared to 1.3ms^{-1} for a planet of mass $7M_{\oplus}$. The next generation of ground-based surveys, such as *MEarth* (Irwin et al., 2009) may discover the first 'habitable' exoplanets, or that honour may fall to a space-based mission.

Going into space removes many of the sources of systematic noise that afflict ground-based surveys, and allows the achievement of greater photometric precision. Missions such

as the recently launched *Kepler* (Borucki et al., 2009) and *CoRoT* (Convection Rotation and planetary Transits; Barge et al. 2008) aim to find smaller planets than those discovered by ground-based surveys.

1.2.4 Gravitational microlensing

When one star passes behind another, the foreground star may act as a gravitational lens, bending light from the background star, resulting in magnification of the background star. This gravitational microlensing effect was predicted by Einstein (1936) and later suggested as a means of exoplanet discovery by Mao & Paczynski (1991). If the lens star is host to an orbiting exoplanet, the planet may cause a secondary magnification of the background source, and detailed modelling of the resulting lightcurve allows, for example, determination of the mass-ratio of the system. The first planet to be discovered in this manner was a 1.5 M_J planet in a $\sim$ 3 au orbit (Bond et al., 2004), and the method is responsible, as of 2009 June, for the discovery of a total of eight exoplanets in seven systems[3].

Microlensing allows planets to be discovered around stars which lie much further from Earth than those discovered by other methods ($\sim$ 1000 pc compared to $\sim$ 100 pc), indeed recent work by Ingrosso et al. (2009a) suggests that it may be possible to find exoplanets beyond our Galaxy, in M31, using microlensing. Microlensing also probes a different area of exoplanet parameter space, able to find low-mass planets at large orbital separations (Fig. 1.2).

The greatest drawback of the method is that the detection of a planet around the lens star is only possible during the unique microlensing event. The host star is distant and faint, so it is not currently possible to gain any further information about such systems from spectroscopic or photometric measurements.

1.2.5 Direct imaging

Attempting to image directly an extra-solar planet poses a significant technical challenge; planets are generally 10^6 to 10^{12} times fainter than their host stars and are typically separated by angles of less than 1 arcsecond, even for nearby systems (Beuzit et al., 2007). Direct imaging favours companions that are young and therefore still warm, large, and which orbit reasonably far from a small star. Early successes include the imaging of a 5 M_J planet

[3] *The Extrasolar Planets Encyclopaedia* – http://www.exoplanet.eu

orbiting a brown dwarf at 55 au (Chauvin et al. 2004, 2005). More recently, planets have been imaged around earlier-type stars, such as the discovery of a planet orbiting the nearby (7.7 pc) A-dwarf Fomalhaut at a distance of 119 au (Kalas et al., 2008). Marois et al. (2008) succeeded in imaging a system of three planets, with masses between 5 and 13 M_J , around HR 8799. They used adaptive optics (AO) to increase the spatial resolution of the images from the limits imposed by the atmosphere, towards those imposed by diffraction. Angular differential imaging (ADI) was also used to distinguish between exoplanets and optical artefacts by allowing the field-of-view to rotate around the star as the telescope tracked the target. To date, a total of eleven planets in nine systems have been imaged. Future instruments such as SPHERE (Spectro-Polarimetric High-contrast Exoplanet REsearch; Beuzit et al. 2008) and GPI (Gemini Planet Imager; Graham et al. 2007) will extend our ability to image planets closer to their stars.

1.2.6 Astrometry

Astrometry has long been suggested as a potential method for discovering exoplanets. Like the RV method (Sec. 1.2.2), it relies on the fact that star and planet orbit a common centre-of-mass and a sufficiently massive planet will cause the movement of its star to be large enough to be measurable. Instead of measuring the movement of the star along the line of sight (like the RV method), astrometry measures the movement of the star in the plane of the sky. Unlike the RV method, however astrometry favours long-period planets Sozzetti (2005). This is because, with astrometry, it is easiest to measure a large orbital reflex displacement, rather than a large orbital reflex velocity, which is preferred by RV.

Several claims to have detected planets via astrometry have been made, almost all of which have later been retracted or discredited. Perhaps most notorious was the announcement of the discovery of two extra-solar planets around nearby Barnard's star by van de Kamp (1969), which have never been confirmed.

More recently, Benedict et al. (2002) used astrometry to measure the mass of the exoplanet Gl 876 b, already known by RV. The combination of astrometry and radial velocity enables the orbital inclination angle to be determined, and thus the true planetary mass. As Tuomi et al. (2009) suggest, high-precision astrometric measurements can be complementary to radial velocity measurements, and enable better characterisation of existing planetary systems.

Even more recently, Pravdo & Shaklan (2009) report what could, if confirmed, represent the first discovery of an exoplanet by means of astrometry. The putative planet has a mass of 6.4 M_J and it resides in a 0.74 yr orbit around the nearby ultra-cool dwarf star, VB 10.

1.2.7 Transit timing

Although no planets have yet been discovered by means of transit timing variations (TTV), the method provides an opportunity to discover multiple planet systems (see Chapter 5) and, potentially, Earth-mass planets. The times of transit of a known transiting planet can be altered by the influence of an additional planet in the system (Agol et al. 2005; Holman & Murray 2005). The TTV method is particularly sensitive to planets in resonant orbit with the transiting planet; such resonant planets are detectable even if they are of very low mass.

1.3 SuperWASP

1.3.1 Instruments

SuperWASP is a consortium comprising members at Queen's University Belfast, the University of St. Andrews, the University of Leicester, Keele University, the Open University, the Isaac Newton Group of telescopes, the University of Cambridge, and the Instituto de Astrofísica de Canarias[4]. This consortium operates two robotic observatories, which are employed as wide-field transit surveys (see Sec. 1.2.3). The first observatory, SuperWASP-N, is located in the Northern hemisphere, at the Observatorio del Roque de los Muchachos on the island of La Palma in the Canaries. The second, WASP-South, is in the Southern hemisphere, at the South African Astronomical Observatory near Sutherland in the Republic of South Africa. SuperWASP-N commenced observations in 2004, followed by WASP-South in 2006.

Each SuperWASP installation comprises an array of eight[5] 200mm f/1.8 Canon camera lenses, each with a 4 mega-pixel CCD recording a 7.8° by 7.8° field (Pollacco et al., 2006). These eight cameras are mounted on a fork mount, which is housed in an enclosure with a hydraulically operated roof (Fig. 1.6), which also houses a weather station.

[4]SuperWASP website – http://www.superwasp.org
[5]although SuperWASP-N operated for the 2004 season with only five cameras

Figure 1.6: The SuperWASP observatories. *Left*: The enclosure of SuperWASP-N on La Palma. *Right*: The eight cameras of WASP-South in South Africa. Photographs taken from the SuperWASP website – http://www.superwasp.org

1.3.2 Observations

The SuperWASP observing strategy is designed to maximise the number of stars that can be hunted for transits, without introducing large numbers of blended objects, which can be a problem given the large pixel size of 13.7″. For this reason, overcrowded fields near the galactic plane are avoided (Christian et al., 2005). The sky is tiled in right ascension, with up to 8 fields being observed at a time. Around a minute is spent on each field, including a 30 s exposure, 4 s of read-out time, and slewing, giving photometry with a cadence of about 8 minutes.

1.3.3 Data reduction

Since each SuperWASP exposure generates an 8.4 Mb image file, a large quantity of data is stored and processed; this is done using a custom-written data reduction pipeline (Pollacco et al., 2006). The pipeline uses the Tycho 2 and USNO B catalogues to prepare an astrometric solution for each field. Aperture photometry is performed on all objects, using three different sized apertures and airmass and CCD position trends are removed from the data before it is archived at the University of Leicester (Pollacco et al., 2006).

Prior to searching the data for transits, the SysRem algorithm of Tamuz et al. (2005) (see Chapter 2) is applied to the data to reduce systematic errors. Four components of systematic error are removed with SysRem; it is thought that two of these are caused by airmass variations and thermal changes in the camera focus, but the causes of the other two are unknown

(Collier Cameron et al., 2006). The HUNTER algorithm of Collier Cameron et al. (2006), which is an adaptation of the box least-squares method (Kovács et al., 2002), is used to search the data for transit-like signatures.

Photometric followup (Chapter 3) and Markov-chain Monte Carlo analysis (Chapter 4) are used to further characterise the resulting planetary candidates, and to eliminate various types of astrophysical false-positive. Candidate planets surviving these and various statistical tests, are then observed with Doppler spectroscopy to confirm that the transit is caused by an object of planetary mass (see e.g. Cameron et al. 2007; Sec. 1.2.2).

1.4 Multiple planet systems

Of the 349 known exoplanets (to 2009 June 08), 91 are known to reside in a total of 37 multiple planet systems[6]. Multiple planet systems are of particular interest for a number of reasons. They are of interest as comparisons to the Solar System, allow multi-body dynamical studies and constrain models of planet formation. Furthermore, additional planets may be detected by their actions on an already known planet, in the same way as Neptune was discovered through its perturbations on the motion of Uranus. The transit-timing method (Sec. 1.2.7) is an example of a method for detecting multiple planets which is complementary to other methods, and has a greater sensitivity to low-mass planets than other methods do at present.

The significance of multiple planet systems in which one or more of the planets exhibits transits is discussed in Chapter 5, along with a description of the various methods proposed to detect such systems.

1.5 Characterising transiting extra-solar planets

As mentioned in Sec. 1.2.3, measurements of transiting planets, in combination with radial velocity data, allow the determination of planetary masses and radii. The discovery of over fifty transiting planets allows the construction of an observational mass-radius diagram (Fig. 1.7). This illustrates the huge variation in mean density for planets of a similar size, the cause of which is, at present, poorly understood; it is not possible to predict whether a given planet will be 'inflated' or not (Charbonneau, 2009). Efforts have been made to model the structure

[6] *The Extrasolar Planets Encyclopaedia* – http://www.exoplanet.eu

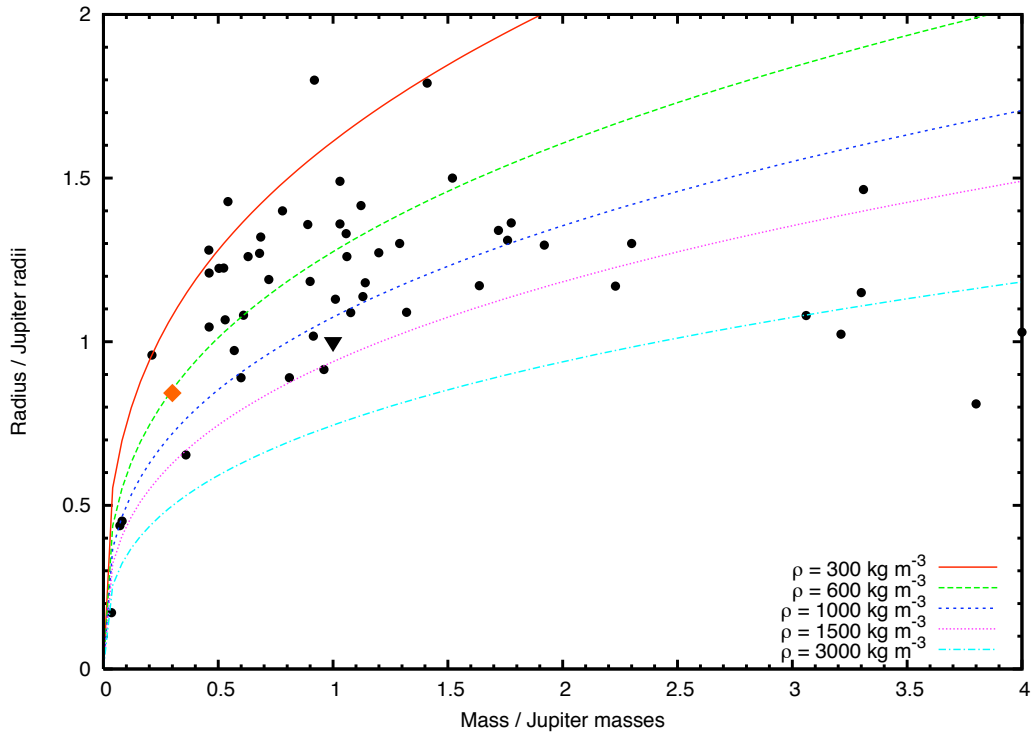

Figure 1.7: Mass-radius relation for extra-solar planets. 53 transiting planets with masses less than 4 M_J are shown (black circles), along with Jupiter (black triangle) and Saturn (orange square). Also shown are lines of constant mean density.

and formation of these hot Jupiters, however, and it is data from transiting planets that will be required to understand fully this issue.

Beyond exploring the structure and formation of exoplanets, transiting planets allow characterisation of their atmospheres without the requirement that we image the planets directly. These techniques exploit the fact that the planet passes directly in front of the star and that, half an orbit later, the planet passes behind the star in secondary eclipse.

Transmission spectra can be used to identify various components of the planetary atmosphere. By subtracting spectra of the star taken in and out of transit, features caused by absorption in the planetary atmosphere can be identified. This technique has been used to detect, for instance, the presence of sodium in the atmosphere of HD 209458 b (Charbonneau et al., 2002), as well as water (Tinetti et al., 2007) and methane (Swain et al., 2008) molecules in the atmosphere of another transiting exoplanet, HD189733 b.

The Spitzer space telescope has been used to detect the secondary eclipse of a number of exoplanets at infra-red wavelengths. The detection of the secondary eclipse of TrES-1 by Charbonneau et al. (2005) represented the first direct detection of (photons from) an extra-

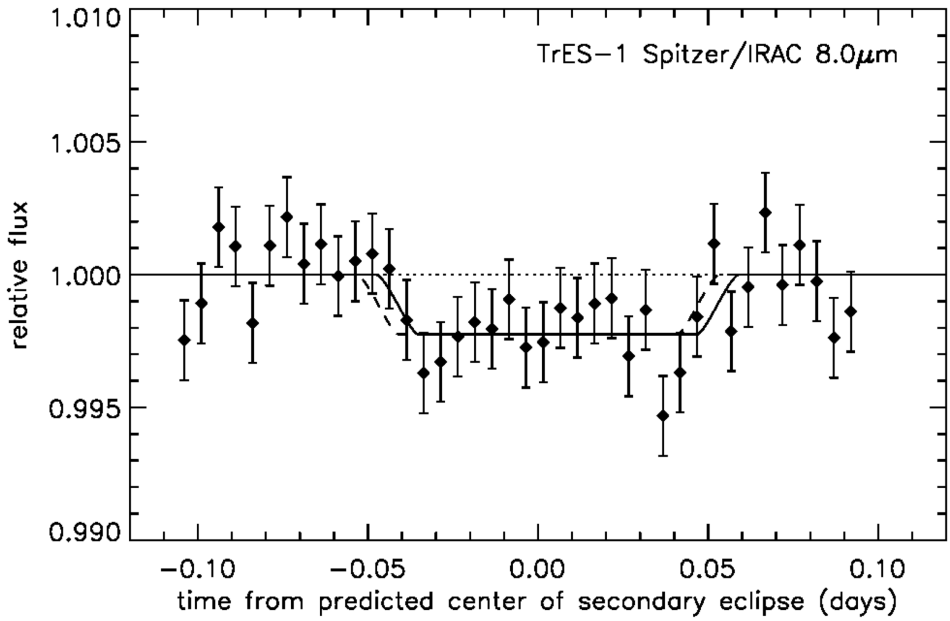

Figure 1.8: The 8.0μm secondary eclipse of TRES-1b. The solid lines is the best-fitting model which has a depth of 0.00225 and a timing offset (from phase 0.5) of +8.3 min. The dashed line is the same, but for a timing offset of zero. Figure taken from Charbonneau et al. (2005).

solar planet, and also allowed the albedo of the planet to be estimated (Fig. 1.8). *Spitzer* data also enabled Knutson et al. (2007) not only to measure the temperature, but to map the distribution of temperatures as a function of planetary longitude (Fig. 1.9).

1.6 Star - planet interaction

Recent studies of hot Jupiter planetary systems have revealed that the star and planet can interact both magnetically and tidally (see e.g. Shkolnik et al. 2009). Through magnetic interactions, the planet can induce activity in the photosphere and upper atmosphere of the star. Tidal interactions commonly result in the planet rotation period and orbital period becoming synchronised.

1.6.1 Low-frequency radio emission from exoplanets

The magnetic field strength of an exoplanet has not yet been measured, but this is thought to be possible through detection of low-frequency radio emission from the planet. Such emission is predicted to occur as a result of magnetic interactions between star and planet, in a manner similar to Jupiter. Jupiter has long been known (Burke & Franklin, 1955) to emit very strongly

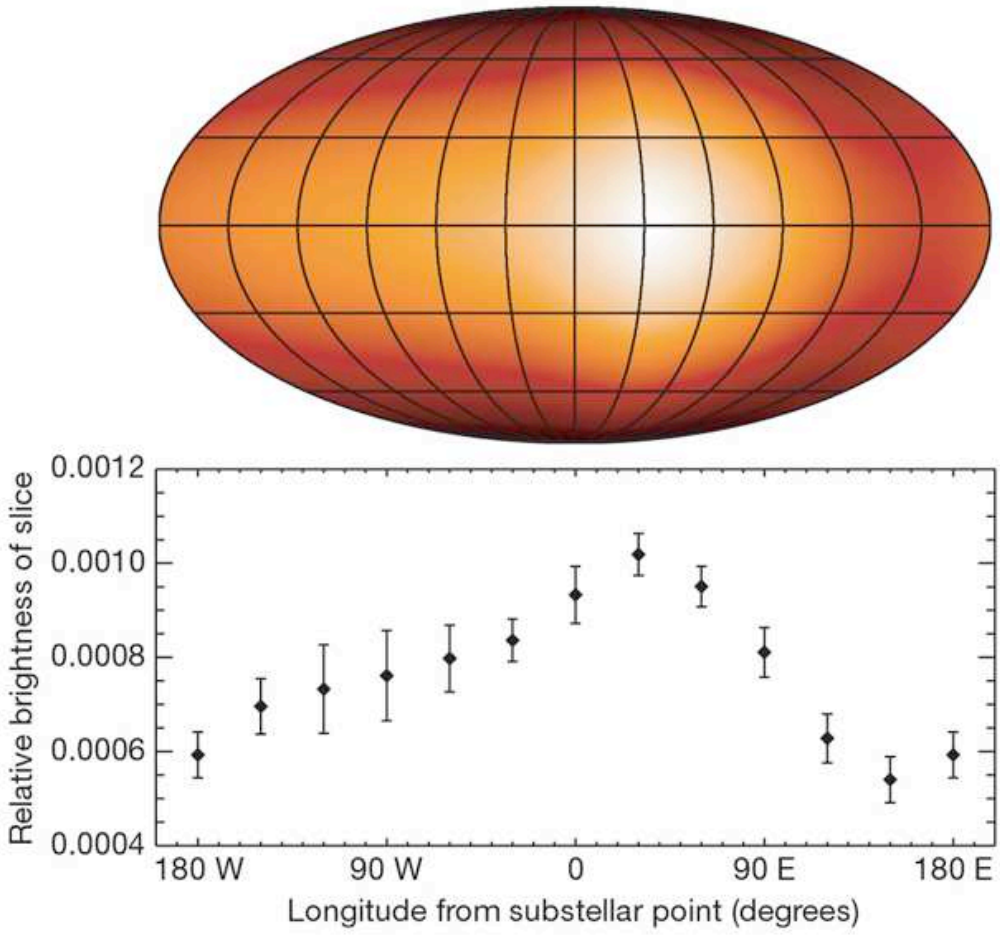

Figure 1.9: Brightness of HD 189733 b. Estimated brightness, assuming the planet is tidally locked, for 12 longitudinal strips of the planet's surface, shown as a contour map, *top* and as a graph, *bottom*. Figure taken from Knutson et al. (2007).

at frequencies of about 30 MHz; this is caused by charged particles from the solar wind interacting with the planetary magnetosphere, resulting in the emission of electron-cyclotron maser emission (see Sec. 6.1 for a more detailed discussion of this).

1.7 Overview of thesis

What follows is a brief description of the content of each of the major chapters of this thesis:

- In chapter 2, I investigate correlated 'red' noise as an explanation for why wide-field transit surveys have not yielded the number of planets originally predicted. The stellar populations in the fields observed by one of the SuperWASP-N cameras in the 2004 observing season are modelled. The number of planets detectable in the presence of red noise is predicted.

- An overview of follow-up photometry to SuperWASP observations is presented in chapter 3. Examples are used to illustrate some of the possible outcomes of follow-up photometry.

- In chapter 4, I describe the development of two Markov-Chain Monte Carlo (MCMC) codes which fit models to transit lightcurves, with the aim of measuring any variation in transit depth with wavelength.

- Chapter 5 is a description of a search of archive SuperWASP photometry for additional transiting planets in known planetary systems. The rotation of a planet host-star is investigated and the ability of SuperWASP to find multiple planet systems is quantified.

- In chapter 6, the first attempt to detect the secondary eclipse of a transiting exoplanet at radio wavelengths is reported. Observations of HD 189733 b are interpreted in the context of electron-cyclotron maser emission, which is predicted to occur when an exoplanetary magnetic field interacts with the stellar wind.

- Finally, the major findings of the previous chapters are summarised in chapter 7, and some possible future work is discussed.

2

The impact of correlated noise on SuperWASP detection rates

This chapter is based on an article published in *Monthly Notices of the Royal Astronomical Society*:

Smith, A. M. S., Collier Cameron, A., Christian, D. J., Clarkson, W. I., Enoch, B., Evans, A., Haswell, C. A., Hellier, C., Horne, K., Irwin, J., Kane, S. R., Lister, T. A., Norton, A. J., Parley, N., Pollacco, D. L., Ryans, R., Skillen, I., Street, R. A., Triaud, A. H. M. J., West, R. G., Wheatley, P. J., & Wilson, D. M., '*The impact of correlated noise on SuperWASP detection rates for transiting extra-solar planets*', 2006, MNRAS, 373, 1151.

All the work described here was conducted by the author.

In this chapter I present a model of the stellar populations in the fields observed by one of the SuperWASP-N cameras in the 2004 observing season. I use the Besançon Galactic model

Above: The five cameras which comprised SuperWASP-N, at the Observatorio del Roque de los Muchachos on La Palma, in 2004. Photograph taken from the SuperWASP website - http://www.superwasp.org.

to define the range of stellar types and metallicities present, and populate these objects with transiting extra-solar planets using the metallicity relation of Fischer & Valenti (2005). The ability of SuperWASP to detect these planets in the presence of realistic levels of correlated systematic noise ('red noise') is then investigated.

2.1 Introduction

Transit surveys have the potential to find numerous hot Jupiter-like planets (HJs), that is Jupiter-sized planets which orbit close to their host star with periods of just a few days. The probability that a HJ system is aligned such that transits will occur is about 0.1; which is much more favourable than planets orbiting at greater distances (for an Earth-like orbit, the probability of transit alignment is 0.0046).

Previous attempts have been made to estimate the expected detection rates of transiting HJs by shallow, wide-field transit surveys similar to SuperWASP (e.g. Brown 2003). Based on an observing pattern consisting of 38 nights of observations spread over 91 days and a requirement that three or more transits are observed, Brown calculated the detection rate of HJs producing a transit of depth 1 per cent or greater to be 0.39 per 10^4 stars. Brown also estimates that, for the same observing window function, 4.51 false alarms will be detected per 10^4 stars – indicating that only eight per cent of transit signals detected will be produced by planets. These planetary transit 'impostors' are grazing eclipsing binaries and eclipsing binaries diluted by light from a third star (either a field star or the third member of a triple system).

The SuperWASP survey has the potential to define the population of extra-solar planets which transit nearby bright stars ($V < 13$). In order for the results of SuperWASP to be properly interpreted, it is essential that the selection effects that operate in the survey are well understood. In this work, I use the findings of Pont (2006) and Pont, Zucker & Queloz (2006) to estimate SuperWASP's detection rate in the presence of realistic levels of systematic red noise. I find that in order to detect a significant number of transiting planets, the existence of red noise necessitates much longer observing baselines than previously thought.

2.2 Observations

Observations were conducted with SuperWASP-N (Sec. 1.3) during 2004, when the instrument was operated using only five cameras. The data were reduced in the standard manner described in Sec. 1.3, and the usual four components of correlated noise (one caused by airmass, one by thermal induced focus variations) are removed by the SysRem algorithm of Tamuz et al. (2005).

2.3 'Colours' of noise in photometric data

Pont (2006) demonstrated that there is likely to be significant co-variance structure in the noise in data from ground-based photometric surveys, such as SuperWASP. Previous forecasts of the planet 'catch' from such instruments (e.g. Horne 2001) have assumed that such noise is un-correlated or 'white' in nature. Pont et al. suggest that the reduced signal-to-noise caused by correlated or 'red' noise can account for an observed shortfall in transiting planet detections.

Noise consisting of white, independent, random noise combined with red, co-variant, systematic noise is termed 'pink'. Unlike white noise, this cannot be removed by averaging the data if the noise is on the time scale of the transits we wish to detect. Pont (2006) showed that systematic noise, correlated on time scales equivalent to a typical hot Jupiter transit (≈ 2.5 hours) cannot be ignored and indeed tends to be the dominant type of noise for bright stars. It therefore seems likely that the noise in SuperWASP data will be pink.

2.4 Characterisation of SuperWASP noise

The simplest method of establishing the level of correlated noise present in the data is to compute a running average of the data over the n data points contained in a transit-length time interval (Pont et al., 2006). The transit duration chosen here is 2.5 hours, which is the transit duration corresponding to a planet orbiting a solar analogue, with a period of 2.6 days – typical of a hot Jupiter. Since exposures are taken at roughly 7 minute intervals, there are about $n = 20$ points in each interval.

If the noise is purely random, the RMS scatter in the average of n data points should be $\sigma_w = \sigma/\sqrt{n}$, where σ is the standard RMS of the whole lightcurve. If, however, there is a

systematic component in the noise, the RMS scatter of the average of n points will be greater than this.

The RMS scatter, σ, is calculated for each of the 822 stars determined to be non-variable in the field centred at 15h17min RA, $+23^\circ\ 26'$ dec for which lightcurves have been produced by the SuperWASP data reduction pipeline. The noisiest 25 per cent of the data points in each lightcurve, corresponding to measurements made around full moon and during Sahara dust events, are excluded from the analysis. Stars are determined to be variable, and excluded from the analysis, if $\sqrt{\sigma_s^2} > 0.005$ mag, where σ_s^2 is the variance caused by intrinsic stellar variability, derived from the χ^2 statistic for a constant-flux model.

The running average, σ_r, over 20 points is also calculated for each of these stars, with the same exclusions of the noisiest data and intrinsically variable stars.

Both σ_w and σ_r are calculated prior to, and after, some red noise has been removed with SysRem. These quantities, and σ, are plotted against magnitude for the 822 non-variable stars in the field in Fig. 2.1.

As indicated by the differences between Figs. 2.1(a) and 2.1(b), the SysRem algorithm is highly effective at reducing the levels of systematic noise present in the data. Fig. 2.1(b) also shows, however, that not all correlation in the noise is removed by SysRem. If that were the case, the σ_r curve would lie over the σ_w curve. Instead, the σ_r curve lies higher than σ_w, and flattens out at about 3 mmag for bright (V=9.5) stars, indicating that systematic trends of this magnitude are present in the data on a 2.5 hour time-scale.

2.5 Simulated planet catch

I model the objects in the 36 fields viewed by one of the SuperWASP cameras in the 2004 season, by using the Besançon model of the Galaxy (Robin et al., 2003) to generate a star catalogue of stars with $9.5 < V < 13.0$ for each of the fields. Planets are then assigned to stars that are of spectral class F, G or K and luminosity class IV or V on the basis of their metallicity, using the planet-metallicity relation of Fischer & Valenti (2005):

$$\mathscr{P}(\text{planet}) = 0.03 \times 10^{2.0[\text{Fe/H}]} \tag{2.1}$$

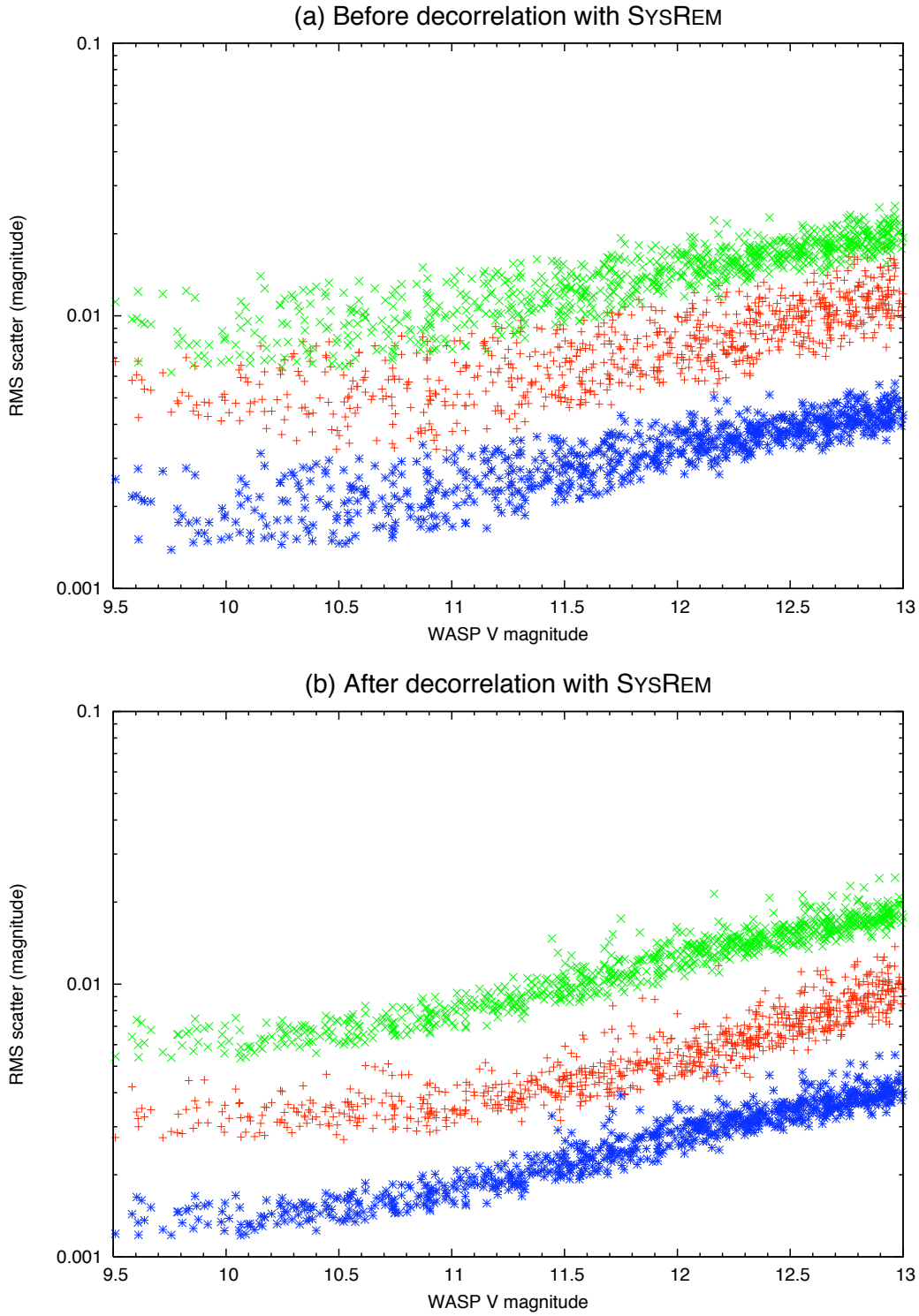

Figure 2.1: RMS scatter versus magnitude for non-variable stars in the field centred at 15h17min RA, $+23^\circ\ 26'$ dec both prior to (a), and after (b) decorrelation with SysRem. The upper (green) curve shows the RMS scatter of the lightcurve of each object, σ. The middle (red) curve shows the scatter, σ_r, after a moving average over a 2.5 hour time interval (20 data points) was calculated. The lower (blue) curve shows the RMS scatter divided by $\sqrt{20}$, σ_w.

where $\mathscr{P}$(planet) is the probability that a particular star of metallicity [Fe/H] is host to a planet. The above equation is used for stars which have metallicities in the range -0.5<[Fe/H]<0.5. For stars with [Fe/H]< -0.5, $\mathscr{P}$(planet) $=$ 0.003, and for [Fe/H]> 0.5, $\mathscr{P}$(planet) $= 0.3$.

Only stars of spectral type F, G and K are allocated a non-zero planet hosting probability, since the Fischer & Valenti (2005) equation is based upon radial velocity observations of stars of this type only. This does not pose a significant problem, however, as early-type stars are not numerous and have radii that are too great for transit detection. M-type stars are not particularly numerous in the Besançon-generated catalogues either (about 2.8 per cent of the stars are of type M or later), because the sample is limited by apparent magnitude, not volume. Although the transit signal produced by a Jupiter-like planet orbiting an M dwarf star will be greater than that produced by, say, a G dwarf star, M dwarfs are thought to be less likely to harbour giant planets (Adams et al., 2005). Similarly, only subgiants and dwarfs are considered planet hosts, since any planet orbiting a giant star would produce an insufficiently deep transit signature to be detected.

The probability that a star hosts a transiting planet is calculated using

$$\mathscr{P}(\text{transit}) = \mathscr{P}(\text{planet}) \times \mathscr{P}(\text{alignment}) \tag{2.2}$$

where $\mathscr{P}$(alignment) is the probability of a given planetary system being aligned with respect to the line of sight such that a transit can be observed. As it was shown in Sec. 1.2.3, this is given by

$$\mathscr{P}(\text{alignment}) = \frac{R_* + R_\text{p}}{a} \approx \frac{R_*}{a} \tag{2.3}$$

where R_* is the stellar radius, R_p the planetary radius and a the semi-major axis of the system. The semi-major axis of each potential planetary system in the model is drawn randomly from a distribution that is uniform in log (a), between $0.02 < a < 5.25$ au.

This simple log-flat distribution of semi-major axes is compared to the actual distribution of a amongst extra-solar planets discovered by Doppler surveys in Fig. 2.2. Our distribution appears to be a poor fit to the observed distribution in the regime favoured by transit surveys ($a \lesssim 0.05$ au), which may lead to an overestimation of the number of very short-period planets. The distributions, however, closely agree on the fraction of planets with $a \leq 0.05$ au - 14 per cent of the Doppler survey planets have $a \leq 0.05$ au, while the model distribution

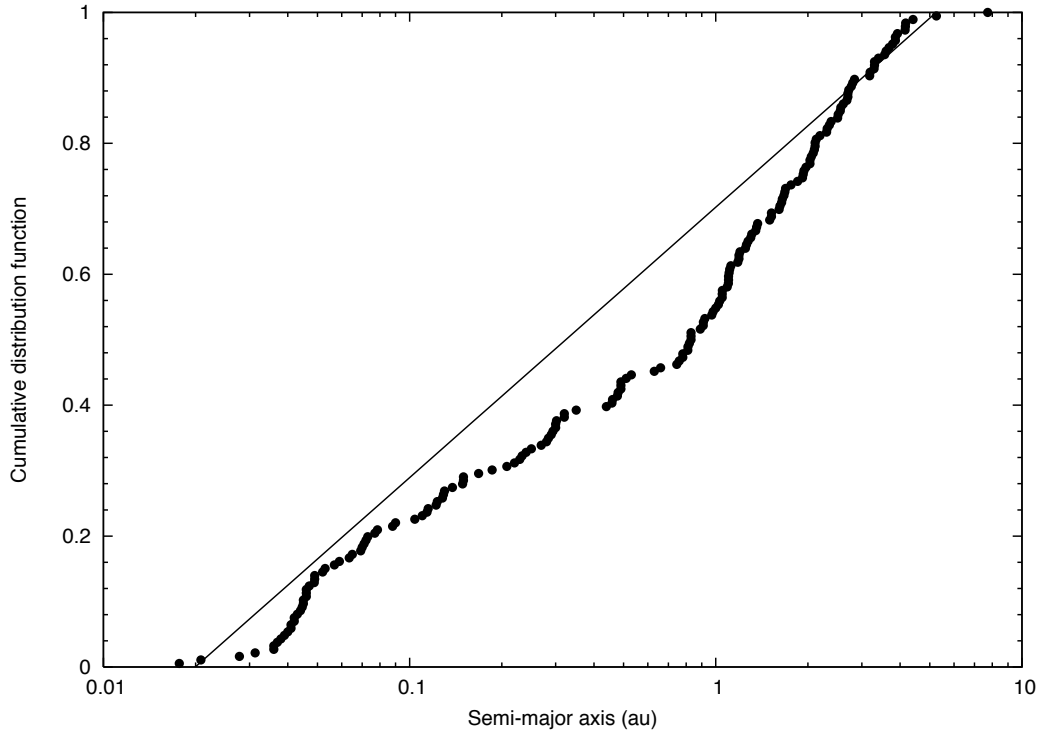

Figure 2.2: Cumulative distribution function of extra-solar planetary semi-major axis. The filled circles represent the 186 planets discovered by radial velocity means, as at 2006 September 15. The solid line is the distribution (uniform in log (a) for $0.02 < a < 5.25$ au) used in our model.

gives 16 per cent.

On the basis of the probability $\mathscr{P}$(transit), for each star, it is determined whether or not a star hosts a transiting planet. It is assumed, for simplicity, that all planets have a radius, $R_{\rm p}$, equal to that of Jupiter, $R_{\rm J}$. The depth of transit, Δm, is determined from the equation of Tingley & Sackett (2005),

$$\Delta m \approx 1.3 \left(\frac{R_{\rm p}}{R_*} \right)^2 \tag{2.4}$$

The factor of 1.3 in the above equation takes account of the effect of stellar limb-darkening, and although this assumes a central transit, off-centre transits will only have a slightly smaller limb-darkening factor (Tingley & Sackett, 2005).

A total of 355,429 stars are generated by the Besançon model in the 36 fields, 165,586 (46.6 per cent) of which are of type F,G or K and class IV or V. The simulation described above results in the allocation of a transiting planet to 329 of these stars, although this number changes each time the simulation is run because it relies on random numbers (see §2.6.2 for discussion of this). The transit depths of these 329 systems are calculated using equation 2.4.

The detection thresholds for planet detection are determined by fitting lines to the white

Table 2.1: Fitted parameters for RMS scatter as a function of magnitude for the white and red noise cases

	c_1	c_2
$\sigma_{\rm w}$	1.40×10^{-3}	1.96×10^{-8}
$\sigma_{\rm r}$	2.88×10^{-3}	4.34×10^{-8}

All variables are defined in the text.

and red noise curves of Fig. 2.1(b). The data is modelled with a constant term and a term which is inversely proportional to the flux of each object. This leads to fitted lines of the form $\sigma = c_1 + c_2 \left(10^{0.4V}\right)$, where c_1 and c_2 are constants which are fitted for, and V is the V-band magnitude. The values of the constants c_1 and c_2, as determined by χ^2 minimisation, for red and white noise are shown in Table 2.1.

These functions, $\sigma_{\rm w}$ and $\sigma_{\rm r}$, of magnitude are the 1-σ detection thresholds for the white and red noise cases respectively. The transit depths of the 329 simulated transiting planets are plotted as a function of magnitude along with the 5-σ detection thresholds for white and red noise in Fig. 2.3. 28 of the 329 planets have transit depths greater than the 5-σ detection threshold for white noise, but only one has a depth greater than the equivalent threshold when red noise is considered.

2.5.1 Signal-to-noise ratios

Although Fig. 2.3 provides a neat illustration of the reduction in planet detection efficiency experienced when red noise is present in the data, an analysis of the signal-to-noise ratio allows a fuller picture of the red noise problem to emerge.

The signal-to-noise ratio, $S_{\rm red}$, is a function of the number of observations made in-transit, as well as the depth of the transit. In the presence of red noise, $S_{\rm red}$ is given by

$$S_{\rm red} = \frac{\Delta m \sqrt{n_{\rm trans}}}{\sigma_{\rm r}(V)} \tag{2.5}$$

where $n_{\rm trans}$ is the number of transits observed.

$S_{\rm red}$ is similar to the S_r statistic of Pont et al. (2006), which also considers white noise. In the regime applicable to this work, where red noise dominates, S_r simplifies to our expression for $S_{\rm red}$.

$S_{\rm red}$ is a criterion used in the selection of planetary transit candidates for follow-up spectroscopic observations (Collier Cameron et al., 2006); a signal-to-noise ratio of 10 or greater

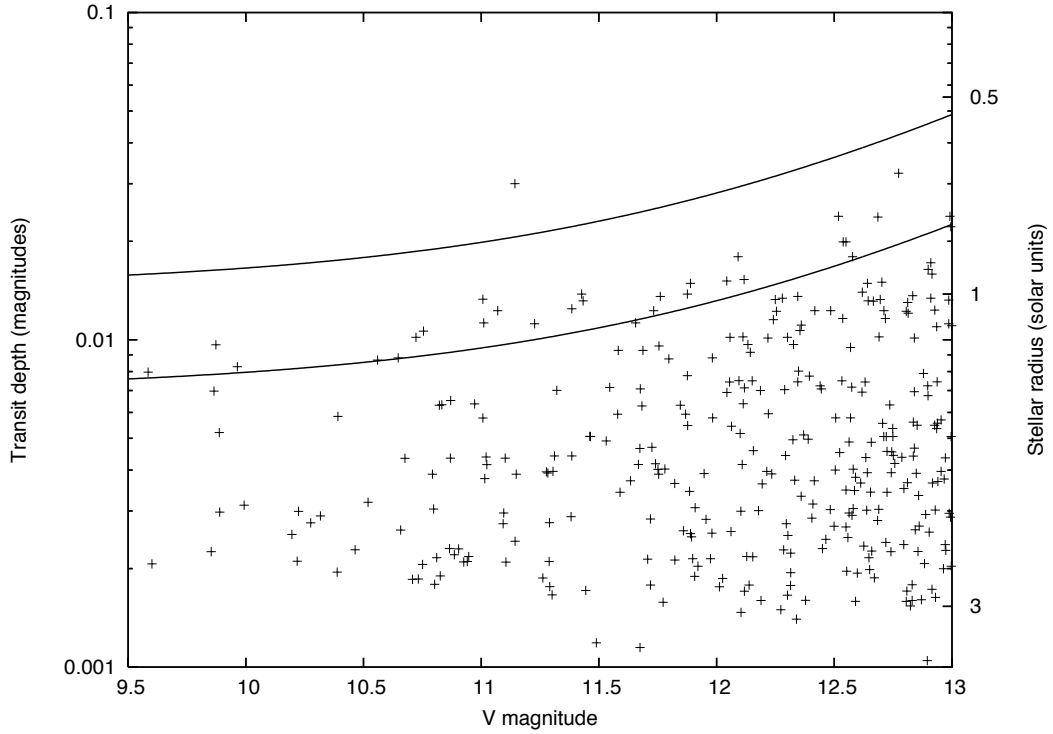

Figure 2.3: Transit depth versus magnitude for 329 simulated transiting extra-solar planets (points), with 5-σ detection thresholds for red (upper curve) and white (lower curve) noise, for a single transit. If more transits are observed, the thresholds are lowered by a factor of $\sqrt{n_{\rm trans}}$. Also indicated is the stellar radius, which is directly related to the transit depth since all planets are of radius R_J.

Table 2.2: The number of nights of observations for the three fields used in the signal-to-noise ratio analysis.

SuperWASP field ID	No. of nights
SW1143+3126	51
SW0044+2826	80
SW1743+3126	130

is required in order for an object to be considered as a viable transit candidate. This is a compromise between allowing too many false positive detections and rejecting large numbers of genuine transiting planets.

The $S_{\rm red}$ values of the simulated planets can be calculated using equation 2.5, since the transit depth, Δm, and the RMS scatter as a function of magnitude for red noise, $\sigma_{\rm r}(V)$, are already known. $n_{\rm trans}$ depends on the observing pattern and observing baseline used; here it is calculated for each simulated transiting planet using the observation times of three SuperWASP fields, the details of which are summarised in Table 2.2.

Each simulated planet is assigned a random epoch which is combined with the orbital period to produce an ephemeris for each simulated planet.

The transit duration, D, is calculated using the following relation,

$$D = \frac{R_* P}{\pi a} \tag{2.6}$$

where P is the orbital period, and circular orbits are assumed. The ephemeris and the transit duration are used to determine whether the system is in or out of transit at each time of observation, and hence $n_{\rm trans}$ is calculated. Here, partially-observed transits with more than five observations are counted towards $n_{\rm trans}$. The signal-to-noise ratio for each simulated planet is calculated for each of the three different observing baselines; the results are plotted in Fig. 2.4.

The number of simulated transiting planets with $S_{\rm red}$ greater than or equal to 10 was also calculated for each of the 20 fields which have at least 10 nights of observations. Each of these fields has a different number of nights of observations, and this is reflected in the simulation, which was conducted 100 times to reduce the problems of small number statistics. A total of 3.72 ± 1.60 planets were detected from a population of 151 ± 13 transiting extra-solar planets. The detailed results of this simulation are shown in Table 2.3, and the detection rate for these fields is plotted as a function of the number of observing nights in Fig. 2.7. Also plotted in Fig.

2.7 are the detection rates produced by the full simulation for the case of both one and two seasons of observing. The detection rate of transiting extra-solar planets increases linearly with the number of observing nights.

2.6 Discussion

2.6.1 Red noise and the SysRem algorithm

The SysRem algorithm is employed to remove four components of systematic error by removing trends which are present in all the stars in a particular field (Collier Cameron et al., 2006). If the implementation of SysRem is changed so that the number of trends set for removal is increased to five or more, no change in the quality of the data is observed. Despite this, however, red noise – as demonstrated in §2.4 – is still present in the data. I postulate that this remaining red noise does not affect stars in all parts of the field and so it cannot be removed by SysRem. Instead, it is suggested that the surviving red noise is localised and is most likely to be caused by variations in detector characteristics coupled with variations in the tracking of the mount. For instance, a particular group of stars may drift over the shadow cast on the CCD by a grain of dust on the optics, producing a regular dimming in a small number of objects.

2.6.2 Limitations of the Besançon-based model

The Besançon-based model used here has certain limitations; it should be noted that the simulation is based only on the observations from one of the SuperWASP-N cameras and it is assumed that none of the stars are blended. Only about two thirds of the generated planets have periods less than 5 days and, at present, Hunter only searches for planets with periods in this range. No planets, however, with $P > 5$ days have $S_{\rm red}$ greater than 10, even with 130 nights of observations. This is because $n_{\rm trans}$, and therefore $S_{\rm red}$, decreases with increasing period.

The number of planets produced in the simulation is determined to an extent by random numbers and so varies if the simulation is repeated. The simulation used here produced 329 transiting planets from a total of 355,429 stars in the magnitude range $9.5 < V < 13.0$, which is a fairly typical number; the simulation was run 15 times and the number of transiting planets produced was found to be 343 ± 25. Additionally, the relatively small number of planets around bright stars somewhat masks the fact that the signal to noise is a function of

magnitude – bright objects tend to have better signal-to-noise ratios.

2.6.3 Detection efficiency

Because SuperWASP can observe only during the hours of darkness, it is impossible to detect transits of planets with certain ephemerides, for instance a planet that orbits with a period of exactly 1 day, where the transits occur at midday. For a relatively modest number of observing nights, if the number of observed transits, n_{trans}, required to detect a planet is small (2 or 4, say), then the detection efficiency decreases with increasing period, but with spikes of reduced efficiency at certain pathological periods (Fig. 2.5(a)).

Increasing the number of transits required for a detection causes the detection efficiency to drop dramatically at most periods. If one requires a larger number (6 or more) of transits for detection, then the detection efficiency is much lower, except for several pathological periods where the detection fraction is such that finding planets with that period is particularly favourable. Increasing the number of observing nights has the effect of increasing the detection efficiency at nearly all periods (Figs. 2.5(b),(c)).

A common property of many SuperWASP transit candidates (e.g. Christian et al. 2006) is their large value of n_{trans}, and that many of the periods coincide with the narrow pathological period ranges where there is a much greater chance of detecting a large number of transits. The effects of red noise can be reduced by increasing the signal-to-noise of the data by requiring that a larger number of transits (≈ 10) are observed. In order to have a reasonable chance of observing this many transits, especially for planets with periods that are not pathologically favourable, longer time-base observations are required.

The S_{red} values of the simulated transiting planets are shown for 2 years of observations (130 nights in 2004, and an identical 130 nights 2 years later) in Fig. 2.6. This simulation shows that many more objects have a signal-to-noise ratio above the threshold of 10 after observing for a further season.

With this in mind, the 2006 SuperWASP-N observing season was dedicated to observing the same fields as in the 2004 season[1]. A further advantage of this policy is that the candidate planets have better determined ephemerides, which will aid follow-up work.

[1] SuperWASP-N did not observe during the 2005 season

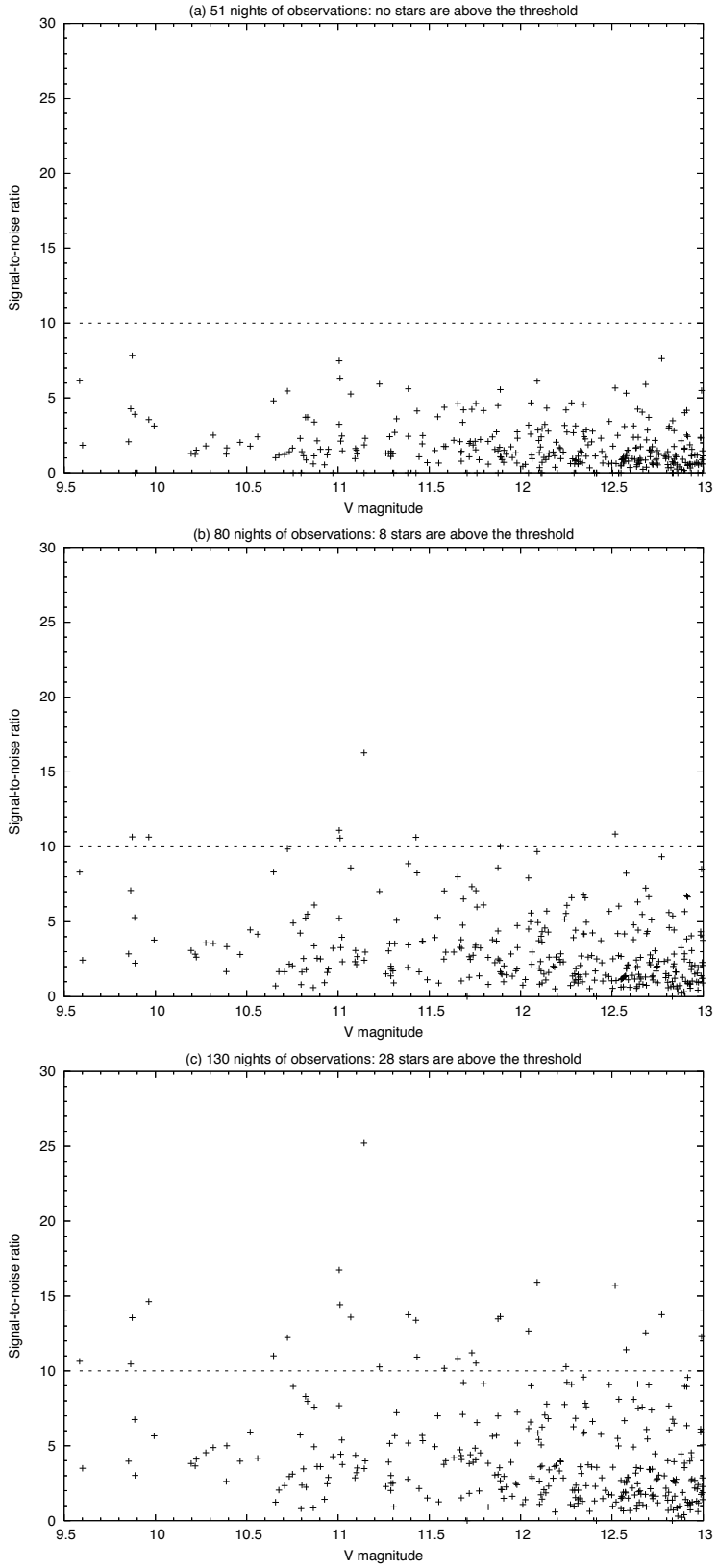

Figure 2.4: Signal-to-noise ratio versus magnitude for 329 simulated transiting extra-solar planets, for 51, 80 and 130 nights of data. The dotted line indicates a signal-to-noise ratio of 10, the threshold used when compiling transit candidate lists.

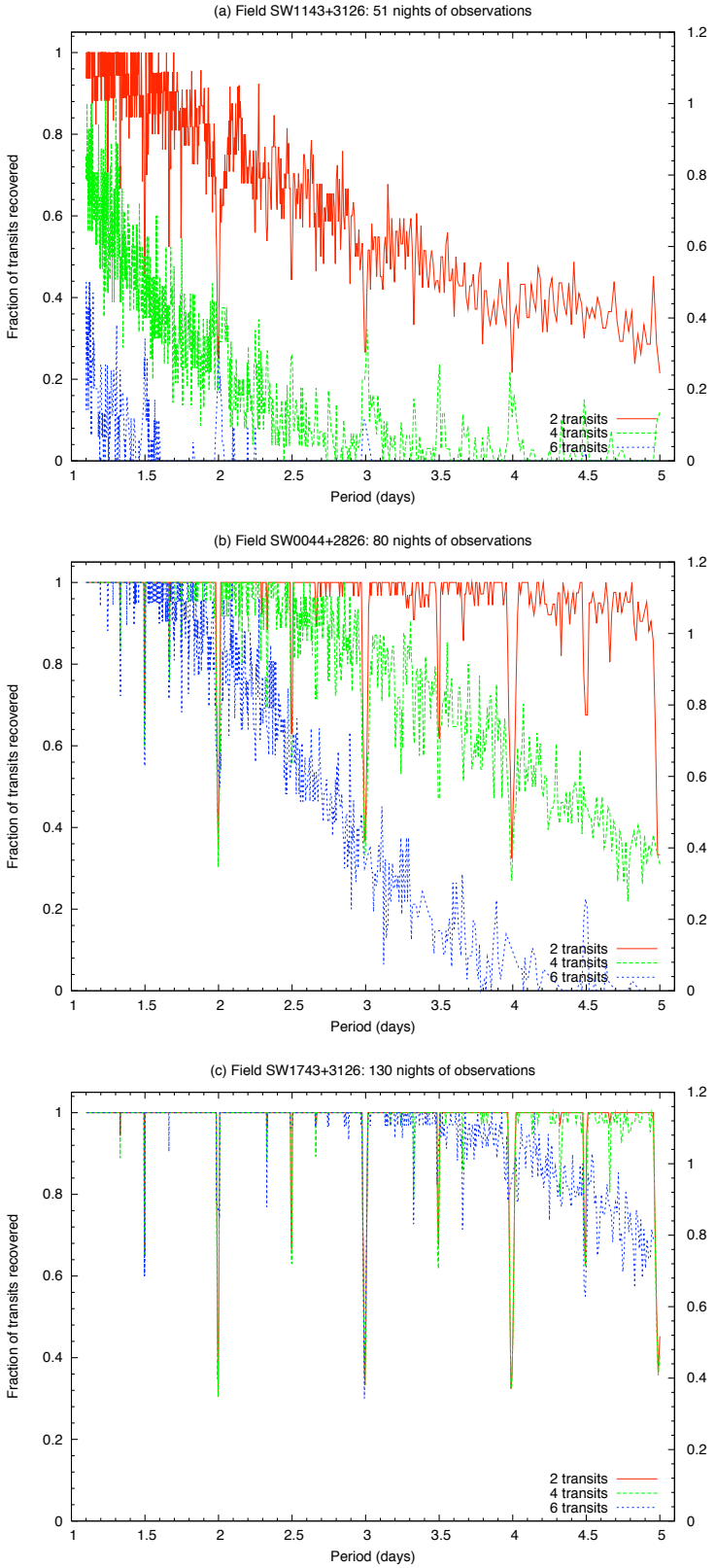

Figure 2.5: Transit detection efficiency as a function of period for fields with observations on 51, 80 and 130 nights. The solid, upper curve is for the requirement that at least 2 transits are observed for a detection; the dashed, middle curve for 4 transits; and the dotted, lower curve for 6.

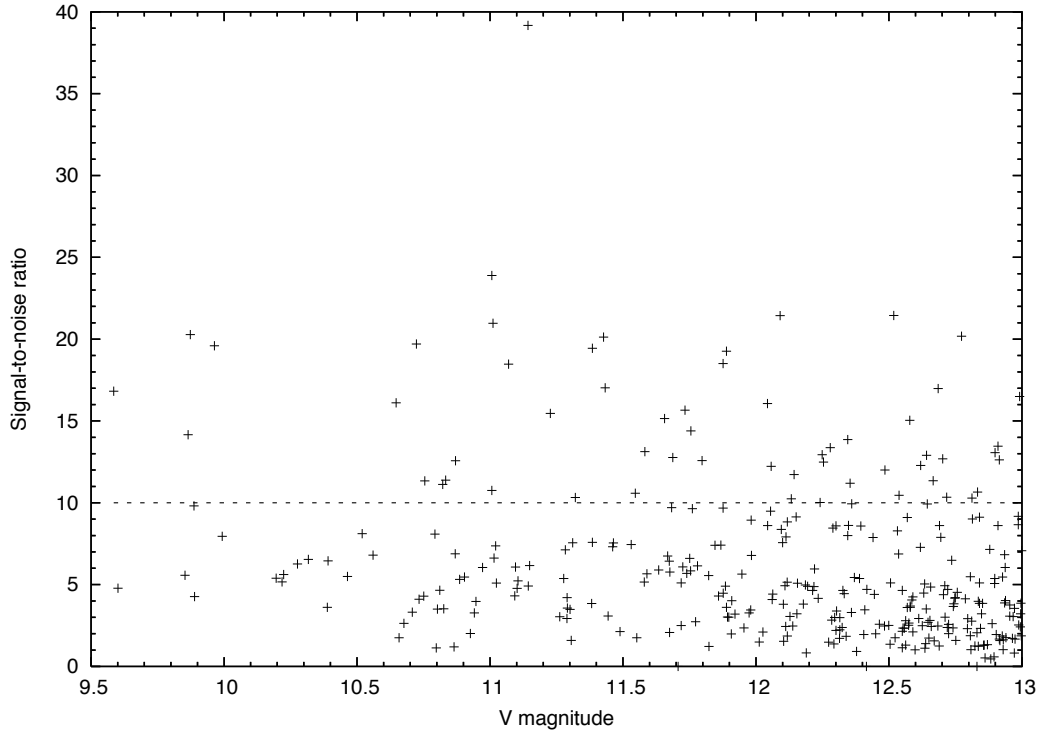

Figure 2.6: As Fig. 2.4, but for 2 seasons each consisting of 130 nights of data. 56 stars are above the $S_{\rm red}$ threshold of 10.

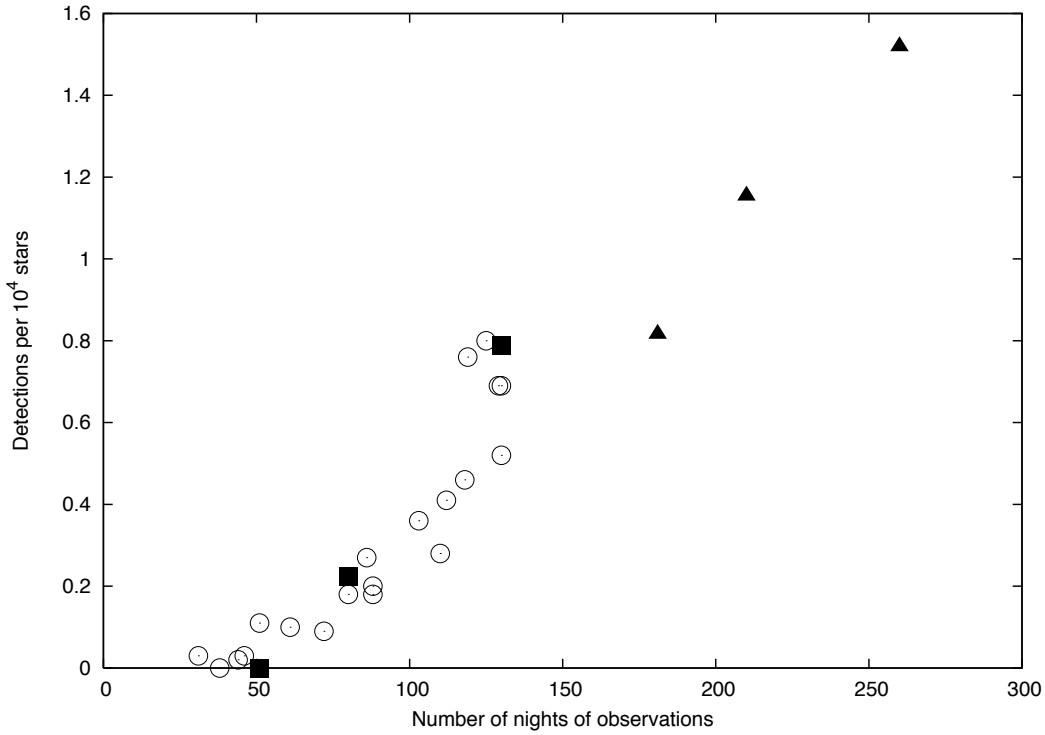

Figure 2.7: Detection rate (a detection is defined as $S_{\rm red} > 10$) of transiting extra-solar planets versus number of nights of observations. The squares correspond to one season of observations, while the triangles represent an additional 130 nights of observations in a second season. The open circles represent the 20 fields included in Table 2.3.

Table 2.3: Simulated planetary detection rates in the twenty fields that were observed for more than ten nights by one of the SuperWASP-N cameras in 2004.

Field ID	No. of nights of observations	No. of observations	No. of stars		No. of planets with $S_{\rm red} \geq 10$ in simulation	Detections per 10^4 stars
			Model	Observed		
SW0043+3126	88	2962	6150	4746	0.12 ± 0.32	0.20
SW0044+2826	80	2851	5684	7353	0.10 ± 0.30	0.18
SW0143+3126	72	2251	6354	7840	0.06 ± 0.24	0.01
SW0243+3126	61	1646	7114	8235	0.07 ± 0.26	0.10
SW0343+3126	46	1286	9630	8465	0.03 ± 0.17	0.03
SW0443+3126	44	911	16062	8314	0.04 ± 0.20	0.02
SW0543+3126	38	539	21255	15021	0.01 ± 0.10	0.00
SW1043+3126	31	473	2939	2775	0.01 ± 0.10	0.03
SW1143+3126	51	813	2628	2508	0.03 ± 0.17	0.11
SW1243+3126	86	2157	2577	2605	0.07 ± 0.35	0.27
SW1342+3824	103	2578	2482	2724	0.09 ± 0.32	0.36
SW1443+3126	125	3618	2988	3071	0.24 ± 0.51	0.80
SW1543+3126	130	4422	3899	3963	0.27 ± 0.47	0.69
SW1643+3126	129	4795	5388	6233	0.37 ± 0.59	0.69
SW1739+4723	119	4401	5361	8791	0.41 ± 0.58	0.76
SW1743+3126	130	5214	8712	11681	0.45 ± 0.65	0.52
SW1745+1727	110	3590	13700	17818	0.38 ± 0.60	0.28
SW2143+3126	88	3672	15145	24129	0.27 ± 0.53	0.18
SW2243+3126	118	4388	9175	14330	0.42 ± 0.60	0.46
SW2343+3126	112	3629	6913	9488	0.28 ± 0.53	0.41
Total			154156	170090	3.72 ± 1.60	0.24

2.6.4 Comparison of detection rates with previous work

The simulation described in this paper allows comparison with the detection rate of transiting HJs estimated by Brown (2003), who takes no account of red noise. Of the planets generated in the simulation, 63 have a transit depth deeper than one per cent, resulting in about 20 detectable planets if it is assumed that the fraction of transits recovered is about 0.3 for the 38 nights of observations described by Brown. Since there are $\sim 3.55 \times 10^5$ stars in our simulation, this gives a detection rate of 0.56 per 10^4, which is comparable to the 0.39 per 10^4 of Brown. However, our signal-to-noise ratio analysis suggests that, in reality, observations must be made for between 80 and 130 nights for the detection rate of HJs to be as high as 0.39 per 10^4 stars (Fig. 2.7).

2.7 Conclusions

In conclusion, there is a significant component of systematic, red noise present in data from SuperWASP-N. The SysRem algorithm of Tamuz et al. (2005) appears highly effective at reducing the level of red noise, but fails to eliminate it entirely. The remaining red noise is present in the data at a level of about 3 mmag on time-scales of 2.5 hours, roughly equivalent to a typical transit duration time. This remaining noise has a significant impact on the efficacy of planet detection, as demonstrated by a Monte Carlo simulation based on the Besançon Galaxy model.

Our analysis reveals that if observations are conducted for only 51 nights, none of the simulated transiting planets produces a transit detection with a signal-to-noise ratio of 10 or more. A total of 3.72 ± 1.60 planets which transit with $S_{\rm red} \geq 10$ are predicted for the fields observed in 2004 by one SuperWASP-N camera, which is representative of the other four cameras, so 18.6 ± 8.0 planets are predicted in total. In order to improve the $S_{\rm red}$, and thus increase the number of detectable planets, a greater number of transits must be observed in the data set of a particular object. This requires observations to be made over a longer time period.

On the basis of the transit detection rates predicted here, the SuperWASP consortium decided to continue observing all the fields that were monitored during 2004. It is expected that this will enhance greatly the number of planetary transit events detected at non-pathological periods.

2.7.1 Postscript

Since the work described in this chapter was carried out and published (Smith et al., 2006), several further seasons of SuperWASP observations have been conducted. These have yielded several confirmed detections of transiting exoplanets, starting with the discovery of WASP-1 and WASP-2 (Cameron et al., 2007). Indeed, the number of known transiting planets has increased greatly, with SuperWASP the most successful of the numerous surveys which have discovered new planets (Sec. 1.2.3). Significantly fewer planets, however, have been discovered than was predicted in Sec. 2.7. The reasons for this are believed to be those already discussed in sections 2.5 and 2.6.2. It should be noted, though, that the predictions made here have proved considerably more accurate than those which do not account for red noise, for instance Horne (2001) predicted a discovery rate of 15 planets per month for SuperWASP-N.

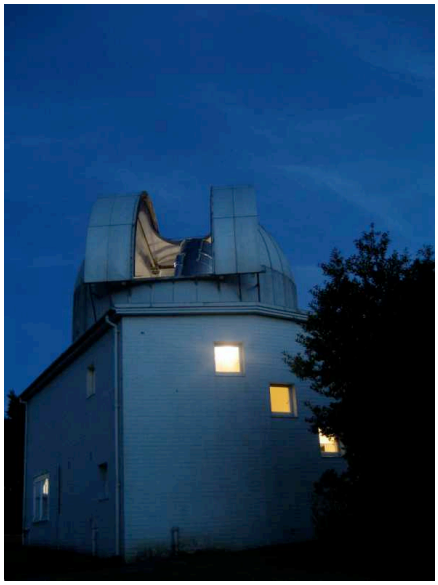

3

Photometric follow-up observations of SuperWASP planetary candidates

In this chapter, I present four examples of follow-up photometry of SuperWASP planetary candidates obtained with larger telescopes. These examples illustrate the various possible outcomes from photometric follow-up observations, and reinforce the importance of such observations when attempting to discover transiting exoplanets with a wide-field survey like SuperWASP.

3.1 Purpose and aims

Many promising planetary candidates arise from systematic searches for periodic transits in SuperWASP data. For a number of reasons, it is generally desirable to devote some observational effort to following up these objects with further, more precise photometry. Photometry

Above: The James Gregory Telescope of the University of St. Andrews Observatory. Photograph by the author.

with a relatively modest-sized telescope ($\sim$ 1 m) can serve to rule out candidate stars as planet hosts before resorting to more expensive radial velocity observations. Such photometry may also be used to refine the ephemeris of the putative planetary system, so radial velocity observations may be optimally scheduled and it can be seen quickly whether the phase of any radial velocity variation is correlated with that of the transits. Refining the ephemerides of these candidate systems is particularly important if the time elapsed since the end of SuperWASP observations is large when compared to the duration of the SuperWASP lightcurve. For instance, the ephemeris of an object observed during only one SuperWASP season and then not observed for $\sim$ 1 year is likely to predict transit times with uncertainties of $\sim$ 1 hour or greater.

Furthermore, if an object is confirmed as a planet, then the SuperWASP lightcurve is not of sufficient quality to constrain tightly planetary parameters such as radius and impact parameter. Instead, follow-up photometry is required to determine, in conjunction with high-precision radial velocity data, the parameters of the planetary system.

3.1.1 Ruling out candidates

Follow-up photometry around the expected time of transit is particularly useful before deciding whether a particular candidate merits radial velocity observations when the SuperWASP lightcurve is of particularly poor quality. For instance, only a small number of transits and/or partial transits may have been observed by SuperWASP, and there may exist doubt as to whether these 'transits' are 'real', i.e. astrophysical in nature. Ambiguities in the period of the transits (or eclipses if they turn out to be entirely stellar in origin) may also be resolved by follow-up photometry. It is often unclear whether the period of a particular object is indeed the best period selected by the HUNTER algorithm (Collier Cameron et al., 2006), or whether it is an alias of that period – most commonly exactly twice or half of that period. Observing, with follow-up photometry, a transit that should only occur if the shorter period is the true one can remove this ambiguity.

Improving our knowledge of the shape of the transit is also possible with higher precision follow-up photometric observations; as previously mentioned, this is important if the object is later confirmed to be a planetary system. Refining the shape can also aid in identifying the object as an eclipsing stellar binary system, the signature of which is a 'V'-shaped transit, rather than one with a flat bottom.

Finally, the improved spatial resolution of follow-up photometry can help identify target objects which appear to exhibit transits, but which are merely close on the sky to an eclipsing binary system. A commonly observed scenario in SuperWASP data is a non-variable object within the normal SuperWASP magnitude limits ($9.5 < V < 13.0$) close on the sky to a significantly fainter ($V < 13$) deeply-eclipsing stellar binary system. Because of the large pixel scale ($13.7''$ per pixel), and hence poor spatial resolution of SuperWASP, the two systems appear as one, often with the deep eclipses diluted to appear about as deep as a typical hot Jupiter transit ($\sim$ 1 per cent). Observations with a larger telescope can often resolve the individual components of these blended objects, and determine which of them is exhibiting transits or eclipses (see Sec. 3.2.1 for an example of this).

3.2 Examples of follow-up photometry

3.2.1 1SWASPJ060553.64+270837.7: an example of an object blended with a deeply-eclipsing stellar binary

The SuperWASP planetary candidate 1SWASPJ060553.64+270837.7 ($V = 11.25$) was identified as such from a HUNTER search of data from the 2006 SuperWASP-N observing season. The ephemeris determined by HUNTER, in the form epoch of mid-transit + period, is:

$$HJD = 2454109.7740 + 1.212878E \tag{3.1}$$

and the transit depth was calculated to be about 30 mmag (Fig. 3.1).

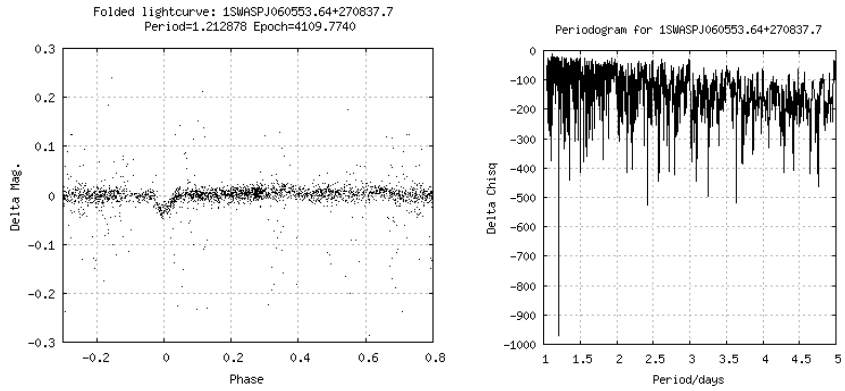

Figure 3.1: HUNTER results for the planetary candidate 1SWASPJ060553.64+270837.7. *Left panel*: phased SuperWASP lightcurve (see text for ephemeris). *Right panel*: periodogram. Plots generated by SuperWASP's HUNTER results interface, which was developed by David Wilson.

Observations

It was known (by looking at the USNO B catalogue) that this object is blended with other stars, and it was decided that follow-up photometry of this object was required to determine which object is responsible for the transits before expending valuable radial velocity observing time. Observations were conducted around the time of a predicted transit on the night of 2007 November 22/23, with the 0.95-m James Gregory Telescope (JGT) of the University Observatory, St. Andrews. The JGT is fitted with a 1024×1024 Andor / e2v CCD at the Cassegrain focus, which covers a $17'$ by $17'$ field with a pixel scale of $1''$ per pixel. A total of 313 images, each with an exposure time of 30 s were made between UT 23:47 and UT 02:59, using an *R*-band filter.

Data reduction and analysis

The data were reduced with a version of the SuperWASP reduction pipeline (Pollacco et al. 2006) adapted for use with the JGT. Differential aperture photometry was performed on the target star using an ensemble of nearby objects as a reference star. The SuperWASP pipeline calculates the flux of each object in each exposure, and these are combined and converted to a single lightcurve in magnitudes, m, as follows,

$$m = -2.5\log_{10}\frac{f_t}{\sum_{r=1}^{n} f_r}, \tag{3.2}$$

where f_t is the flux of the target star and a total of n reference stars with fluxes $f_1, f_2, ..., f_n$ are combined to act as a single reference star. The uncertainty (assuming independent errors) on this magnitude, σ_m, is calculated using standard error manipulation and a conversion to magnitudes,

$$\sigma_m = \frac{2.5}{\log_e 10}\sqrt{\left(\frac{\sigma_t}{f_t}\right)^2 + \left(\frac{\sqrt{\sum_{r=1}^{n} {\sigma_r}^2}}{\sum_{r=1}^{n} f_r}\right)^2}, \tag{3.3}$$

where σ_t is the uncertainty on the target flux and σ_r the uncertainty on the reference flux.

The resulting lightcurve was phase folded using the ephemeris given earlier (Eqn. 3.1) and is shown in Fig. 3.2 over-plotted with the phase-folded SuperWASP lightcurve. No transit

was observed around phase zero, although there is an apparent reduction in flux around phase 0.03, believed to be caused by thin, patchy cloud.

A visual inspection of two images revealed an apparent reduction in flux from a fainter (USNO $R = 11.34$ compared to $R = 10.77$ for the target), closely neighbouring star (Fig. 3.3). Aperture photometry performed on this object which lies approximately $16''$ from the target (well within the 3.5 pixel radius SuperWASP aperture) reveals a deep (~ 0.4) mag eclipse at almost exactly the time of predicted transit (Fig. 3.2).

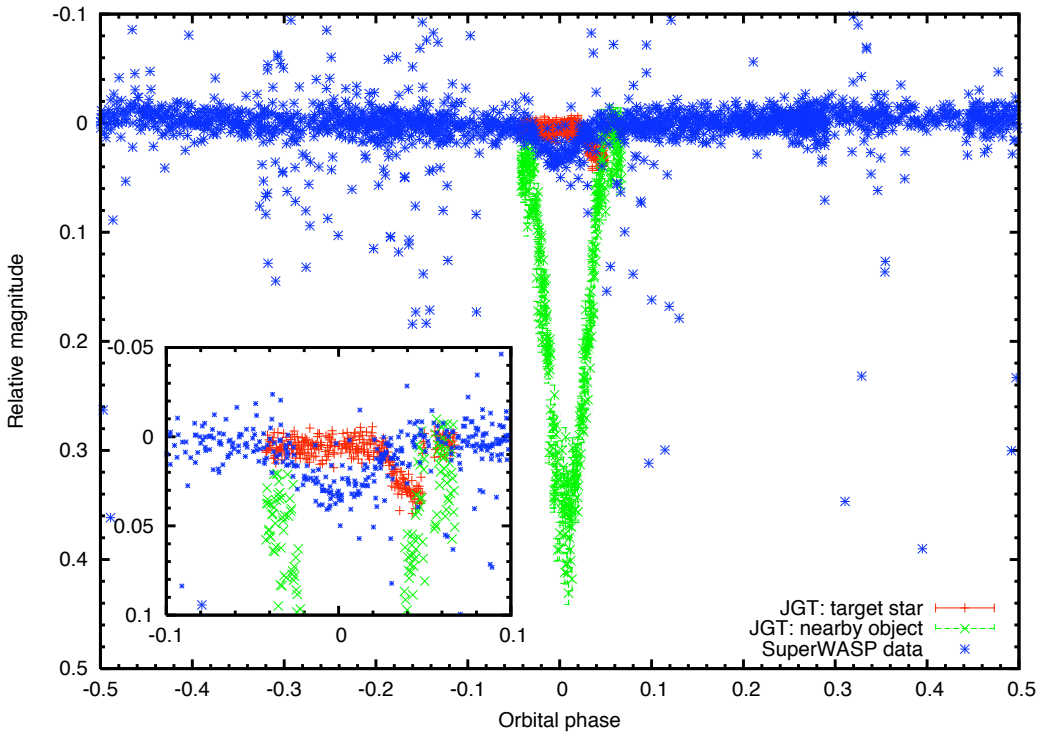

Figure 3.2: Phase-folded lightcurves of 1SWASPJ060553.64+270837.7. Shown are the 2006 season SuperWASP data (blue), the 2007 November 22 JGT target lightcurve (red) and nearby object lightcurve (green). Inset: a zoomed-in plot of the area around transit, with error bars removed for clarity.

Conclusions

In summary, follow-up photometry of this object enabled a nearby fainter eclipsing binary system to be identified as the true cause of the observed 'transits' for this object. 1SWASPJ060553.64+270837.7 was therefore rejected as a planetary candidate without resort to spectroscopic observations.

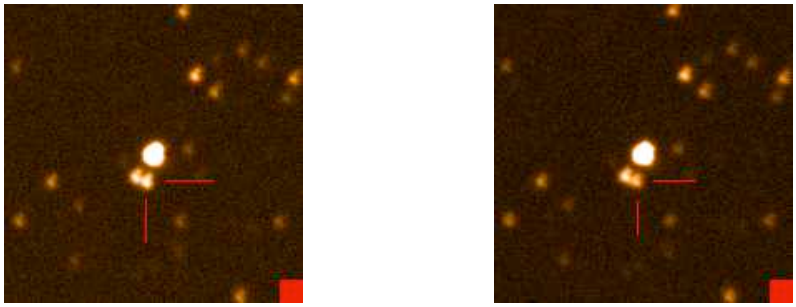

Figure 3.3: JGT images of 1SWASPJ060553.64+270837.7. *Left*: at the start of the 'transit' (phase = -0.0454). *Right*: close to the centre of the 'transit' (phase = 0.00543). Both images measure 3′ on each side and are centred on the target star. The nearby object indicated by red lines is responsible for the 'transit' and can be seen to be fainter in the image on the right. For comparison purposes, the size of a SuperWASP pixel is indicated by the red square in the lower-right corner. North is up, and East to the left.

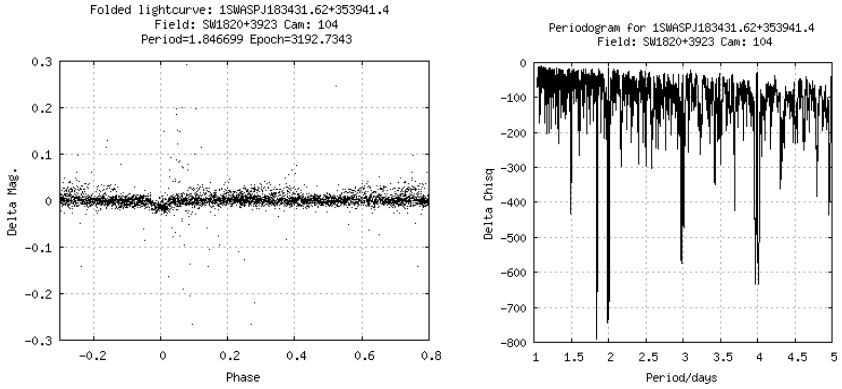

Figure 3.4: HUNTER results for the planetary candidate 1SWASPJ183431.62+353941.4. *Left panel*: phased SuperWASP lightcurve (see text for ephemeris). *Right panel*: periodogram. Plots generated by SuperWASP's HUNTER results interface, which was developed by David Wilson.

3.2.2 1SWASPJ183431.62+353941.4: an example of an extra-solar planet

The SuperWASP planetary candidate 1SWASPJ183431.62+353941.4 ($V = 10.64$) was identified as such from a HUNTER search of data from the 2004 SuperWASP-N observing season (Fig. 3.4).

Two partial transits of this object were observed by the author and Leslie Hebb on the nights of 2007 August 02 and 2007 August 04, using the 0.8-m Instituto de Astrofísica de Canarias IAC-80 telescope. The telescope, located at the Observatorio del Teide on Tenerife, is fitted with a 2148 × 2148 pixel CCD which covers 10.6′. Observations were conducted in the V-band and the I-band, with exposure times of 30 s and 20 s, respectively. The data were reduced by Leslie Hebb in a similar fashion to that described in Sec. 3.2.1, albeit with different software. This data reduction is described in more detail by Pollacco et al. (2008),

and the resulting lightcurves, phase-folded on the SuperWASP ephemeris, are shown in Fig. 3.5. Also shown in Fig. 3.5 are the best-fitting models to the transit photometry obtained with the Markov-chain Monte Carlo (MCMC) code 4DEPTHS which is described in Chapter 4.

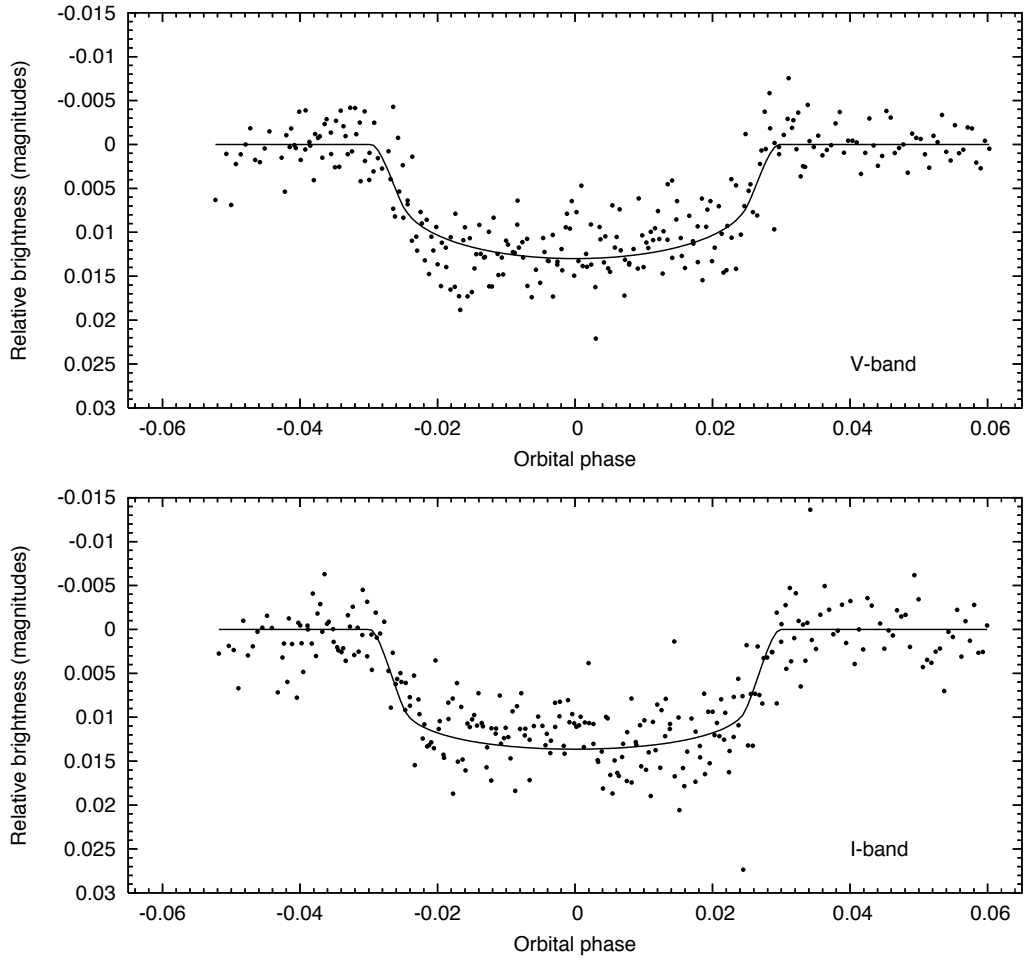

Figure 3.5: Transit lightcurves of 1SWASPJ183431.62+353941.4 (WASP-3), obtained with the IAC-80 telescope of the Observatorio del Teide on 2007 August 02 and 04. *Upper panel*: V-band lightcurve, *Lower panel*: I-band lightcurve. In each case, the best-fitting model obtained with Markov-chain Monte Carlo modelling (see Chapter 4 for details) is plotted as a solid line.

The higher-precision photometry obtained with the IAC-80 confirmed that the candidate object is responsible for the transits, and that the transits are consistent with a hot Jupiter planet. This object was confirmed as a transiting planetary system shortly after the IAC-80 observations were made, using radial velocity observations conducted with the SOPHIE spectrograph on the 1.93-m telescope at the Observatoire de Haute-Provence (Pollacco et al., 2008). The IAC-80 transit photometry, along with further, R-band, follow-up photometry and the SuperWASP photometry allowed determination of the planetary parameters and ephemeris by other members of the SuperWASP team. All the aforementioned photometry and the radial

velocity measurements were modelled simultaneously using the MCMC techniques described in Collier Cameron et al. (2007) to determine the parameters listed in Pollacco et al. (2008).

3.2.3 1SWASPJ211059.34+015711.9: an example of a blended eclipsing binary

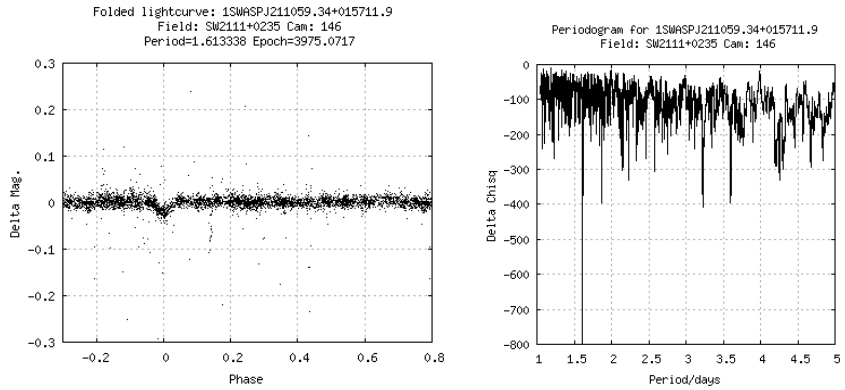

Figure 3.6: HUNTER results for the planetary candidate 1SWASPJ211059.34+015711.9. *Left panel*: phased SuperWASP lightcurve. *Right panel*: periodogram. Plots generated by SuperWASP's HUNTER results interface, which was developed by David Wilson.

The SuperWASP planetary candidate 1SWASPJ211059.34+015711.9 (Fig. 3.6) was observed on 2007 August 02 with the 0.8-m IAC-80 telescope (see Sec. 3.2.2 for further details of this instrument). Although a partial transit of this object was obtained at approximately the time predicted by the SuperWASP ephemeris, a single image was enough to rule this candidate out. Although not apparent from looking at the image, a cut through the point spread function of the target revealed that the star is clearly not a single object (Fig. 3.7). One of these two stars is presumed to be an eclipsing binary, since the transit depth is too great to be caused by a planet. This hypothesis was further confirmed by the partial transit obtained with the IAC-80, which appears to be rather more 'V'-shaped than would be expected for a planetary transit (Fig. 3.8).

3.2.4 1SWASPJ062430.87+261906.0: an example of a low-mass eclipsing binary

The SuperWASP planetary candidate 1SWASPJ062430.87+261906.0 ($V = 11.80$, Fig. 3.9) was observed on 2008 January 11 with the JGT (see Sec. 3.2.1 for details of this instrument and data reduction technique). A partial transit (missing ingress) was observed at the time predicted by the ephemeris determined by the SuperWASP photometry (Fig. 3.10). A visual inspection of this lightcurve indicated that the transit is flat-bottomed, and therefore could be

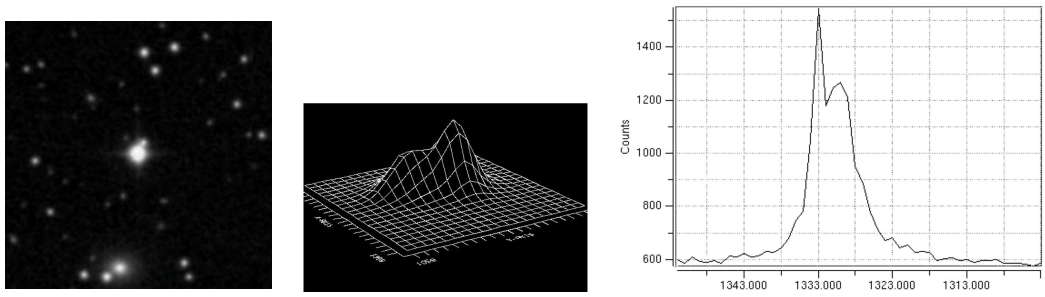

Figure 3.7: Photometry of 1SWASPJ211059.34+015711.9. *Left*: an ESO Digitised Sky Survey (DSS) image centred on the target, measuring 3′′ on each side, with North up and East to the left. Analysis of the point spread function of the target in an IAC-80 image (*centre* and *right*) reveals that the target is a blend of two stars, in addition to the nearby object to the NW that can be seen in the DSS image.

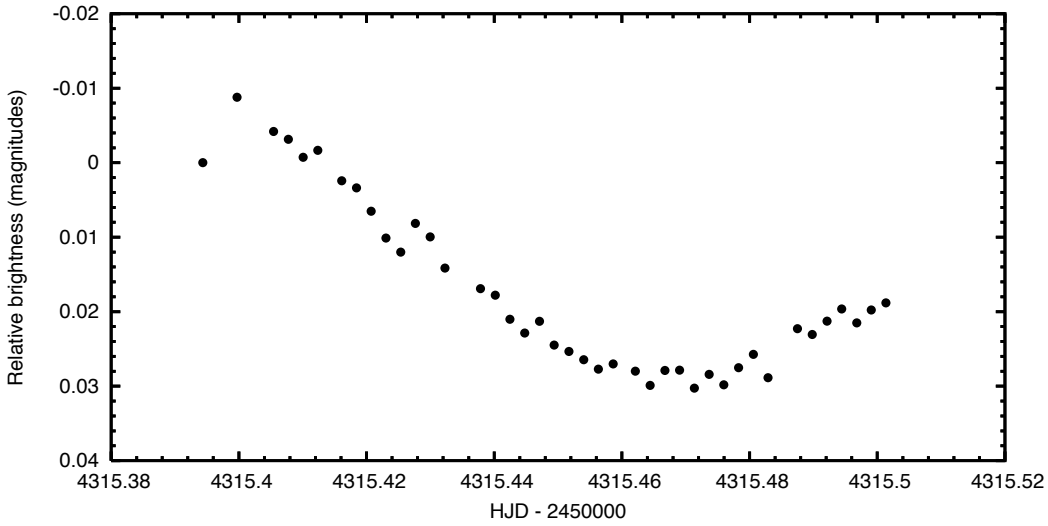

Figure 3.8: Partial transit lightcurve of 1SWASPJ211059.34+015711.9, obtained with the IAC-80 telescope at the Observatorio del Teide on 2007 August 02

of planetary origin. Furthermore, the JGT observations established the eclipse as astrophysical in nature, and confirmed that the target, not a neighbouring object, is responsible for the eclipses.

MCMC analysis of the combined SuperWASP and JGT photometry carried out by Andrew Cameron gave a large planetary radius ($\approx 2\ R_{\rm J}$) as the best-fitting solution. This suggested that the eclipses may be caused by a stellar object rather than a planet, but it was decided that spectroscopic observations were required to determine the nature of this candidate. Spectra of the object were obtained by Elaine Simpson using the Nordic Optical Telescope (NOT) at the Observatorio del Roque de los Muchachos, on the island of La Palma, Spain. These spectra indicate that the target is a fast-rotating star, with $v\sin i \approx 40$ kms^{-1}, confirming that the eclipses are caused by a low-mass stellar companion to the target star, rather than an orbiting

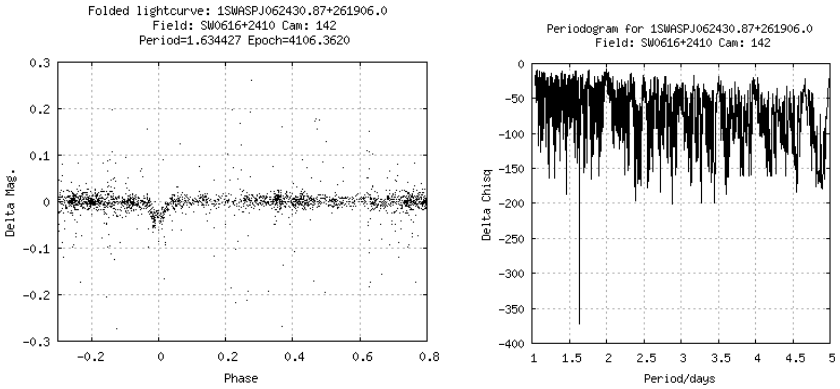

Figure 3.9: HUNTER results for the planetary candidate 1SWASPJ062430.87+261906.0. *Left panel*: phased SuperWASP lightcurve. *Right panel*: periodogram. Plots generated by SuperWASP's HUNTER results interface, which was developed by David Wilson.

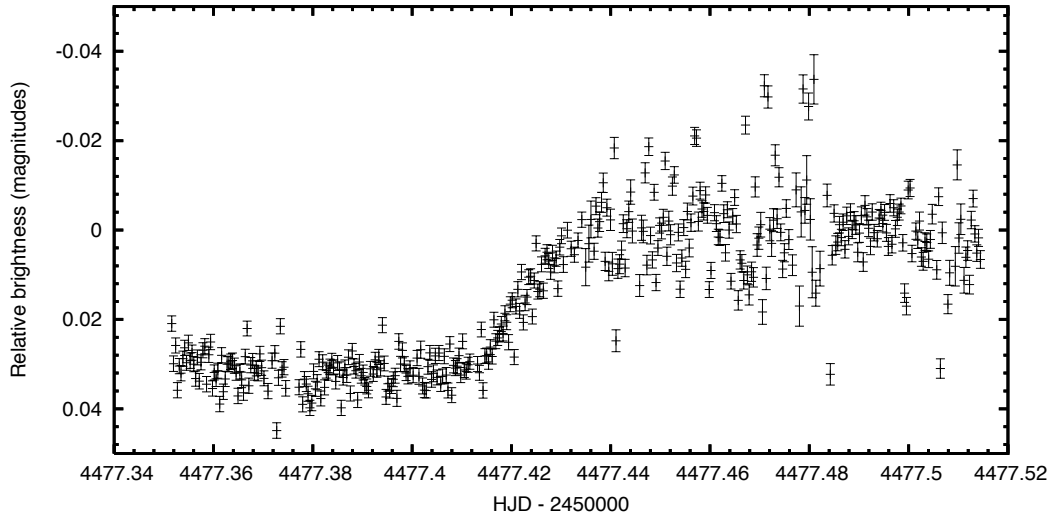

Figure 3.10: Partial transit lightcurve of 1SWASPJ062430.87+261906.0, obtained with the JGT at the University Observatory, St. Andrews on 2008 January 11. The increased scatter in the data after 2454477.44 is due to thin cirrus cloud.

planet.

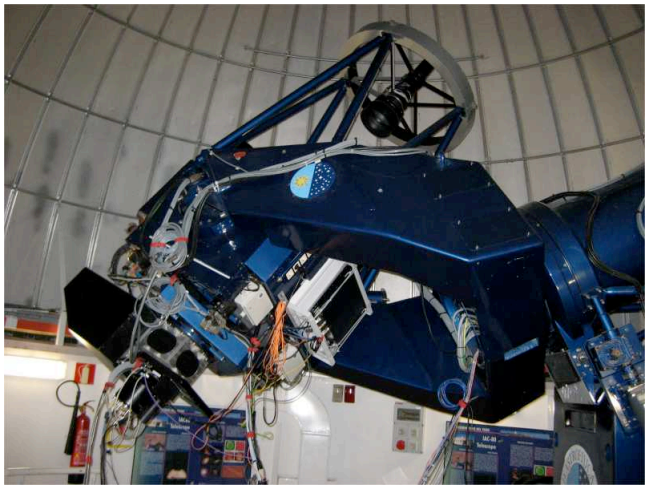

4

A Markov-chain Monte Carlo code to measure transit depth as a function of wavelength

This chapter describes the development of two Markov-chain Monte Carlo (MCMC) codes to fit models to follow-up photometry of transiting exoplanets, with the goal of measuring any variation in transit depth with wavelength. The first code, MCMCFIT, determines the best-fitting parameters to a single transit lightcurve. These parameters are then input as initial parameters to a second code, DEPTHCOM, which fits models to multi-band photometry to determine the transit depth at each of several wavelengths.

4.1 Introduction

Ordinarily, one does not expect the depth of transit caused by an exoplanet to vary with wavelength, indeed if the transit depth of a planetary candidate is observed to vary significantly

Above: The IAC-80 telescope of the Instituto de Astrofísica de Canarias, Observatorio del Teide, Tenerife, Spain. Photograph by the author.

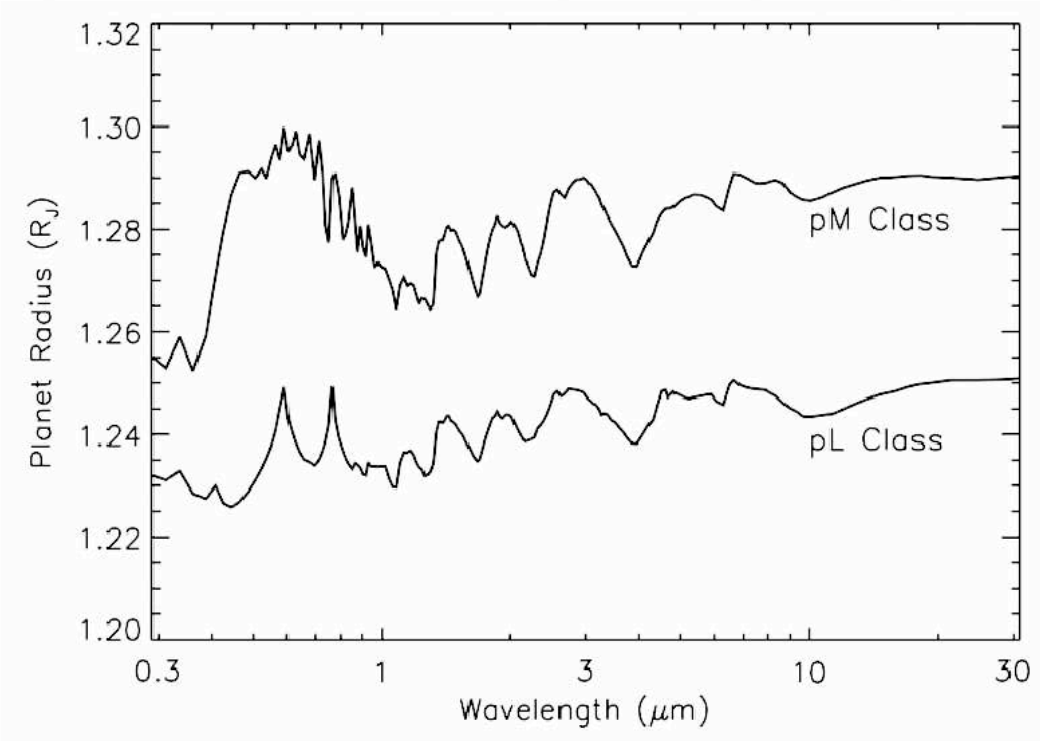

Figure 4.1: The predictions of Fortney et al. (2008) for the radius that one would observe as a function of wavelength for a pL and pM Class planet with a 1 bar radius of 1.20 R_J and $g = 15\text{ms}^{-2}$. Figure taken from Fortney et al. (2008).

with colour, the candidate is likely to be rejected. This is because stellar eclipsing binary systems, which may mimc planetary transits (Chapter 3), may well exhibit transits that vary with wavelength. For example, consider an M-dwarf partially eclipsing a star of earlier spectral type – the eclipse will be deeper at shorter (more blue) wavelengths, since the M-dwarf contributes less blue light than red light to the unresolved system. An opaque, non-radiating planet, however, should block the same fraction of the star's light at all wavelengths, resulting in a constant transit depth.

Recent theoretical work, however, suggests that planetary atmospheres may induce some variation of transit depth with wavelength, albeit small. In a recent theoretical study, Fortney et al. (2008) suggest dividing hot Jupiters into two classes based on their atmospheric chemistry. They name these classes "pM Class" and "pL Class", by analogy to the atmospheres of M- and L-type dwarf stars. The pM Class have hotter atmospheres containing gaseous titanium oxide (TiO) and vanadium oxide (VO) causing opacity. The cooler pL Class by contrast, have their Ti and V largely in solid condensates.

Fortney et al. (2008) performed calculations to determine the effects of each of these

atmospheric types on the apparent transit radius of a typical hot Jupiter planet, the results of which are shown in figure 11 of Fortney et al. (2008), which is reproduced as Fig. 4.1 here. The hotter atmosphere of the pM Class results in a more extended atmosphere and a larger apparent radius, as well as a larger apparent radius across a wide range of optical wavelengths due to opacity caused by the TiO and VO. Although such predictions are at a relatively preliminary stage, it would clearly be of interest to confront them with observational data, and attempt to determine whether two such classes of atmosphere exist. It is for this reason that it was decided to develop a code to fit the depths of transits observed at different wavelengths.

4.2 Methodology

Given a set of data, D, and model parameters, θ, Bayes' theorem states that the posterior distribution of θ is given by

$$P(\theta|D) \propto P(\theta)P(D|\theta) \tag{4.1}$$

where $P(\theta)$ is the prior distribution and $P(D|\theta)$ is the likelihood (see e.g. Gilks et al. 1996). The Markov chain Monte Carlo technique allows an exploration of the joint posterior probability distribution of a number of model parameters. In order to place constraints on a particular parameter, it is necessary to marginalise over the other parameters in the model. The use of MCMC and the Metropolis-Hastings algorithm allows this marginalisation to occur (Gilks et al. 1996; Tegmark et al. 2004).

4.2.1 Metropolis-Hastings algorithm

At the core of both MCMC programs is the Metropolis-Hastings algorithm (Metropolis et al. 1953; Hastings 1970), which determines when a new set of parameters is accepted. Consider the case of a model dependent on just a single parameter, p. In this 1-D example, p, is altered by adding a random number drawn from a Gaussian distribution, to create a new proposal parameter, $p\prime$.

The chi-squared statistic is then calculated for models based on both p and $p\prime$. These values of chi-squared are denoted by χ^2_p and $\chi^2_{p\prime}$ respectively. If the newly-proposed model is a better fit to the data, i.e. if $\chi^2_{p\prime} \leq \chi^2_p$, then the new proposal is accepted, and the cycle is repeated. If, however, the new model is a worse fit to the data ($\chi^2_{p\prime} > \chi^2_p$), the new proposal

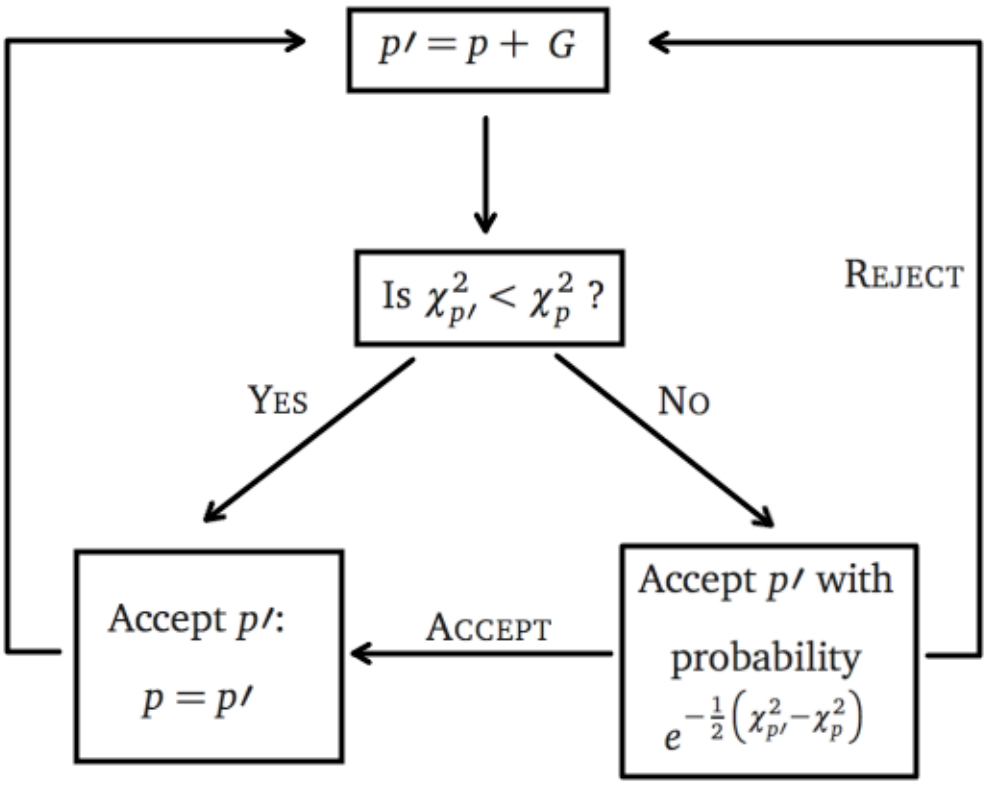

Figure 4.2: Flow chart describing the Metropolis-Hastings decision for a 1-dimensional model determined by the parameter, p. Further explanation is given in the text.

Table 4.1: The six parameters varied in the MCMCFIT code, and their prior distributions.

Parameter	Symbol	Prior
Epoch of mid-transit	t_0	-
Orbital period	P	-
Ratio of squares of planetary and stellar radii $\left(\frac{R_p}{R_*}\right)^2$	Δm	$\Delta m \geq 0$
Duration of transit (first contact to fourth contact)	t_{T}	$t_{\mathrm{T}} \geq 0$
Transit impact parameter	b	$10^{-10} \leq b \leq 1.0$
Stellar mass	$M_\star$	$M_\star > 0$

may still be accepted, but could instead be rejected. The probability that the proposal is accepted is given by $e^{-\frac{1}{2}\left(\chi^2_{p\prime}-\chi^2_p\right)}$. This decision process is illustrated in Fig. 4.2.

This simple 1-D example can be generalised to an n-parameter model, in which each new proposal requires the individual modification of each of the n parameters, in the same way as p was modified to $p\prime$ in the aforementioned 1-D example.

A Markov chain is created by storing the parameters associated with each acceptance of a new parameter-set. When such a step results in a rejection of the new model, the parameters associated with the previously accepted model are saved again. The length of the Markov chain is, therefore, equal to the number of proposal iterations.

A 'burn-in' phase of operation is required in order to allow the chain to reach the parameter space that it will explore. During this phase, the values of the parameters of accepted proposals which comprise the Markov chain are not stored, and thus do not form part of the posterior distribution. Additionally, during burn-in, the size of the jumps made in parameter space are altered so that the region of lowest χ^2 can be found relatively quickly. This is done by altering the properties of the Gaussian distributions from which the random numbers that alter the proposal parameters are drawn. At the end of the burn-in phase (defined as a pre-determined number of proposal steps, e.g. 1000), the properties of the aforementioned Gaussian distributions, and hence also the jump size, are fixed.

4.2.2 The MCMCFIT code

The first code, MCMCFIT, determines the best-fitting parameters which describe a transit lightcurve. The approach adopted is very similar to that of Collier Cameron et al. (2007); the parameters that are fitted for are the six listed in Table 4.1, which are close to being mutually uncorrelated.

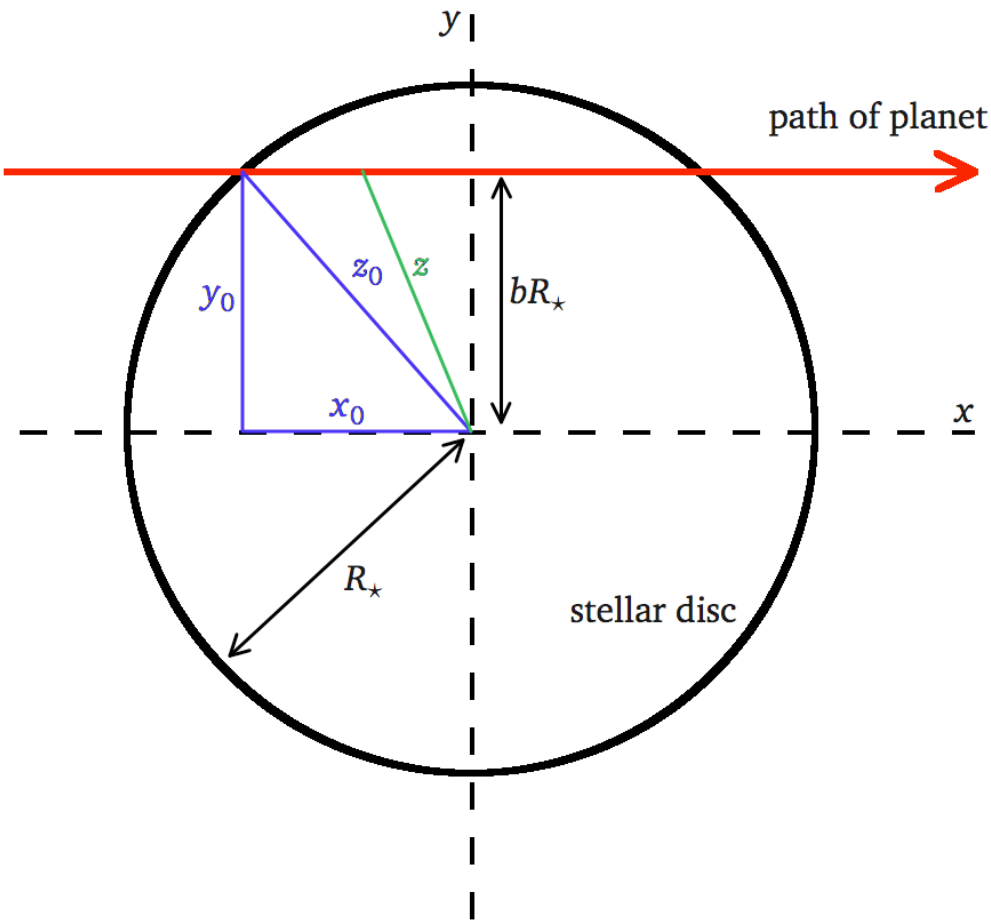

Figure 4.3: Geometry of a planetary transit. The path of the transiting planet across the stellar disc, with impact parameter b, is indicated by the red arrow. The projected distance of the centre of the planet from the centre of the star is z. See text for full description of symbols.

The inputs to the code are (i) the lightcurve(s) used to constrain the parameters – comprising the SuperWASP lightcurve of the object, and optionally a follow-up lightcurve; (ii) the appropriate non-linear quadratic limb-darkening coefficients for the host star, taken from Claret (2000); (iii) the initial values of the parameters listed in Table 4.1, which define the starting point in 6-D parameter space for the MCMC chain; and (iv) the priors ($P(\theta)$), which in this instance are merely the requirement that the values of the parameters retain physical meaning (see Table 4.1 for details of these priors). The initial parameters are those determined by the transit search algorithm HUNTER (Collier Cameron et al., 2006), with $M_\star$ calculated from the $J-H$ colour, using the method described in Appendix B of Collier Cameron et al. (2007).

First, the inherent correlation between the epoch and period is reduced by re-defining the epoch of mid-transit to be the mid-point of the transit that lies closest to the middle of the

duration of the SuperWASP lightcurve. The small-planet approximation of Mandel & Agol (2002) is used to fit a model to the data; the OCCULTSMALL subroutine calculates the relative observed flux for a given value of z, the projected distance between the centres of star and planet (Fig. 4.3). The x and y positions of the planet as it crosses the limb of the star are denoted by x_0 and y_0, which are given by

$$x_0 = R_\star \sqrt{1 - b^2} \tag{4.2}$$

and

$$y_0 = bR_\star \tag{4.3}$$

where b is the impact parameter and $R_\star$ the stellar radius.

The stellar radius can be calculated from the proposal parameters, t_T, P and b, and the semi-major axis of the orbit, a,

$$R_\star = \frac{\pi a t_\mathrm{T}}{P\sqrt{1 - b^2}}. \tag{4.4}$$

The semi-major axis of the planetary orbit is given by Kepler's third law,

$$\frac{a}{\mathrm{au}} = \left(\left[\frac{P}{\mathrm{yr}} \right]^2 \frac{M_\star}{M_\odot} \right)^{\frac{1}{3}} \tag{4.5}$$

where $M_\odot$ is the mass of the sun.

The projected distance of the centres of star and planet at this point, z_0 is given by

$$z_0 = \sqrt{x_0^2 + y_0^2} \tag{4.6}$$

which reduces to $z_0 = R_\star$ if Eqns. 4.2 and 4.3 are substituted into Eqn. 4.6. More generally, the value of z at an arbitrary time can be calculated thus,

$$z = \sqrt{\left(x_0 \left[1 - \frac{2\Delta t}{t_\mathrm{T}} \right] \right)^2 + y_0^2} \tag{4.7}$$

where t_T is the transit duration and Δt is the time since the start of the most recent transit.

The chi-squared statistic is calculated for this model, and an additional term, $\frac{M_\star - M_{\star i}}{\sigma_{M_\star}}$ is added to χ^2 to restrict the stellar mass from varying too far from the original inputted value,

$M_{\star i}$. Here, $\sigma_{M_\star}$ is the standard deviation of previously accepted values of $M_\star$.

A new set of parameters is proposed, as described in Sec. 4.2.1, and the χ^2 of the new model is then compared to the χ^2 of the previous model and the Metropolis-Hastings algorithm is used to decide whether or not to accept the new set of parameters (Fig. 4.2).

A set of parameters corresponding to either the new model (in the case where that model has been accepted) or the previously accepted model (in the case of a rejection) is appended to the end of the stored Markov chain.

During the burn-in phase (see Sec. 4.2.1), the jump size is tuned by altering the Gaussian distributions from which numbers are drawn to create the new proposal parameters. This distribution, for a given parameter, p, is given by

$$G_p = \sigma_p G(0,1) F \tag{4.8}$$

where σ_p is the standard deviation of previously saved values of the parameter p, $G(0,1)$ is a number drawn randomly from a Gaussian distribution of mean zero and variance unity, and F is a scaling factor common to all the parameters. The new value of each parameter, $p\prime$, is given by

$$p\prime = p + G_p \tag{4.9}$$

The σ values are initially held constant (see Table 4.2 for initial values), until 100 proposals have been made. At that point, the standard deviation of the saved values of each parameter is calculated. These σ values are re-calculated after every 100 iterations until the end of burn-in. The scaling factor F is initially set to equal 1.0, and thereafter re-calculated after every 100 proposals during burn-in, according to

$$F\prime = F\frac{n_{acc}}{25}, \text{ or } F\prime = 0.1 \tag{4.10}$$

whichever value is the greater, where $F\prime$ is the new value of the scaling factor, F the previous value, and n_{acc} the number of proposals which were accepted from the last 100 made. F is tuned so that an acceptance rate of approximately 0.25 is achieved, which Tegmark et al.

Table 4.2: Initial standard deviation values for each proposal parameter, used until 100 proposals have been accepted.

Parameter	Symbol	Initial value
Epoch of mid-transit	σ_{t_0}	0.02 d
Orbital period	σ_P	0.02 d
Depth of transit	$\sigma_{\Delta m}$	2 mmag
Duration of transit (first contact to fourth contact)	σ_{t_T}	0.02 d
Transit impact parameter	σ_b	0.1 $R_\star$
Stellar mass	$\sigma_{M_\star}$	0.2 $M_\star$

(2004) suggest is optimal.

At the end of the burn-in phase, the σ values and F are frozen, and remain constant for all subsequent proposals. Also at the end of burn-in, the error bars on the data are rescaled to give a reduced χ^2 of 1.0.

The code is usually run for a total of 10,000 steps or, if fewer than 2000 acceptances have been made, until that condition has been satisfied. The saved proposal which produces the model with the lowest value of χ^2 is selected as the best-fitting model. 1-σ uncertainties are generated for each parameter by selecting values of that parameter from the posterior probability distribution that enclose the 68.2 per cent of points with the lowest χ^2 values (see Fig. 4.4 for an example of this).

4.2.3 The DEPTHCOM code

The second MCMC code, DEPTHCOM, was developed to fit simultaneously transit photometry in several wavelength bands, and to determine whether any variation in transit depth with wavelength is observed, and with what significance. It uses the parameters established by MCMCFIT, namely t_0, P, t_T, b, and $M_\star$, and holds them constant, while fitting for the transit depth in each passband. Although different parameters are varied in this code, the program operates in exactly the same fashion as MCMCFIT (Sec. 4.2.2). From this point onwards, it will be assumed that the program is being used to fit lightcurves from three passbands, specifically the V, R, and I bands, although the code can be modified to fit data from a greater or lesser number of passbands. In this instance, the only parameters that DEPTHCOM fits for are the depths of transit in these three bands, Δm_V, Δm_R, Δm_I.

Table 4.3: The fitted depths of transit and associated 1-σ uncertainties for WASP-3 b, as determined by the DEPTHCOM code.

Passband	Fitted depth of transit	Uncertainty
V	0.00940	$^{+0.000181}_{-0.000181}$
R	0.01023	$^{+0.000195}_{-0.000182}$
I	0.01069	$^{+0.000213}_{-0.000230}$

4.3 Testing: WASP-3 b

Photometry of very high precision, such as that obtained from space, or from large ground-based telescopes such as the VLT (see e.g. Gillon et al. 2009b) will probably be required to probe the predictions of Fortney et al. (2008) (Sec. 4.1). Some testing of the DEPTHCOM code, as a 'proof of concept', however, can be done with lower-precision data, such as that obtained from the IAC-80 telescope (Sec. 3.2.2).

4.3.1 Observations

Transit observations of WASP-3 b were obtained in 3 different passbands, V, R, and I. The V- and I-band lightcurves are those taken with the IAC-80 telescope at the Observatorio del Teide, and already described in Sec. 3.2.2 and displayed in Fig. 3.5. The R-band photometry was carried out by Iain McDonald using the 0.6-m Thornton Reflector of the Keele University Observatory, and is described more fully by Pollacco et al. (2008).

4.3.2 Results

MCMCFIT was first used to calculate the parameters listed in Table 4.1, and then DEPTHCOM used to determine the transit depths of each of the three aforementioned lightcurves. The distribution of Δm_V values produced by DEPTHCOM is shown in the form of a χ^2 vs. Δm_V plot in Fig. 4.4. The resulting transit depths and associated 1-σ uncertainties are displayed in Table 4.3, and plotted against wavelength in Fig. 4.5.

4.3.3 Conclusions

The apparent variation in transit depth (Fig. 4.5) is greater in magnitude than that predicted by Fortney et al. (2008); the difference in depths between V and I corresponds to a change in

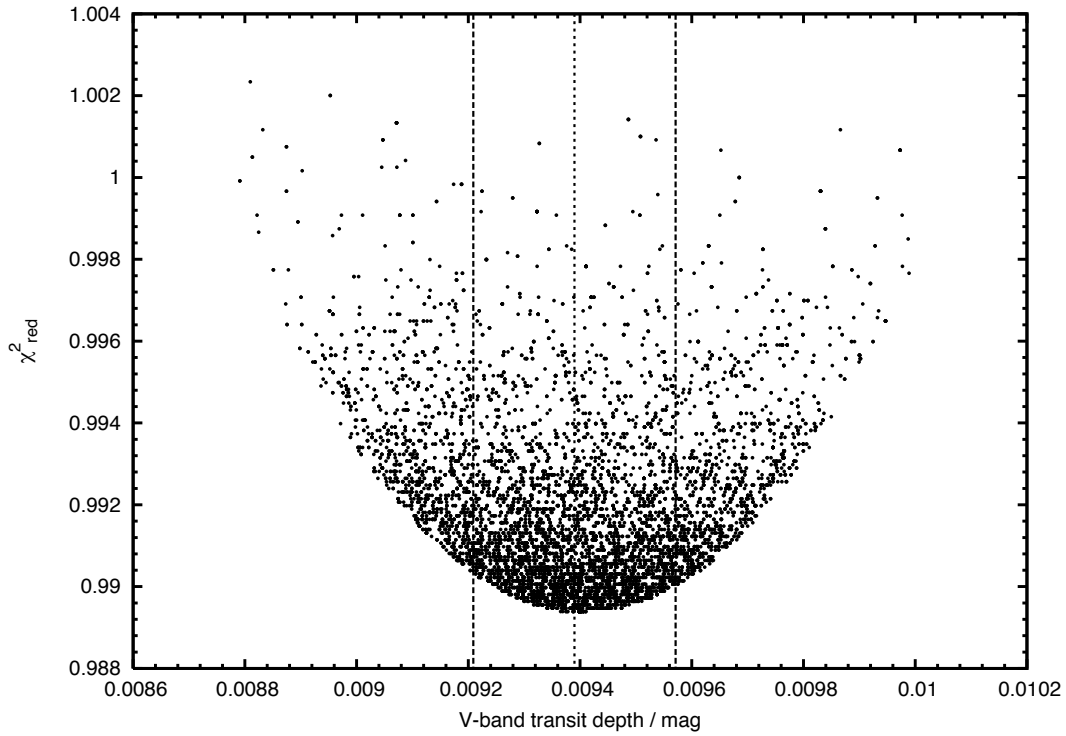

Figure 4.4: The distribution of values of the transit depth in the V-band produced by the DEPTHCOM code. Reduced χ^2 is plotted against Δm_V. The most likely value of Δm_V is indicated by the dotted line, and the 1-σ limits by dashed lines.

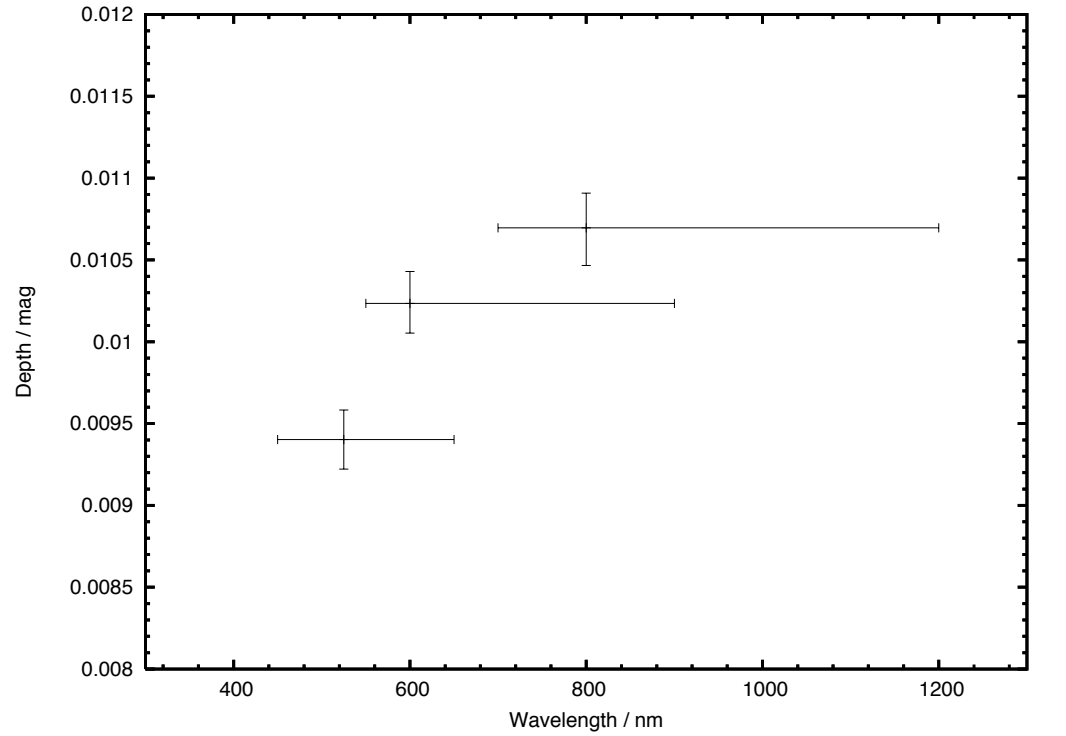

Figure 4.5: Fitted transit depth for WASP-3 b against wavelength. The wavelengths plotted are the peaks of the V, R, and I passbands, and the extent of each band is indicated. The 1-σ uncertainties in the depth are also shown.

planetary radius of about 0.08 R_J. Given the quality of the transit photometry, it is more likely that the changes in depth measured here are caused by systematic errors rather than by any real variation. Furthermore, the improvement in the reduced chi-squared statistic, χ^2_{red} as a result of fitting for different depths rather than a single depth is small ($\chi^2_{red} = 0.989$ compared to $\chi^2_{red} = 1.0997$, with the errors re-scaled by the same amounts in both cases). This provides further confirmation that no real depth variation has been measured. This test using WASP-3 proved useful in developing the DEPTHCOM code, however, and it would be interesting to use it in conjunction with higher-precision photometry in the future.

5

A SuperWASP search for additional transiting planets in 24 known systems

This chapter is based on an article published in *Monthly Notices of the Royal Astronomical Society*:
Smith, A. M. S., Hebb, L., Collier Cameron, A., Anderson, D. R., Lister, T. A., Hellier, C., Pollacco, D., Queloz, D., Skillen, I., and West, R. G., '*A SuperWASP search for additional transiting planets in 24 known systems*', 2009, MNRAS, 398, 1827.

All the work described here was conducted by the author. Some computer codes used in this work were developed by other people, this is stated explicitly in the text.

In this chapter, results are presented from a photometric search for additional transiting planets in 24 systems already known to contain a transiting planet. The transits due to

Above: The WASP-South enclosure (second building from left) at the South African Astronomical Observatory, Sutherland, RSA. Photograph taken from the SuperWASP website - http://www.superwasp.org.

the known planet in each system are modelled and these models are then subtracted from lightcurves obtained with the SuperWASP survey instruments. These residual lightcurves are then searched for evidence of additional periodic transit events. The ability to find such planets is characterised by means of Monte Carlo simulations. Artificially generated transit signals corresponding to planets with a range of sizes and orbital periods are injected into the SuperWASP photometry and the resulting lightcurves searched for planets. As a result, the detection efficiency as a function of both the radius and orbital period of any second planet, is calculated. Additionally, previous evidence of the rotational stellar variability of WASP-10 is confirmed, and the period of rotation refined.

5.1 Introduction

5.1.1 Multiple planet systems

Of the 347 presently known extra-solar planets, 90 are known to reside within multiple planet systems[1]. All of these systems, however, have been discovered by radial velocity measurements alone; none of them were discovered via the transit method, nor have any been later discovered to transit their host stars (see Gregory 2007 for an example of a multiple planet system detected using a Bayesian periodogram on radial velocity data). The study of multiple planet systems enables greater understanding of theories of planet formation and migration, and affords us the opportunity to study planetary dynamics in action, as well as helping us answer fundamental questions such as 'how common is the Solar System?'.

Planets that transit their host stars allow us to measure fundamental properties such as the planetary radius and remove much of the uncertainty on the value of the planetary mass by constraining the orbital inclination angle. This is just as true for multiple-planet systems, and further properties such as dynamical evolution time-scales can be measured for transiting systems (Fabrycky, 2009).

5.1.2 Detecting transiting multiple planet systems

It has been noted that, given that there are now in excess of 50 known transiting planets, there is a good chance that at least one of these systems may harbour additional planets which should be detectable (Fabrycky, 2009). There are three methods for detecting further

[1] *The Extrasolar Planets Encyclopaedia* – http://www.exoplanet.eu, 11th May 2009

planets in known transiting systems (Fabrycky, 2009), namely (i) searching for transit timing variations (TTV) or variations in other transit parameters; (ii) searching for long-term radial velocity trends; and (iii) searching for additional transits.

In a multi-planet system, one planet can have a perturbing effect upon the orbit of a second planet, the effects of which can include small variations in the timings of transits caused by the second planet, such that the transits are no longer spaced periodically (Agol et al. 2005; Holman & Murray 2005). Many searches for further planets have been conducted, and continue to be conducted, using TTV, which has great sensitivity to planets in resonant orbits with the first planet, even if the second planet has an extremely low mass.

It is also possible to infer the presence of additional planets by measuring long-term trends in other transit parameters. For instance, Coughlin et al. (2008) report observed increases in the orbital inclination, transit width and transit depth of Gl 436 b, which may indicate the presence of another planet.

In general, the discovery lightcurves of transiting planets, such as those produced by SuperWASP, are of insufficient quality to measure transit timings and other parameters with the required precision to discover additional planets; predicted timing variations, for instance, are typically on the order of seconds or tens-of-seconds. Additional resources must therefore be expended to obtain high precision lightcurves.

Secondly, known planets continue to be monitored for long-term trends in the radial velocity data, as is common practice with planets discovered by that means alone. Many longer-period additional planets have been found around stars around which a relatively short-period planet has been discovered by radial velocity measurements. Long-term monitoring of RV systems has yielded planets with periods of several years (the longest such period is 14.3 yr). This too, requires a modest expenditure of telescope time in order to obtain radial velocity data points at suitable intervals to detect longer-period planets.

Finally, photometric monitoring of known transiting systems may reveal transits caused by a second planet in the system. The inclination angle of this second planet must be sufficiently close to that of the first planet, that the second planet can be seen to transit its star as well as the first. This method, unlike the other two, does not necessarily require the allocation of further observing resources; instead the data archives of transit surveys can be searched for such transit signals. Such surveys often observe the same fields for several seasons, and

so have a large quantity of data on known transiting systems. In this chapter, results are presented from a search of the data archive of SuperWASP (Wide Angle Search for Planets), one such wide-field transit survey (Pollacco et al., 2006).

5.1.3 Detecting transiting multiple planet systems by transit photometry

Only two of the 58 known (to 2009 March) transiting planets have orbital periods, P, greater than 10 d (these were both detected initially by radial velocity means and were only later discovered to transit); indeed only six transiting planets have periods longer than 5 d. This is largely due to the selection effects present in wide-field surveys: (i) in general, a relatively large number of transits are required to boost the signal-to-noise sufficiently that the transit may be detected in the presence of correlated ('red') noise (Smith et al. 2006; Chapter 2). This requirement for many transits leads to the preferential detection of short-period planets that exhibit frequent transits. (ii) The probability that a given planetary system exhibits transits is inversely proportional to the orbital semi-major axis, a, and so this again causes a bias towards the detection of short period planets.

Any additional transiting planet is likely to orbit with a period greater than the currently known planet. Several factors militate against the usual difficulties in detecting long-period ($P > 5$ d) planets, however. Most significantly, the probability that any second planet will transit should be greatly enhanced by the fact that there is already one transiting planet in the system. This is because the orbits of exoplanets in multiple systems are generally predicted to be close to coplanar, because such systems are believed to form from a flat disc in a similar fashion to the Solar System (e.g. Bouwman et al. 2006). In the Solar System, this results in all planetary orbits being coplanar to within a few degrees.

If co-planarity to within 5 deg is assumed, the probability that the second planet transits is approximately equal to the ratio of the semi-major axes of the inner and outer planets, $a_{\rm in}/a_{\rm out}$ (Fabrycky, 2009). This means, for example, the probability of a planet orbiting a solar analogue with a 10 day period is increased from about 5 per cent to around 45 per cent if an inner transiting planet exists with a period of 3 days.

The above relation for the probability of a second planet transiting is an approximation of the relation given by Koch & Borucki (1996),

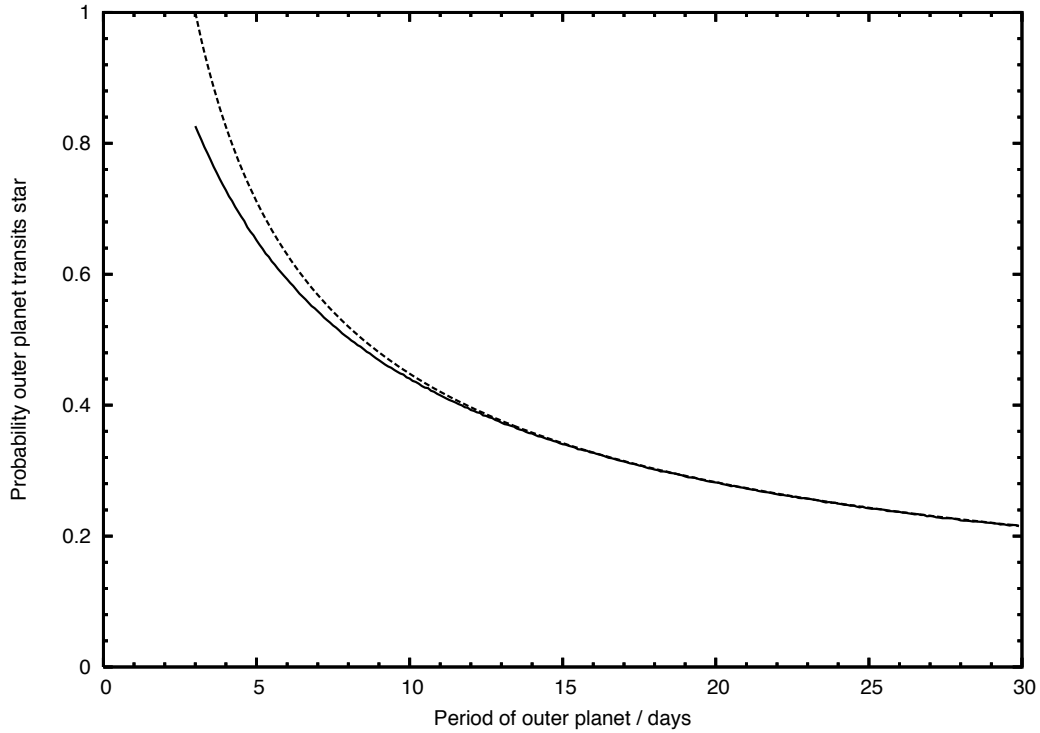

Figure 5.1: The probability that an outer planet transits, given that an inner planet with a period is observed to do so. The solid curve is the result of simulations (described in the text) where an outer planet is placed around a solar analogue which already hosts a transiting planet in a 3 d orbit. The maximum mutual inclination angle is 5 °. The dashed curve is simply the ratio $a_{\rm in}/a_{\rm out}$.

$$P_{21} = \frac{2}{\pi}\sin^{-1}\left(\frac{R_\star}{a\sin\phi_i}\right) \tag{5.1}$$

where ϕ_i is the relative inclination of the orbital planes.

Some simulations were conducted to establish the accuracy of the $a_{\rm in}/a_{\rm out}$ relation. A large number of outer planets were simulated at each of a number of periods, along with an inner planet with $P = 3$ d each orbiting a solar analogue. The orbital inclination angle of the inner planet was drawn from a uniform random distribution, the limits of which were the maximum inclination angle for a transit to occur. The mutual inclination angle was drawn from a uniform random distribution between -5° and +5°. It was then analytically determined whether this hypothetical outer planet would exhibit transits. In Fig. 5.1, the probability of the outer planet transiting is shown as a function of period for both the aforementioned models, and using the ratio of the orbital semi-major axes. The two are in very close agreement, particularly at longer periods, and the difference between them becomes even smaller if a smaller maximum mutual inclination angle is chosen.

Some previous attempts have been made to detect additional transiting planets. Croll et al.

(2007a,b) used the *MOST* (Microvariability and Oscillations of STars) satellite to place upper limits on the presence of additional transiting planets in two systems (HD 209458 and HD 189733) known to harbour a transiting exoplanet. They were able to rule out the presence of additional planets larger than about 0.2 R_J orbiting with periods less than 14 d for HD 209458 and planets larger than about 0.15 R_J orbiting with periods less than 7 d for HD 189733.

This chapter reports results from an extensive search of archival SuperWASP data for additional transits of stars known to host transiting exoplanets. Constraints on the existence of additional transiting planets in such systems are provided.

5.2 Observations

Time-series photometry of 24 stars which host transiting exoplanets was obtained by the SuperWASP instruments, which are wide-field, multi-camera survey instruments described in Sec. 1.3 and in Pollacco et al. (2006).

Fifteen of these planets were observed by SuperWASP-N, located at the Roque de los Muchachos Observatory on La Palma in the Canary Islands, and nine by WASP-South, at the South African Astronomical Observatory in Sutherland. The objects observed are the first eighteen planetary systems discovered by SuperWASP (with the exception of WASP-9, for which follow-up observations are still ongoing) and seven similar systems discovered by other transiting planet surveys and retrospectively detected in SuperWASP data. Details of all these objects are given in Table 5.1. SuperWASP has an extensive archive of data on these objects. Many of them have been monitored for several observing seasons, dating back to 2004 in some cases.

5.3 Search for additional planets

To search the SuperWASP lightcurves for additional transits, first all the existing lightcurves on a particular object are taken from the SuperWASP archive. Several lightcurves may exist if the star has been observed in several seasons and/or with more than one camera.

A systematic re-analysis of each of these systems was performed using all the photometric data either publicly available[2] or held by the WASP consortium. The transits caused by

[2]via the NASA/IPAC/NExScI Star and Exoplanet Database, which is operated by the Jet Propulsion Laboratory, California Institute of Technology, under contract with the National Aeronautics and Space Administration. – http://nsted.ipac.caltech.edu

Table 5.1: Planetary systems searched for additional transiting bodies. The instrument used to observe the system is indicated in column 2: 'N' represents SuperWASP-N on La Palma and 'S' represents WASP-South in South Africa. Columns 3 to 9 are the parameters of the known planet used to subtract the transits of the first planet. They are the orbital period, P, the epoch of mid-transit, t_0, the transit duration, w, the impact parameter, b, the depth of the transit, $(R_\mathrm{p}/R_*)^2$, the stellar density, ρ_*, and the orbital inclination angle, i. Also shown is the number of data points in the lightcurve, n_phot.

Star	Obs.	MCMC fitted parameters used to subtract transits from lightcurves								
		P /d	t_0 /HJD - 2450000	w /d	b	$(R_\mathrm{p}/R_*)^2$	ρ_* / $\rho_\odot$	i/°	n_phot	Discovery reference
WASP-1	N	2.519951	3998.19239	0.1551	0.056	0.01004	0.38709	89.44	13630	Cameron et al. (2007)
WASP-2	N	2.152227	3978.60091	0.0736	0.729	0.01742	1.51264	84.80	7941	Cameron et al. (2007)
WASP-3	N	1.846833	4214.03159	0.1112	0.446	0.01067	0.59680	85.20	5167	Pollacco et al. (2008)
WASP-4	S	1.338232	4387.32776	0.0881	0.055	0.02366	1.29600	89.44	10112	Wilson et al. (2008)
WASP-5	S	1.628428	4373.99598	0.0987	0.314	0.01180	0.88028	86.85	15003	Anderson et al. (2008)
WASP-6	S	3.361010	4593.07139	0.1068	0.204	0.02071	1.70136	88.96	14083	Gillon et al. (2009a)
WASP-7	S	4.954746	4133.65826	0.1555	0.183	0.00538	0.67368	89.02	24547	Hellier et al. (2009b)
WASP-8	S	8.158754	4679.33741	0.1457	0.332	0.01088	1.33364	88.67	16773	Queloz et al. (in prep.)
WASP-10	N	3.092718	4299.09114	0.0944	0.225	0.02501	2.32879	88.94	8546	Christian et al. (2009)
WASP-11	N	3.722464	4473.05587	0.1066	0.065	0.01620	1.89252	89.70	8367	West et al. (2009b) & Bakos et al. (2009)
WASP-12	N	1.091423	4506.79316	0.1168	0.395	0.01390	0.33880	82.24	7233	Hebb et al. (2009)
WASP-13	N	4.352999	4491.61656	0.1647	0.653	0.00886	0.28496	84.92	8661	Skillen et al. (2009)
WASP-14	N	2.243738	4555.56986	0.1145	0.488	0.00979	0.61661	85.06	6817	Joshi et al. (2009)
WASP-15	S	3.752087	4577.19424	0.1527	0.456	0.00953	0.45322	86.65	20442	West et al. (2009a)
WASP-16	S	3.118600	4578.19167	0.0796	0.817	0.01208	1.13688	85.00	12237	Lister et al. (2009)
WASP-17	S	3.735456	4566.65221	0.1777	0.103	0.01534	0.40353	89.21	16084	Anderson et al. (ApJ, submitted)
WASP-18	S	0.941453	4600.88702	0.0895	0.336	0.00871	0.64012	84.47	8593	Hellier et al. (2009a)
HAT-P-4	N	3.056544	4099.10073	0.1707	0.040	0.00616	0.33246	89.63	6546	Kovács et al. (2007)
HAT-P-5	N	2.787765	3871.02389	0.1220	0.019	0.00626	0.83380	89.86	9081	Bakos et al. (2007)
HAT-P-6	N	3.853041	3931.62934	0.1648	0.054	0.00568	0.46098	89.61	20718	Noyes et al. (2008)
HAT-P-7	N	2.204799	4010.72625	0.1544	0.029	0.00258	0.30042	89.65	3647	Pál et al. (2008)
TrES-2	N	2.470625	4011.98837	0.0750	0.864	0.01615	0.95940	83.46	6268	O'Donovan et al. (2006a)
TrES-4	N	3.553964	4063.88015	0.1218	0.434	0.00769	0.84448	87.31	13790	Mandushev et al. (2007)
XO-4	N	4.123971	4477.65872	0.1488	0.050	0.00680	0.68468	89.70	2589	McCullough et al. (2008)

the known planet were modelled using the Markov-chain Monte Carlo (MCMC) technique described by Collier Cameron et al. (2007), which uses the analytic model of Mandel & Agol (2002) (see Table 5.1 for details of the parameters fitted). The resulting fitted parameters are within the joint error bars of the best published parameters. The modelled transits were then subtracted from the lightcurves, and the resulting residual lightcurves concatenated into a single residual lightcurve for each object.

Each of these residual lightcurves is searched using HUNT1STAR, a modified version of the adapted Box Least-Squares (BLS) algorithm used for routine SuperWASP transit hunting (Collier Cameron et al. 2006; Kovács et al. 2002), which was developed by Andrew Cameron and Leslie Hebb. The HUNT1STAR routine searches the lightcurve of a single object for transits, and it is able to handle large quantities of photometric data spanning multiple seasons and cameras, with a finely-sampled period grid.

The lightcurves of a total of 24 transiting planet host stars (see Table 5.1 for the details of these objects) were searched for additional transits with periods of between 5 and 25 days using HUNT1STAR. This lower limit of 5 d was chosen because, with the exception of WASP-8 b with a period of 8.16 d, all of the original planets have periods between 0.9 and 5.0 d, and so have been searched at sub-5 d periods previously. The upper limit of 25 d was chosen after consideration of the length of the observing baselines and because for this period, the orbital inclination angle, i, must be greater than about 88° in order for transits to be exhibited by a Jupiter-sized planet (Fig. 5.2). The probability of such a planet transiting is around 2 – 3 per cent assuming nothing about the system, and about 25 per cent if co-planarity to within 5 degrees with a $P = 3$ d planet is assumed.

A periodogram is produced for each object, and the parameters of the five strongest peaks in the periodogram are refined. The resulting candidates are loosely filtered according to the criteria usually used for SuperWASP planet hunting (Collier Cameron et al., 2006). These criteria are (i) At least two transits must be detected; (ii) the reduced χ^2 of the model must be less than 2.5; (iii) the phase-folded lightcurve must not consist of a high proportion of gaps; and (iv) the signal-to-red-noise ratio (the $S_{\rm red}$ statistic defined by Collier Cameron et al. (2006)) must be -5 or less (the convention here is that negative values indicate transits, whereas positive values indicate brightening events). Stricter filtering is not applied, since there are only a small number of objects, so the risk of false positives is small.

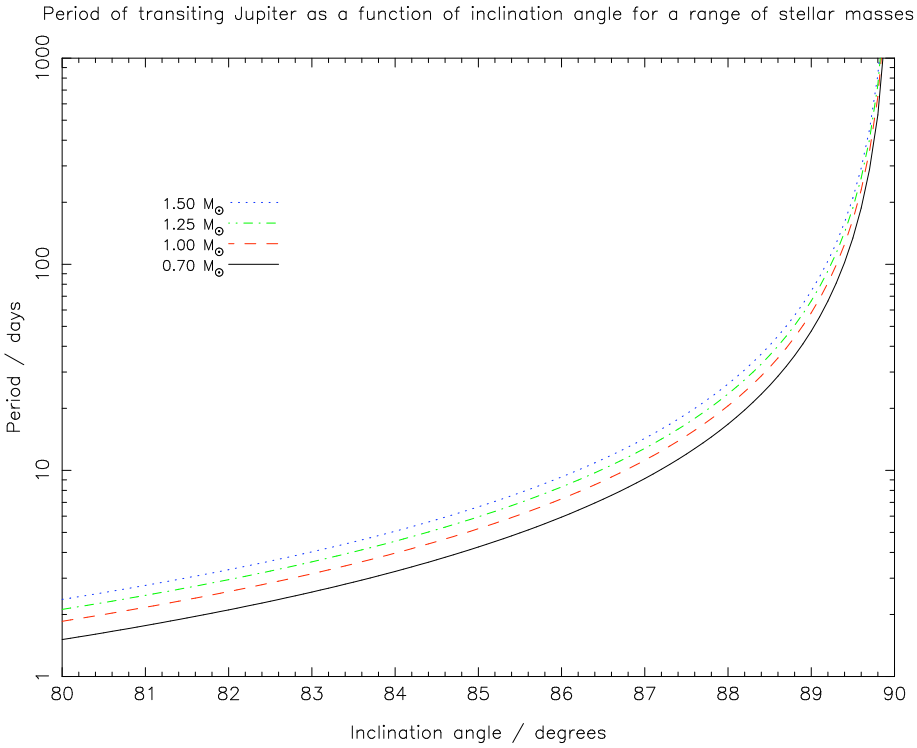

Figure 5.2: Plot indicating the maximum period for a planet to exhibit transits, as a function of orbital inclination angle for a range of stellar masses. The host star is assumed to be on the main sequence and the planet is assumed to be Jupiter-sized.

5.4 Results of search for additional planets

Of the five best peaks for each of the 24 planets (120 peaks in total), 75 pass the criteria outlined in Sec. 5.3, but our initial rejection criteria lean strongly towards retaining candidates.

As a small number of objects are being dealt with, I choose not to apply further cuts on, for example signal-to-noise, but instead visually inspect all 24 periodograms and all 120 phase-folded lightcurves. The periodograms produced for each of the 24 stars were inspected for any strong peaks indicative of a genuine transit, and the phase-folded lightcurves were checked for transit-like signals. Most of the objects do not display any noteworthy periodogram peaks (Fig. 5.3). For comparison, Fig. 5.4 is a periodogram typical of a genuine transiting planet. None of the phase-folded lightcurves were observed to display any transit-like signal.

Five phase-folded lightcurves were also plotted for each object, corresponding to each of the five strongest peaks in the periodogram. These were inspected for signs of a transit at phase 0, but no such signals were observed, even in the handful of objects that exhibit at least one reasonably strong periodogram peak.

5.4.1 WASP-10

Although a strongish peak at about 12 d is observed in the periodogram for WASP-10 (Fig. 5.5), no transit is seen in the corresponding phase-folded lightcurve. This peak is less well-defined than the typical peak produced by planetary transits (Fig. 5.4). Instead, this peak is attributed to stellar rotation, the period, $P_{\rm rot}$, of which is known to be about 12 d (Christian et al., 2009). The stellar rotation hypothesis is confirmed by fitting a sine curve of the form $\delta + A\sin(\omega t + \theta)$, where $\omega = 2\pi/P_{\rm rot}$ to the data (Fig. 5.6), using code written by Leslie Hebb. The best-fitting parameters for data taken in SuperWASP-N's 2004 and 2006 observing seasons are given in Table 5.2. The same period of rotation (11.95 d) is found in both seasons of data, but both the phase of rotation and the amplitude of the variability differ between the two seasons. The auto-correlation function (Edelson & Krolik, 1988) of the data is also computed, using a code developed by Andrew Cameron; the period determined by this method is 11.84 d.

Using a generalised Lomb-Scargle periodogram (e.g. Press et al. 1992), as described in Zechmeister & Kürster (2009) and implemented in code developed by Andrew Cameron, I am able to calculate the false alarm probability for the signal detected by sine fitting. Despite our

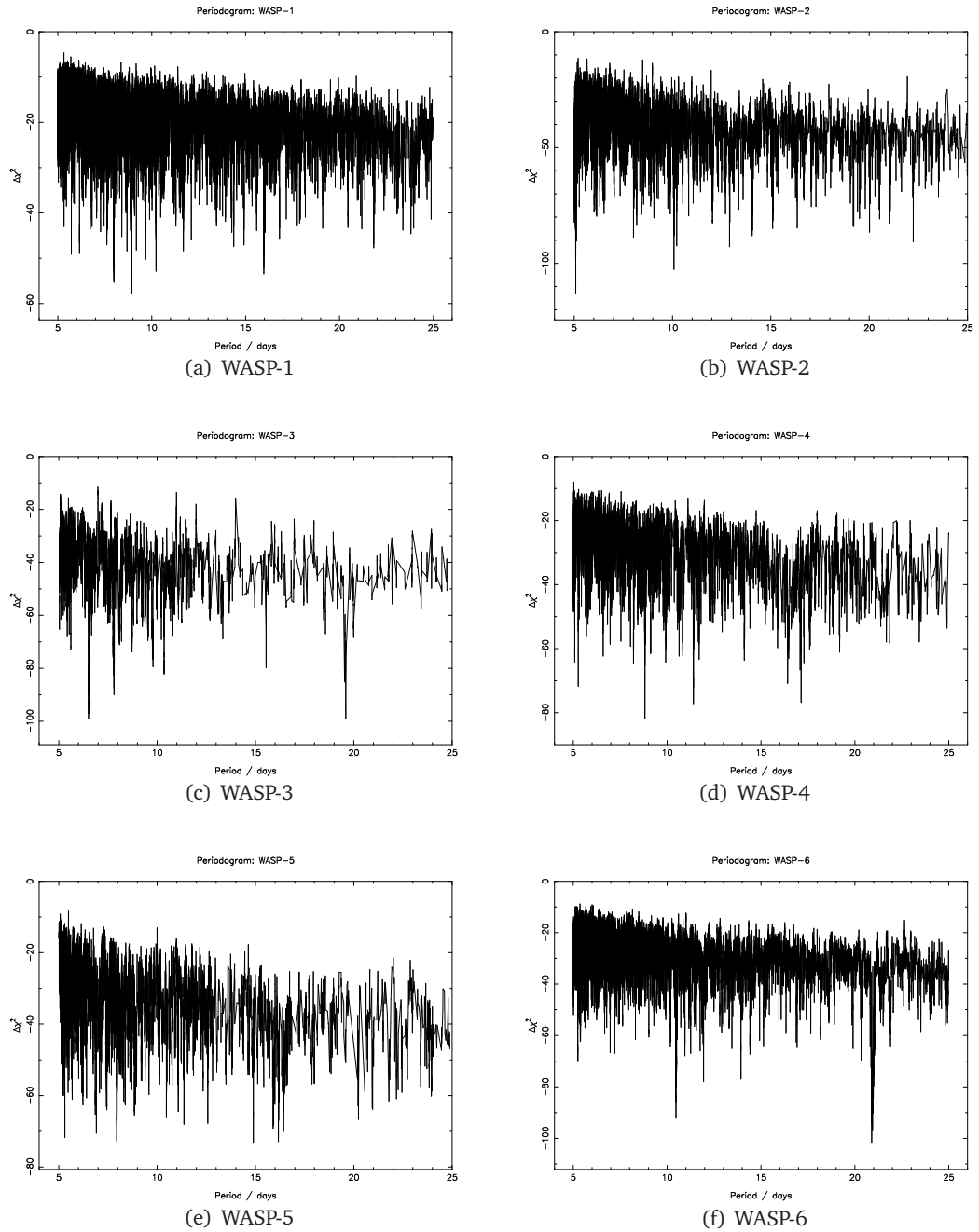

(a) WASP-1 (b) WASP-2

(c) WASP-3 (d) WASP-4

(e) WASP-5 (f) WASP-6

Figure 5.3: (continued on next page)

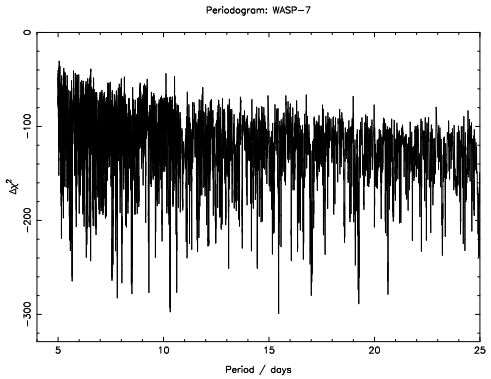

(g) WASP-7

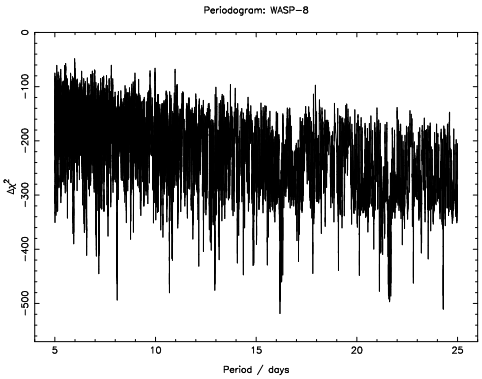

(h) WASP-8

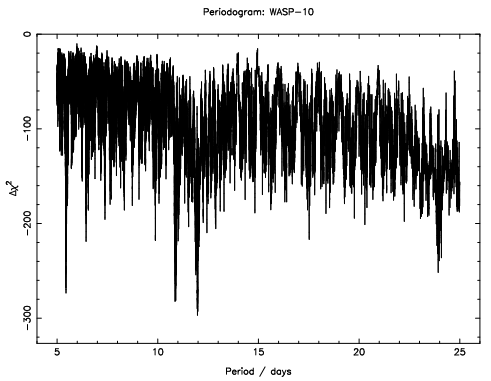

(i) WASP-10

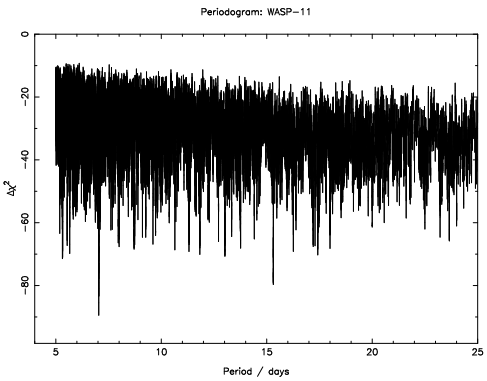

(j) WASP-11

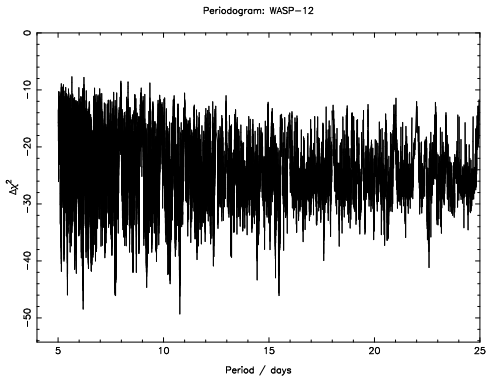

(k) WASP-12

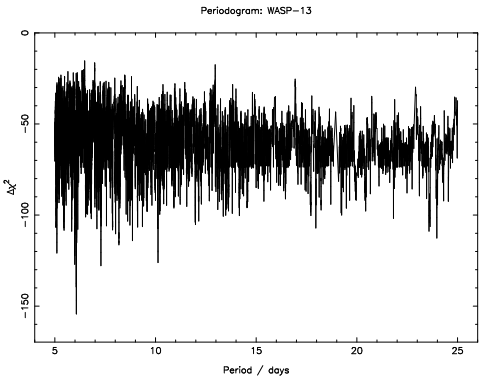

(l) WASP-13

Figure 5.3: (continued on next page)

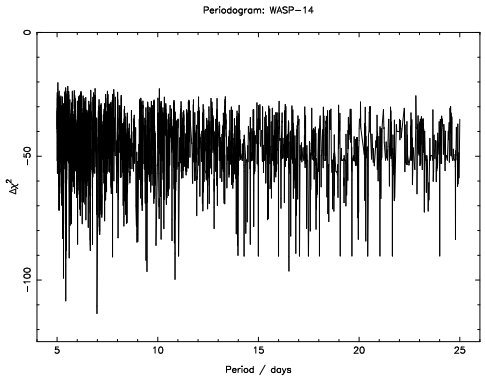

(m) WASP-14

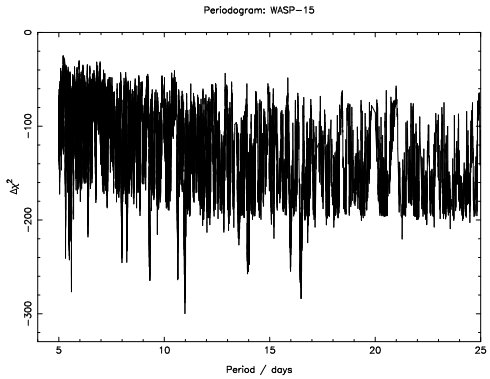

(n) WASP-15

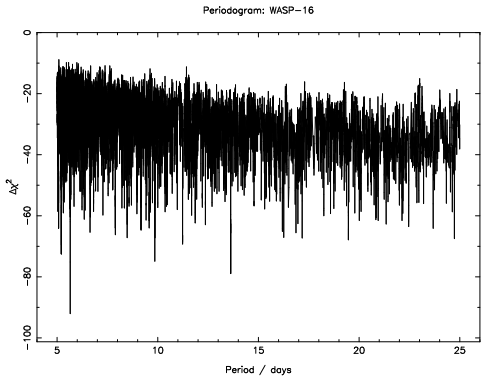

(o) WASP-16

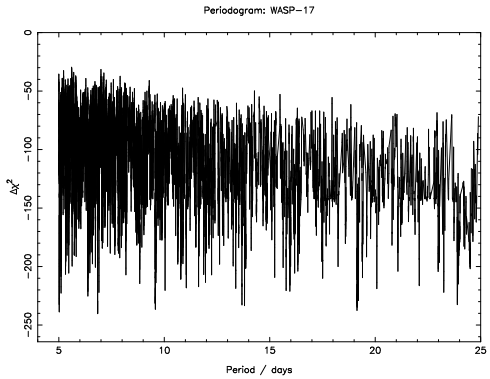

(p) WASP-17

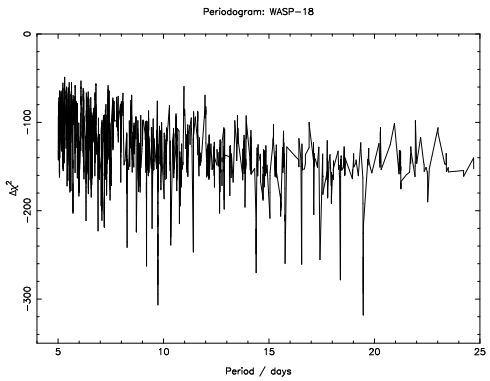

(q) WASP-18

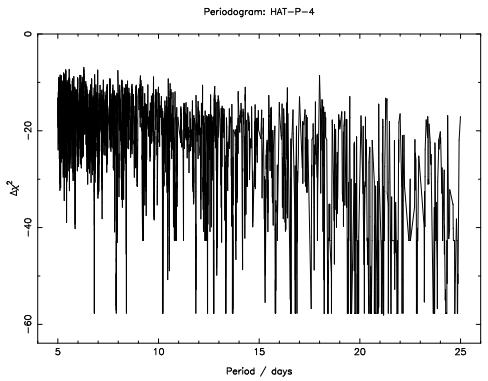

(r) HAT-P-4

Figure 5.3: (continued on next page)

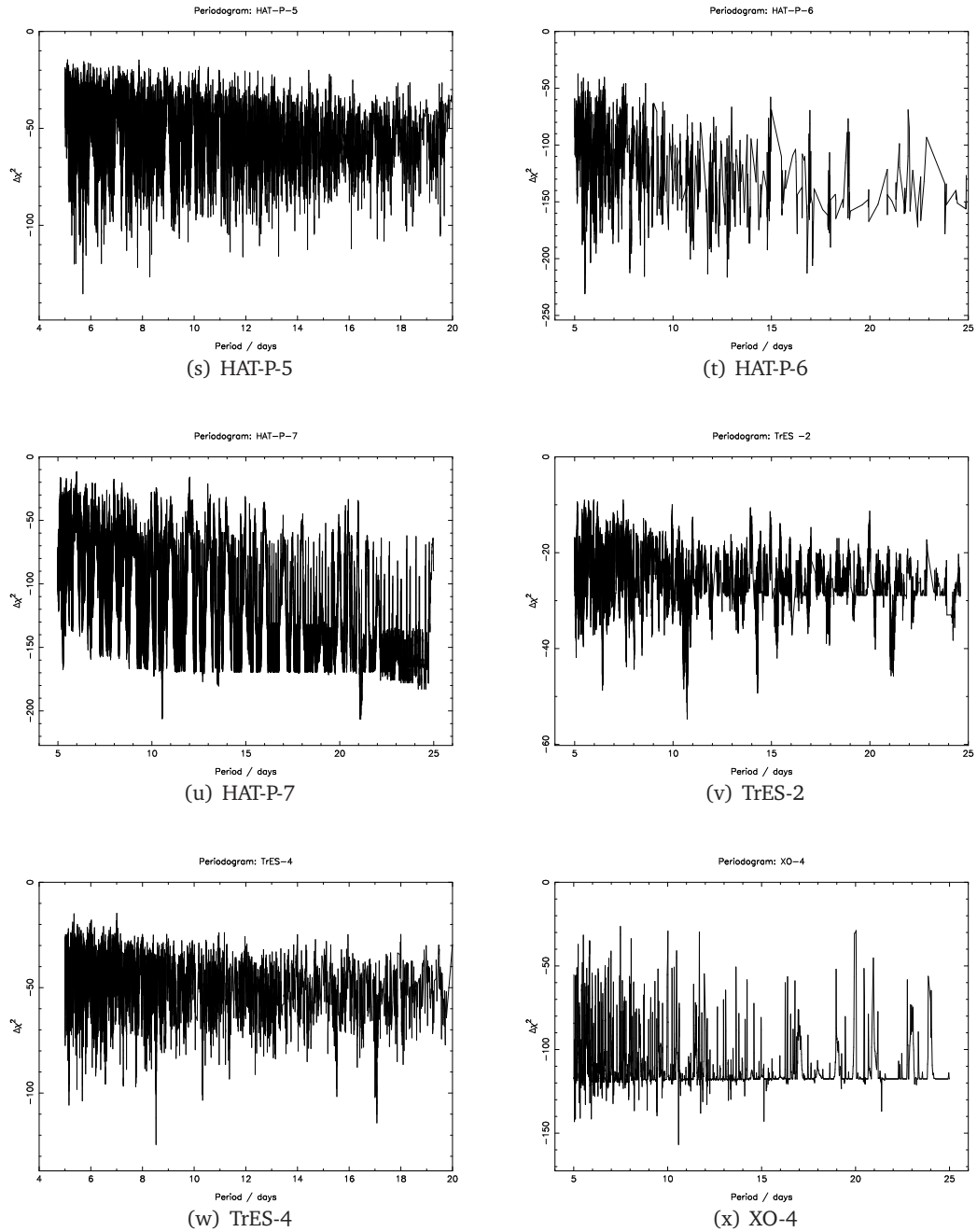

(s) HAT-P-5 (t) HAT-P-6

(u) HAT-P-7 (v) TrES-2

(w) TrES-4 (x) XO-4

Figure 5.3: Periodograms produced by HUNT1STAR for each of the 24 systems searched. Positive values of $\Delta\chi^2$, which correspond to brightening events ('anti-transits') are not plotted for clarity. This results in some periodograms (e.g. that in panel (t)) appearing somewhat 'gappy' in nature.

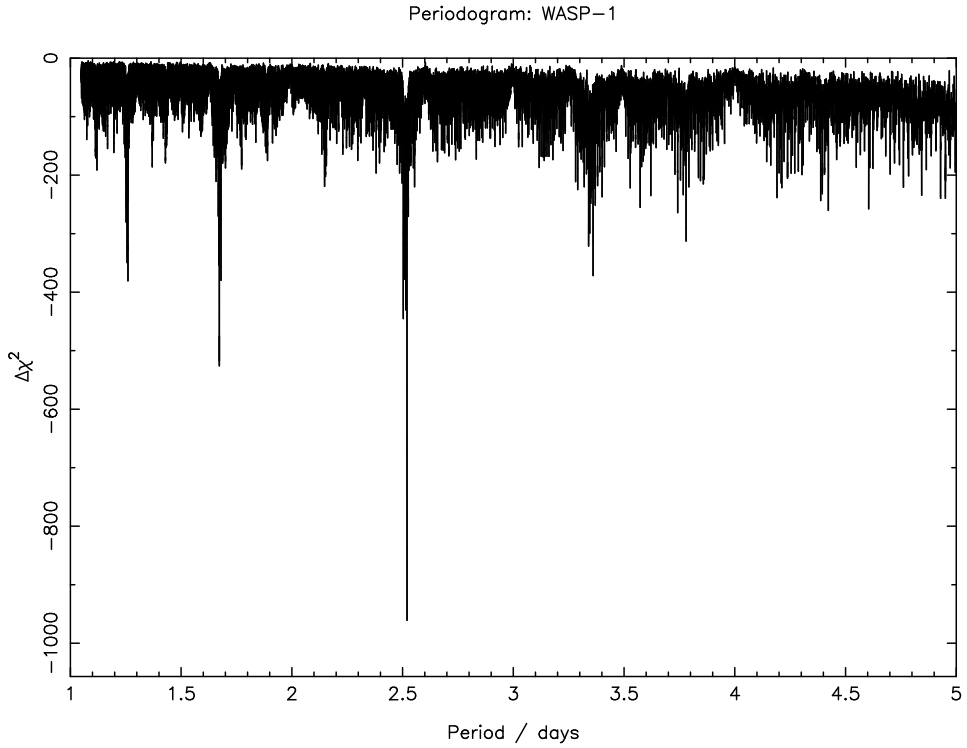

Figure 5.4: Periodogram output of HUNT1STAR for the unadulterated SuperWASP lightcurve of WASP-1. This is typical of the periodogram indicating the presence of a transiting planet, in this case WASP-1 b, which orbits with a period of about 2.52 d.

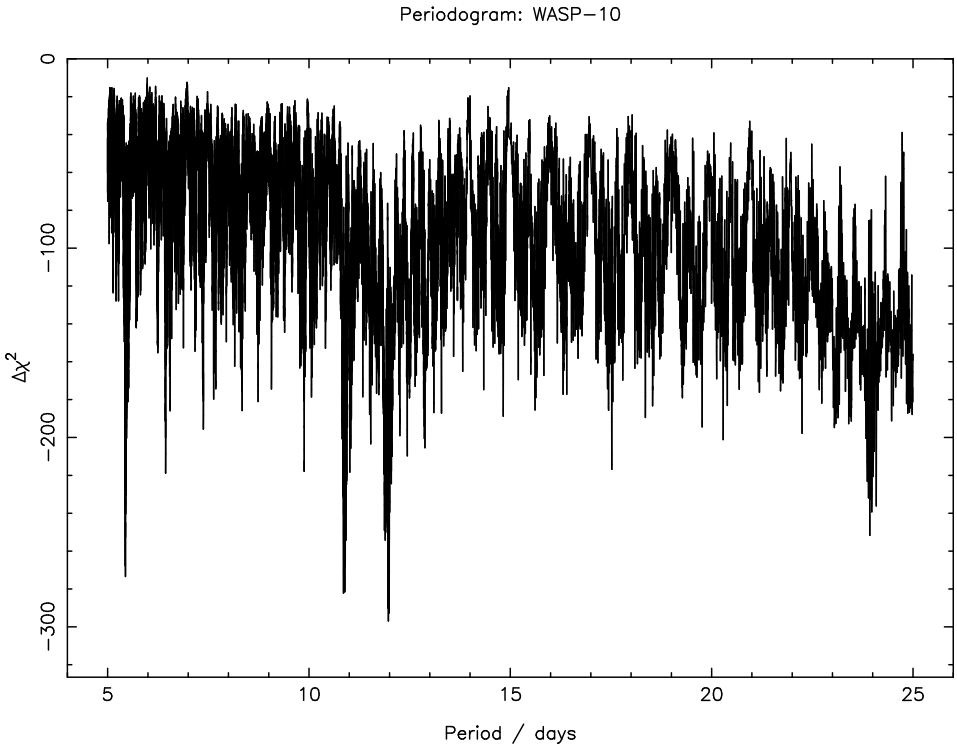

Figure 5.5: Periodogram output of HUNT1STAR for WASP-10. The strong peak observed at about 12 d is caused by stellar rotation with that period.

Table 5.2: Best fitting parameters of a sine curve fitted to the lightcurve of WASP-10. The parameters are described in the text.

	δ/mmag	A/mmag	$P_{\rm rot}$/d	θ/rad
2004 data	0.3	10.1	11.949984	-0.6351
2006 data	0.8	6.3	11.946772	1.0950

lightcurve consisting of 8546 points, because of red noise the effective number of independent data points, $n_{\rm eff}$, is significantly smaller. To calculate $n_{\rm eff}$, the individual nights of data are shuffled, destroying the rotation signal, but maintaining the red noise. By assuming the highest peak in the resulting periodogram has a probability of 0.5, I calculate $n_{\rm eff} = 949$. The number of independent frequencies is calculated to be 1135, according to the approximation of Cumming (2004). Using these values, and equation 24 of Zechmeister & Kürster (2009), the false alarm probability is calculated to be 3.8×10^{-13}.

This extremely low probability confirms the reality of this variation, as does the fact that very similar periods were detected in different seasons of data, and with different methods. Taking the mean of all the periods detected, it is concluded that the star rotates with $P_{\rm rot} = 11.91 \pm 0.05$. This variability is likely to be caused by starspots; such variability is not unusual amongst K-dwarfs.

5.5 Monte Carlo simulations

In conclusion, none of the 24 lightcurves that were analysed show any evidence for further transiting planets. Although no additional planets were detected in Sec. 5.4, it is a useful exercise to quantify our ability to detect such planets, and hence to determine upper limits to the sizes and orbits of planets that have been ruled out. To do this, I test the ability to detect planetary transits with various parameters, through the use of Monte Carlo simulations.

5.5.1 Generation of artificial lightcurves

The two parameters that most affect the ability of a survey such as SuperWASP to detect a planet are the size of the planet and the period of its orbit. It was therefore chosen to determine our ability to detect additional planets as a function of these two parameters, following an approach similar to that used by the *MOST* team to place upper limits on the presence of additional companions in the HD 209458 and HD 189733 systems (Croll et al. 2007a; Croll et al. 2007b).

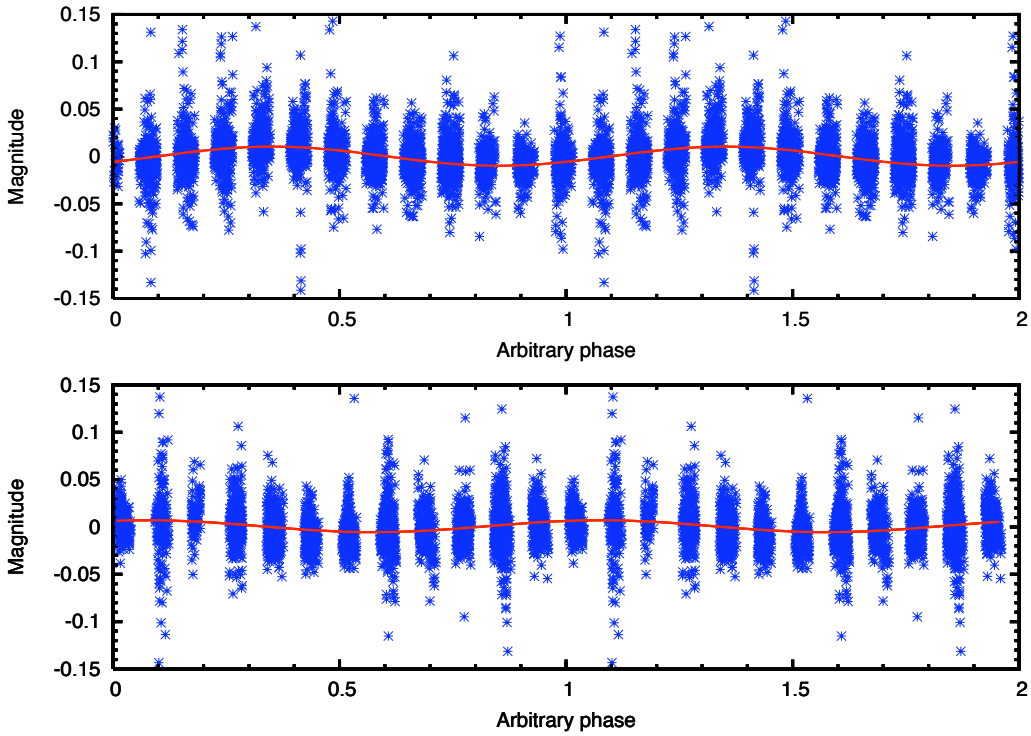

Figure 5.6: Stellar rotation of WASP-10. The 2004 data are phased on a period of 11.949984 d *(upper panel)* and the 2006 data on a period of 11.946772 d *(lower panel)*. Over-plotted in each case is the best-fitting model of the form $\delta + A\sin(\omega t + \theta)$; the values of δ, A and θ are given in Table 5.2.

The residual lightcurves described in section 5.3 are taken, and artificial transits are injected into them, using the small planet approximation of Mandel & Agol (2002). The inputs to the Mandel & Agol (2002) model are the stellar mass, stellar radius, effective stellar temperature ($T_{\rm eff}$), stellar limb-darkening parameters and the planet radius and orbital inclination angle. Values of M_*, R_*, and $T_{\rm eff}$ are taken from the *Extrasolar Planets Encyclopaedia*[3], the non-linear limb-darkening coefficients of Claret (2000) are used, and an orbital inclination angle of 89° is adopted. Model planetary transits are injected at a range of 15 different orbital periods and 10 different planetary radii, giving a grid of 150 models (see Table 5.3 for all values of P and $R_{\rm p}$). One hundred different lightcurves are created for each of these points in $P - R_{\rm p}$ space, each with a randomly generated epoch of mid-transit, t_0.

5.5.2 Searching for injected transits

Each of the 15,000 lightcurves generated for each object is searched for transits by HUNT1STAR, in exactly the same way as were the real data (Sec. 5.3). The detection efficiency for a planet of a given size and orbital period is determined by the fraction of transits recovered for planets

[3]http://www.exoplanet.eu

Table 5.3: Model planet parameters used in simulations. Ten different planetary radii and fifteen periods give a total of 150 combinations.

Periods used / d:							
5.100	6.529	7.957	9.386	10.814	12.243	13.671	15.100
16.529	17.957	19.386	20.814	22.243	23.671	25.100	
Radii used / R_J :							
0.40	0.55	0.70	0.85	1.00			
1.15	1.30	1.45	1.60	1.75			

of those characteristics.

Since searching a single lightcurve of the typical size and duration used here takes around 20 minutes using HUNT1STAR on a 2.2 GHz processor with 2 GB of RAM, the lightcurves are distributed to a number of similar machines[4], making use of otherwise idle computing resources. The time taken to search the 15,000 lightcurves associated with one star is reduced from several hundred days to of order one week.

Whilst the periodograms and five best lightcurves of each of the 24 planets were inspected visually when searching the real data (Sec. 5.4), this is clearly an unfeasible proposition for 15,000 lightcurves per object. Instead, for lightcurves identified as candidates by HUNT1STAR, it is required that the injected period, or an alias thereof, *and* the injected epoch of mid-transit are successfully recovered in at least one of the five best periodogram peaks. To do this, I define the statistic,

$$\eta = \frac{|P_{\rm meas} - P_{\rm inj}|}{P_{\rm inj}}, \tag{5.2}$$

where $P_{\rm meas}$ and $P_{\rm inj}$ are the orbital periods measured by HUNT1STAR, and injected into the lightcurves, respectively. It is then required that $\eta < 0.001$ (corresponding to a detection at the injected period), or $0.4995 < \eta < 0.5005$ or $-0.0005 < \eta^* < 0.0005$, where $\eta^* = nint(\eta) - \eta$ (corresponding to detections at an alias of the injected period). These thresholds were designed to encapsulate clearly-defined populations of objects clustered around $\eta = 0$, $\eta = 0.5$ and $\eta = 1, 2, ...$ These populations are clearly visible when η is plotted against the signal-to-red noise, $\sigma_{\rm r}$, for instance. This is done in Fig. 5.7(a) for all injected transits which are regarded as candidates by HUNT1STAR.

Furthermore, it is required that $\Delta t_0 \leq 0.10$ d, where $\Delta t_0 = |t_{0inj} - t_{0meas}|$, and t_{0inj} and t_{0meas} are the injected and measured epochs of mid-transit, respectively. This limit of 0.10 d

[4]Using software from the Condor Project (http://www.condorproject.org)

was determined by plotting Δt_0 against t_{0inj} for all those objects which survived the cuts on η outlined above (Fig. 5.7(b)).

Periodograms and phase-folded lightcurves for several of the injected transits detected in this manner were inspected in the same fashion as the real data (Sec. 5.3), in order to ensure that these objects could have been detected without prior knowledge of the orbital period. The periodogram and recovered lightcurve of one such injected transit is shown in Fig. 5.8.

5.5.3 Results of simulations

WASP-1

The results of our simulations of extra planets in the WASP-1 system are presented in a series of 2 dimensional cuts through the parameter space (Figs. 5.9 & 5.10). Fig. 5.9 shows detection efficiency plotted against the radius of the simulated additional planets for a variety of orbital periods, whereas in Fig. 5.10, detection efficiency is shown as a function of orbital period for a range of orbital periods.

The full dataset is shown as a contour map in Fig. 5.11(a), although the results from the models with periods of 7.957 and 17.957 d are excluded as they are very close to an integer number of days. The sharp drops in detection efficiency observed at these periods (Fig. 5.10) are manifestations of the well-known 1 d alias phenomenon, which can cause either a sharp reduction or sharp increase in detection ability at periods which are almost exactly an integer number of days (e.g. Smith et al. 2006; Sec. 2.6.3).

Further modelling of WASP-1 with an additional planet of Jupiter radius was conducted with greater period resolution (periods were evenly sampled at intervals of 0.2 d) than the other simulations. The results of these simulations reveal the familiar pattern of lower than normal detection ability at short-integer periods and higher than normal detection at longer-integer periods (Fig. 5.12).

Other systems

Similar simulations were conducted for several of the 24 systems which were searched for additional transits in Sec. 5.3. Contour plots were also produced for these systems (Fig. 5.11). Our ability to detect additional planets in these other systems is very similar to that for WASP-1; there are variations in detection efficiency, but this correlates with the length of the

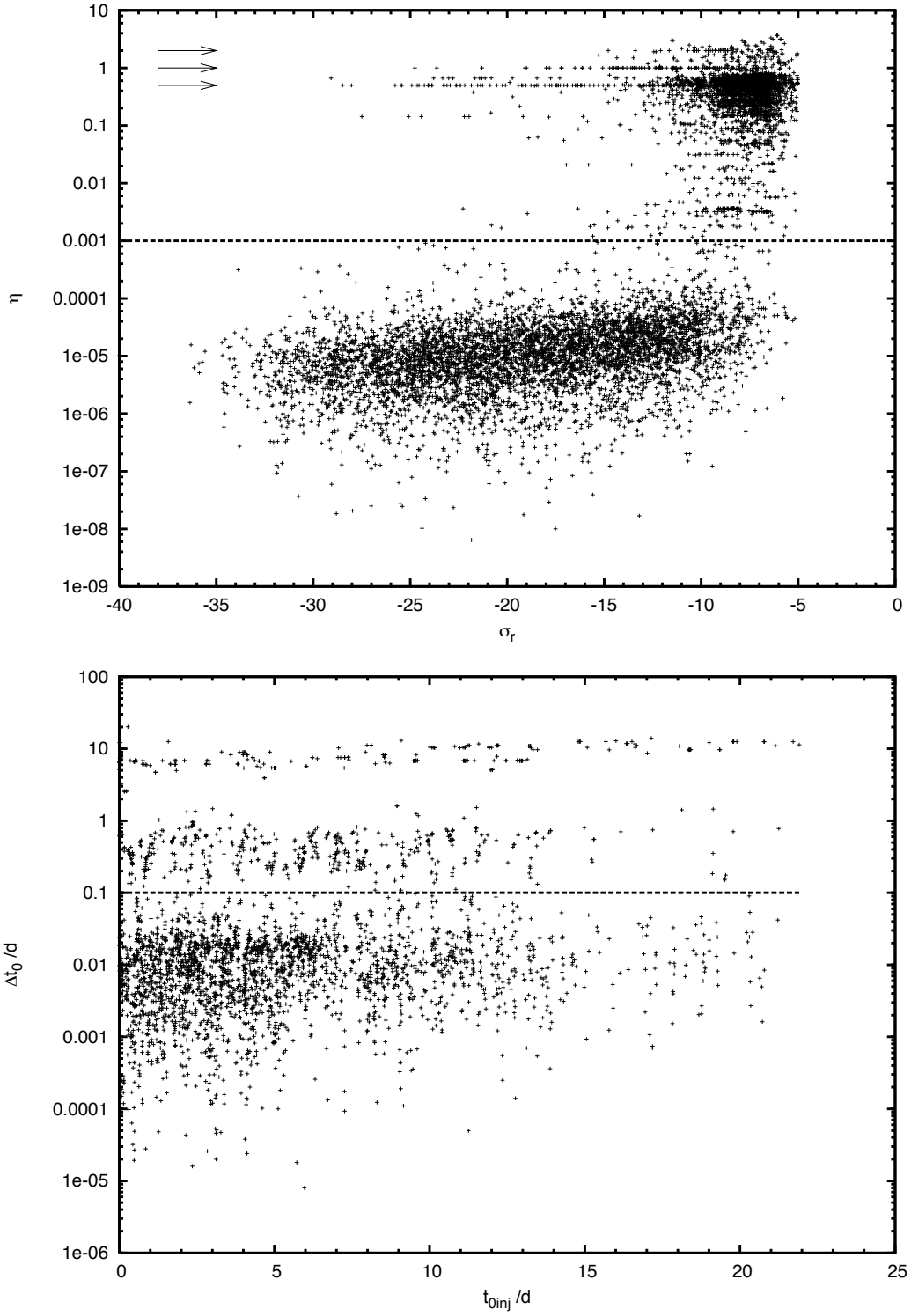

Figure 5.7: Detection criteria for simulated transits. *Upper panel*: Period. η (see text for definition) against the signal-to-red-noise, σ_r for modelled lightcurves regarded as candidates by HUNT1STAR. The dotted line is the $\eta < 0.001$ threshold used to define candidates detected at the correct period. Clusters of detections with $\eta = 0.5, \eta = 1.0$ *and* $\eta = 2.0$ corresponding to detections at aliases of the injected period are indicated by arrows. *Lower panel*: Epoch of mid-transit. Difference between the injected and measured epochs of mid-transit against the injected epoch of mid-transit for the simulations of WASP-2. The adopted threshold of 0.10 d is indicated by the dotted line.

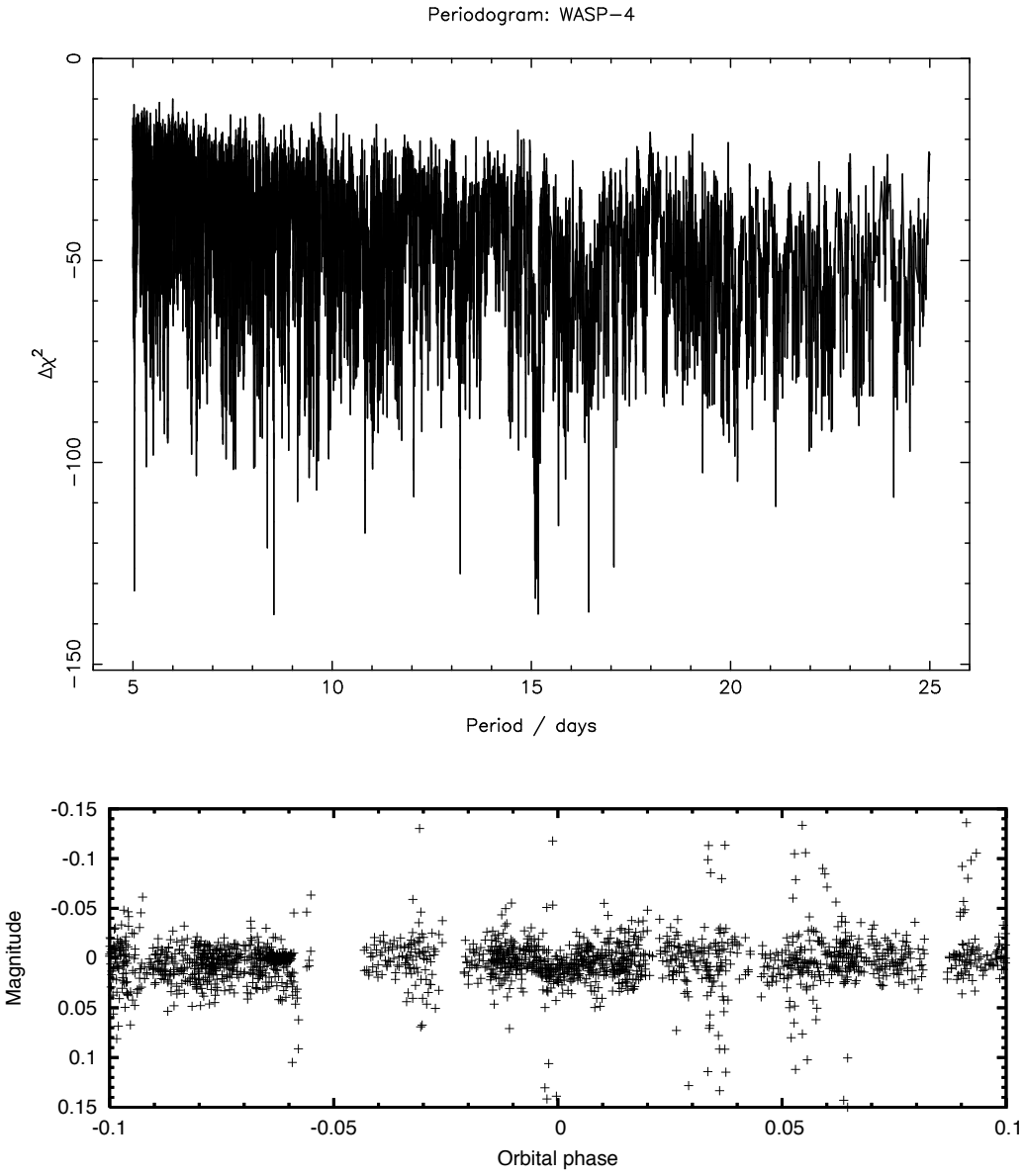

Figure 5.8: An example of an artificial transit which is successfully recovered in our simulations. Shown are the HUNT1STAR results from transits corresponding to a planet with $P = 15.100$ d and $R_p = 0.85R_J$, which were injected into the WASP-4 lightcurve. The planet is detected with $P = 15.10138$ d in the strongest peak of the periodogram *(upper panel)*. The lightcurve, folded on the recovered period using the recovered epoch of mid-transit, exhibits a clear transit at phase = 0 *(lower panel)*.

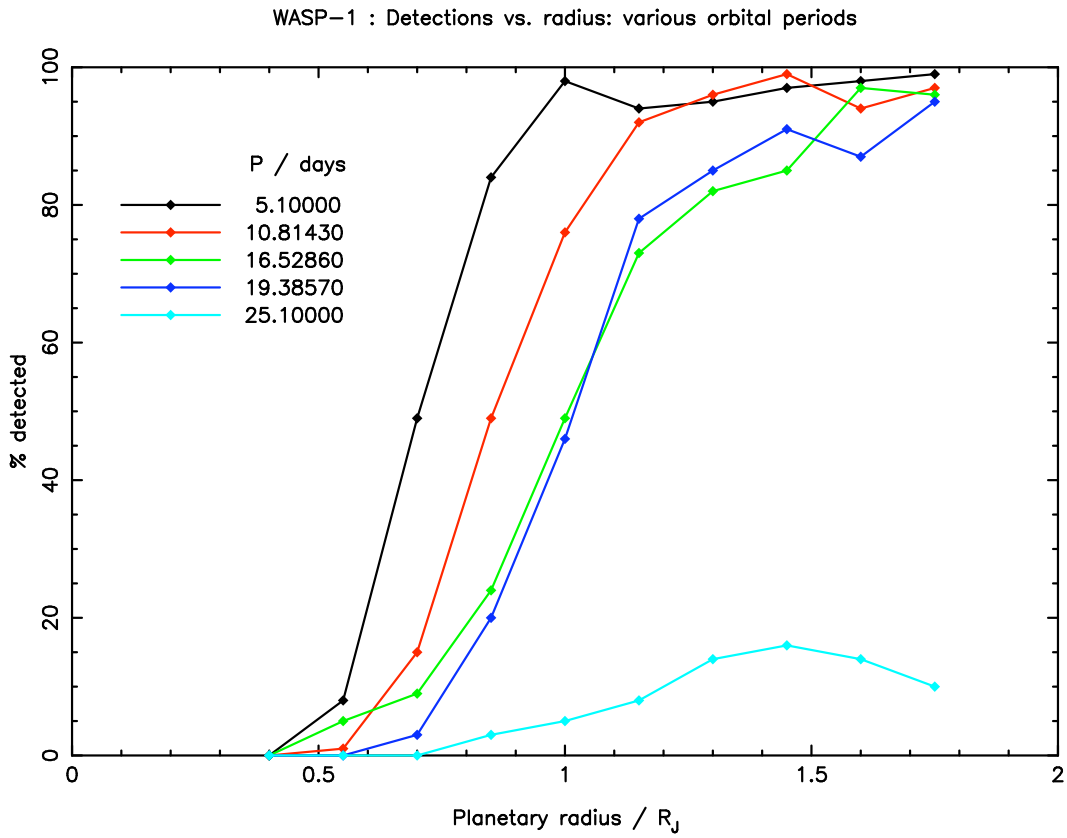

Figure 5.9: Simulation results (i) – WASP-1. Detection efficiency as a function of planetary radius for a second planet orbiting WASP-1 for several orbital periods.

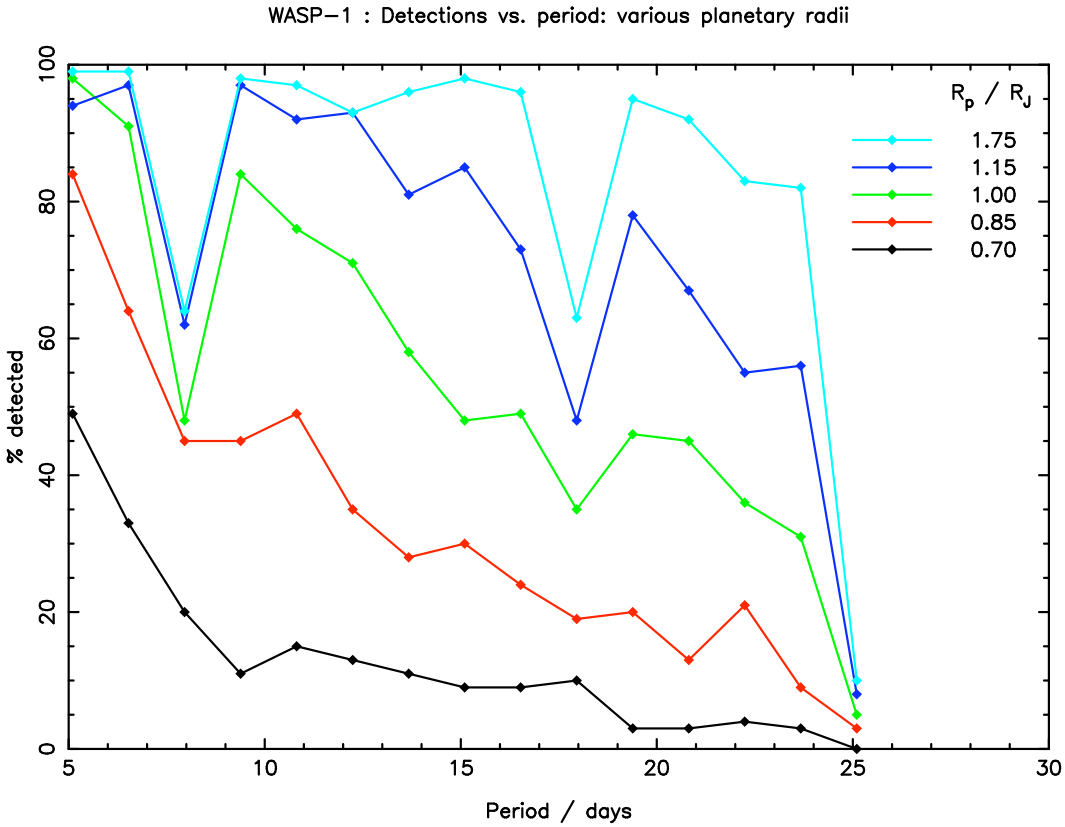

Figure 5.10: Simulation results (ii) – WASP-1. Detection efficiency as a function of orbital period for a second planet orbiting WASP-1 for several planetary radii.

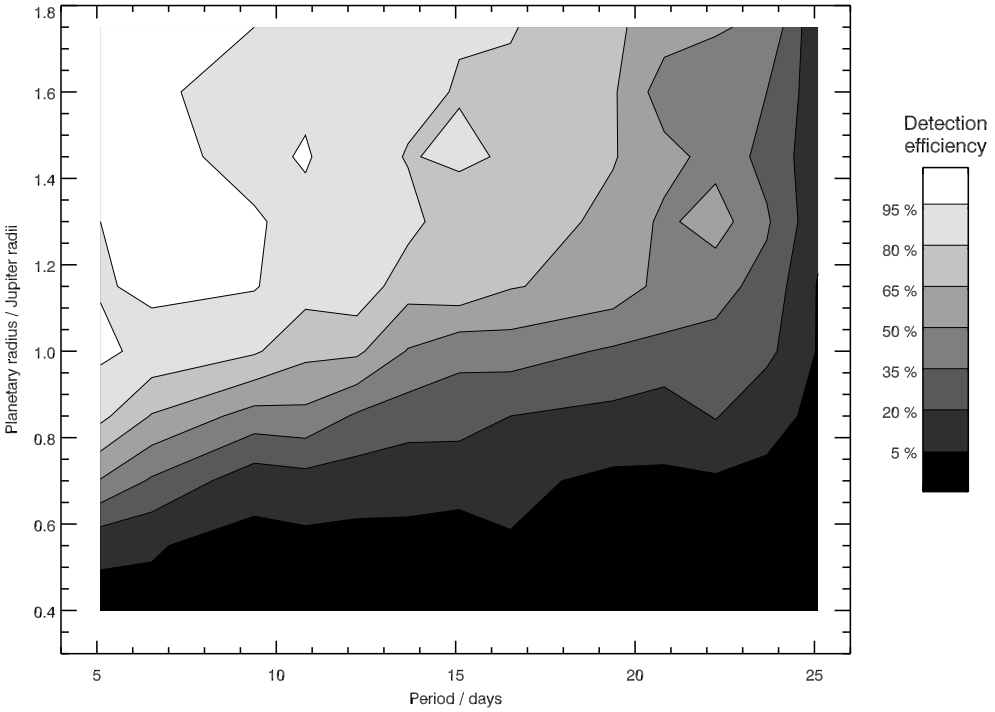

(a) WASP-1

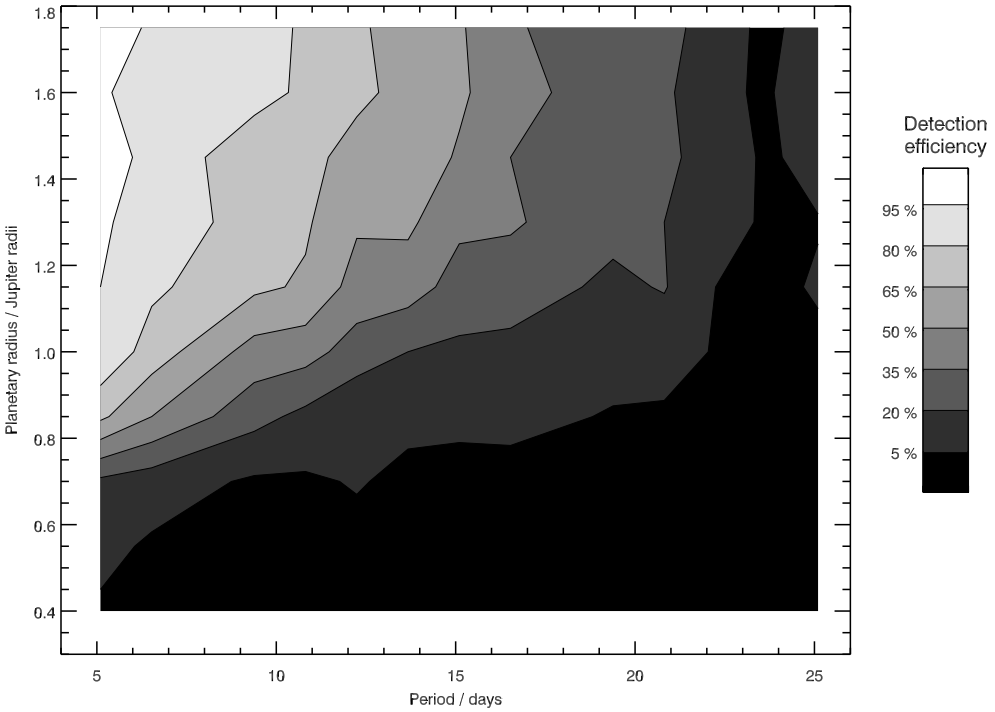

(b) WASP-2

Figure 5.11: (continued on next page)

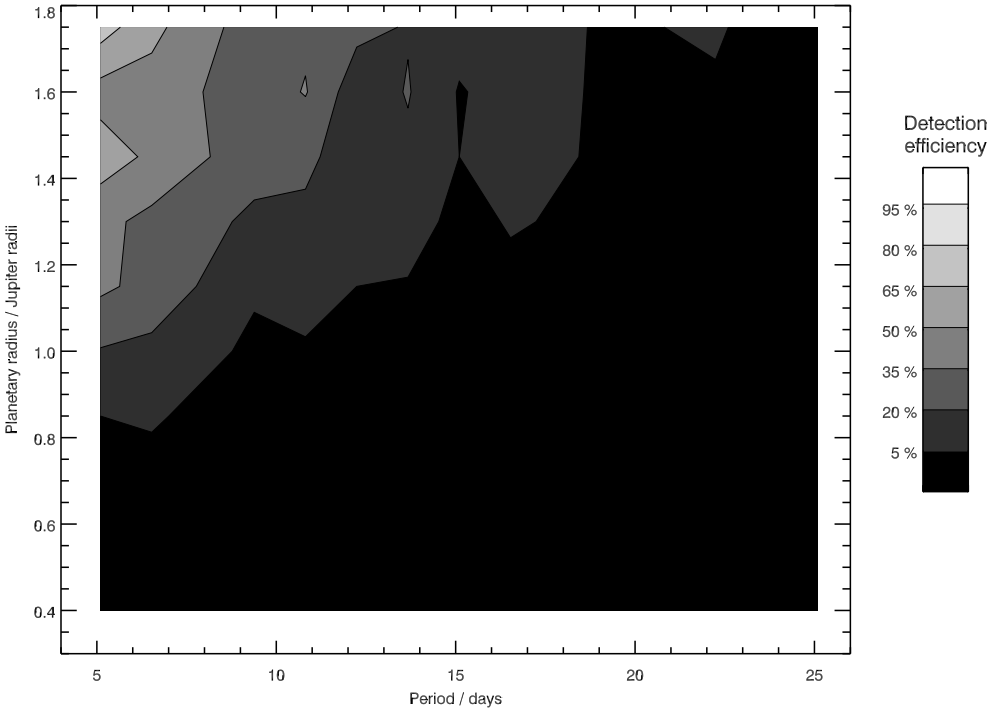

(c) WASP-3

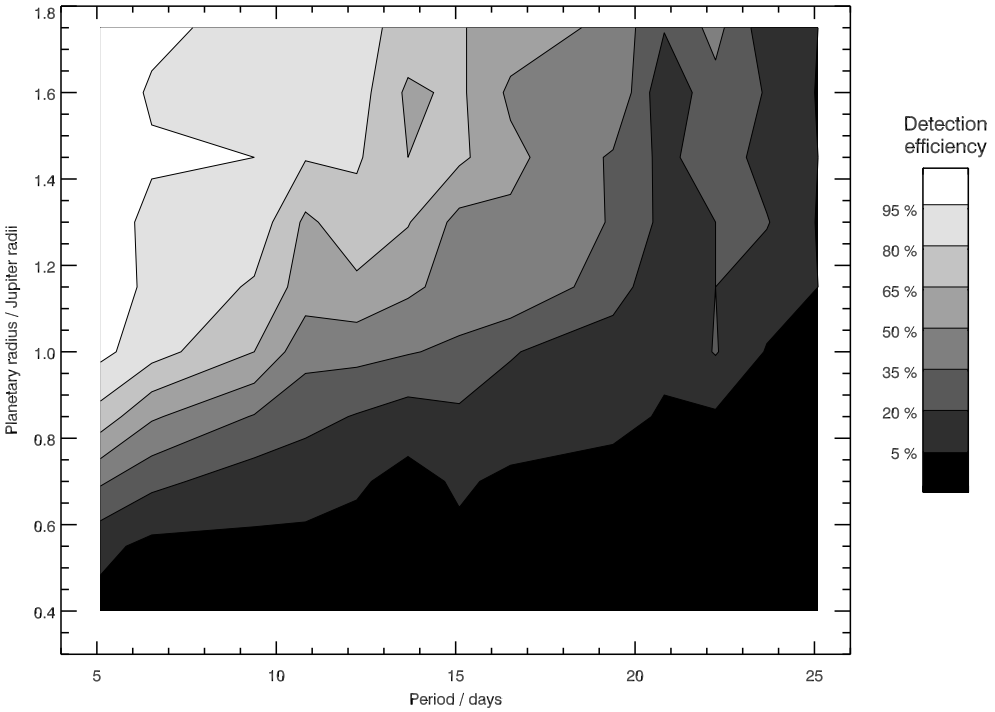

(d) WASP-4

Figure 5.11: (continued on next page)

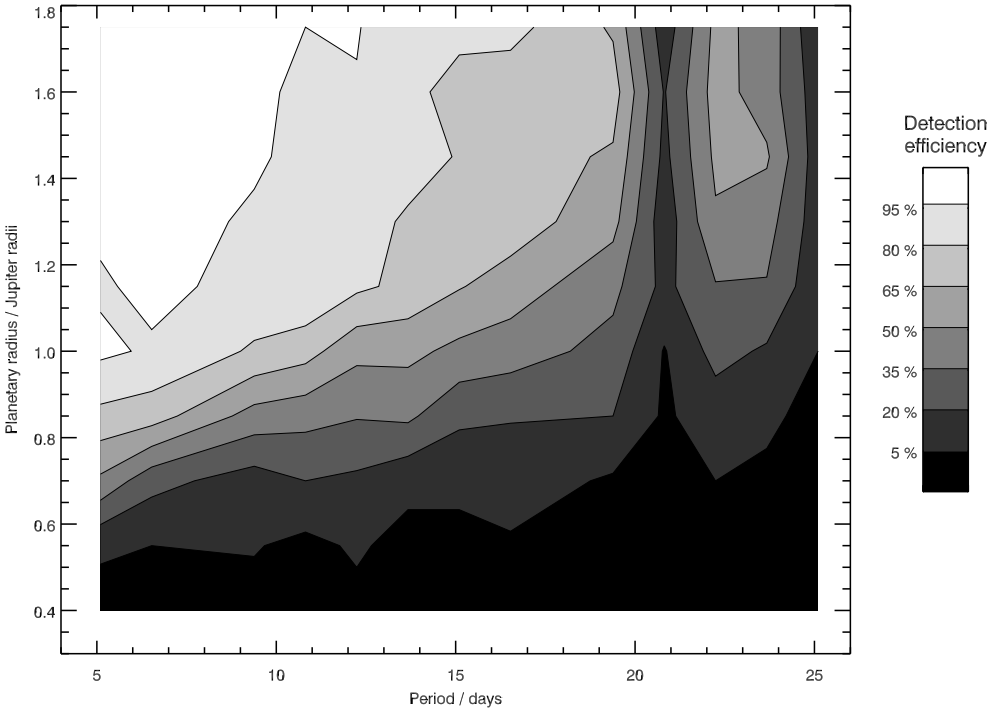

(e) WASP-5

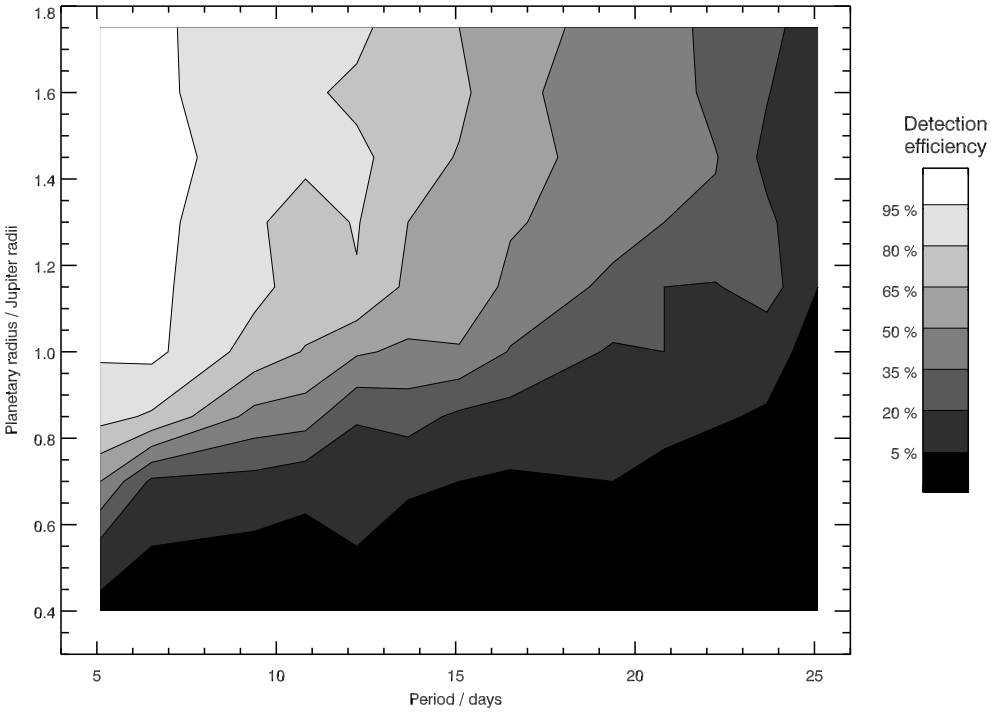

(f) WASP-6

Figure 5.11: (continued on next page)

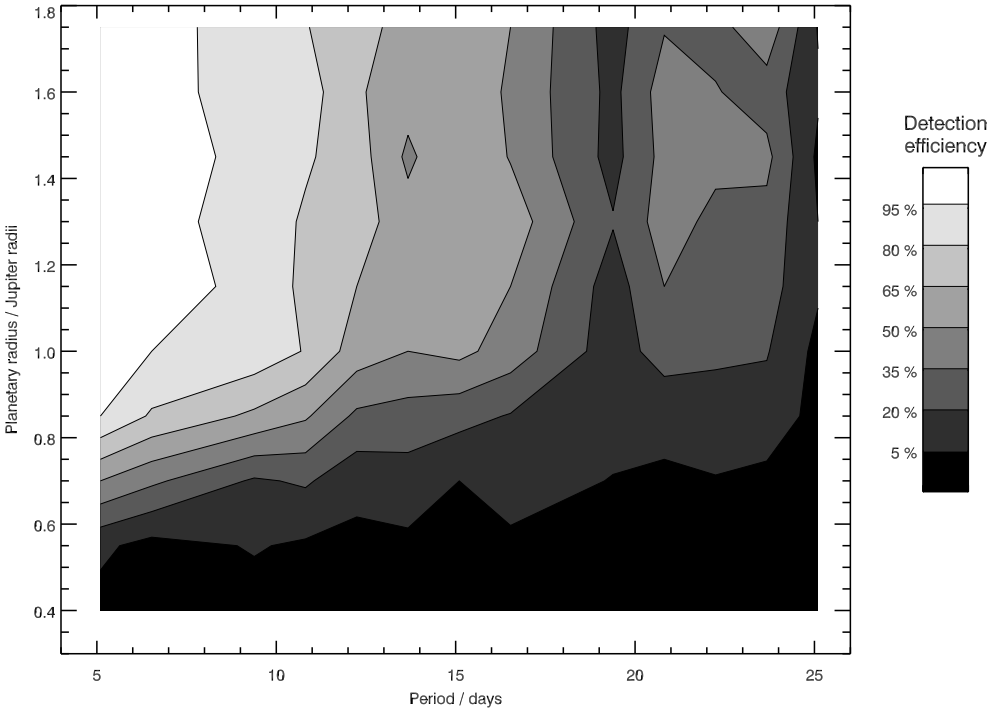

(g) WASP-7

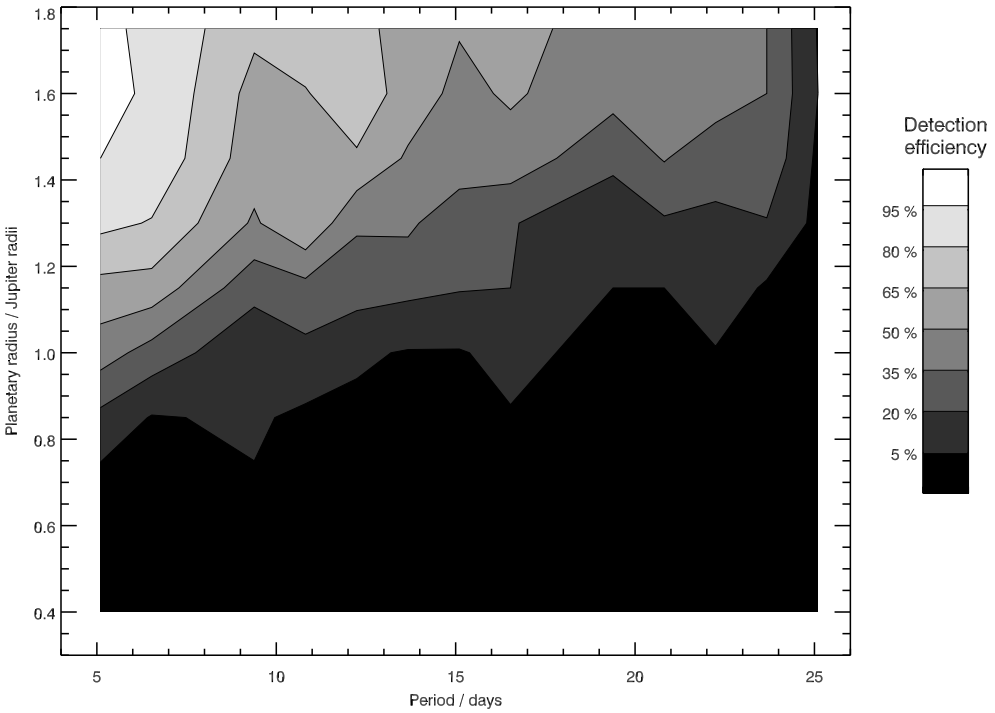

(h) WASP-15

Figure 5.11: (continued on next page)

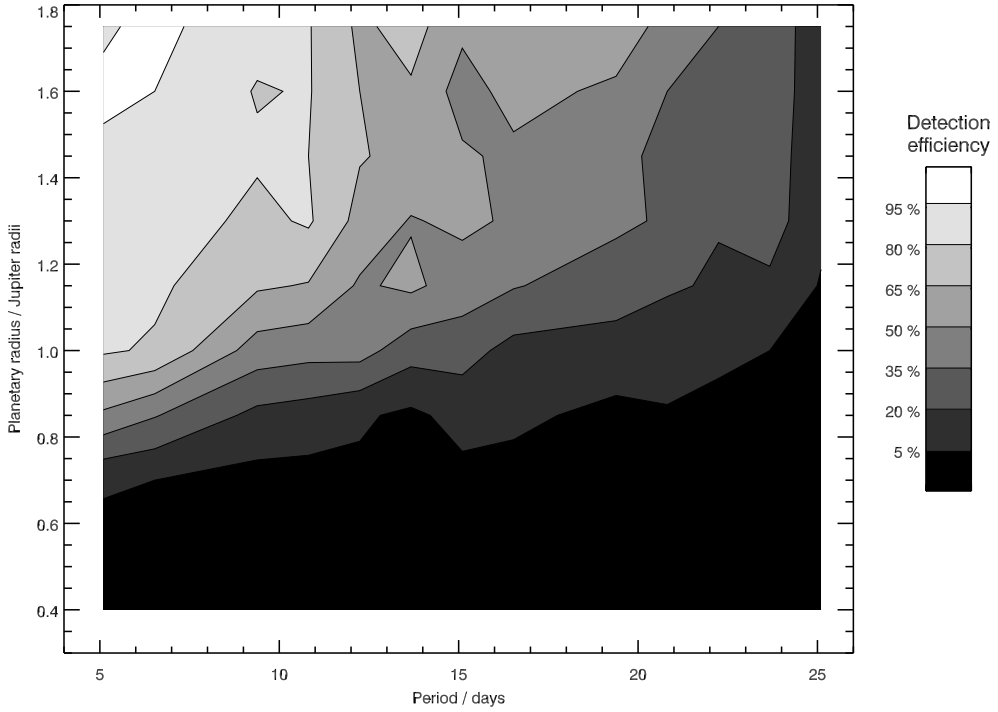

(i) HAT-P-4

Figure 5.11: Simulation results (iii) – selected planets. Contour maps showing detection efficiency as a function of orbital period and planetary radius.

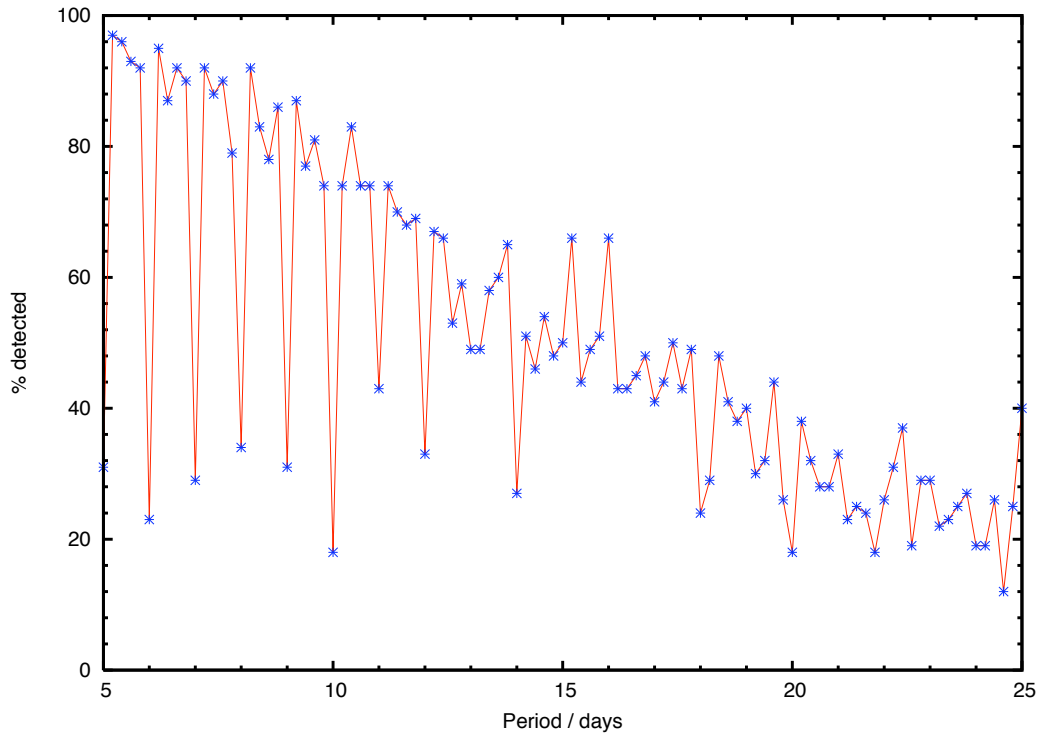

Figure 5.12: Simulation results (iv) – WASP-1 with an additional planet of Jupiter radius, at higher period resolution than the main simulations.

original lightcurve. There is more data on WASP-1 than most of the other objects – 13,630 data points spanning the 2004, 2006, and 2007 observing seasons. At the other extreme is HAT-P-4, which has a significantly shorter SuperWASP lightcurve, comprising just 6,546 data points, a few hundred of which are from 2006, with the rest from 2007. The contour plot for HAT-P-4 is shown in Fig. 5.11(i), where it can be seen that the detection efficiency is poorer, particularly at relatively long periods, than for WASP-1 (Fig. 5.11(a)).

5.6 Discussion

5.6.1 Limits of simulations

When considering the reliability of the upper limits established in Sec. 5.5.3, an obvious question to ask is 'could systems in which multiple planets exhibit transits have been detected by SuperWASP (and HAT, TrES, and XO) in the first place?'. Although objects which exhibit photometric variability are generally rejected as planet candidates, I argue that systems with a sub-5 d transiting planet and a further transiting planet with a period greater than 5 d would be unlikely to be rejected. In general, very few transits caused by the longer period planet would be present in the discovery lightcurve and that, combined with the shallow depth of planetary transits would prevent the candidate from failing test designed to eliminate variable stars. This is borne out by simulations conducted on lightcurves containing the transits caused by two planets, where the HUNT1STAR algorithm was still able to detect the inner planet, despite the presence of additional transits.

In particular, I consider the example of additional transits corresponding to a large, fairly short-period planet ($P = 12.243$ d; $R_{\rm p} = 1.45 R_{\rm J}$) which had been successfully recovered by HUNT1STAR when injected into the residual WASP-4 lightcurve (Sec. 5.5). These same artificially generated transits were injected into the unmodified WASP-4 b lightcurve, in order to ascertain whether WASP-4 b could still be detected. WASP-4 b was indeed still detected, with only a very slightly reduced signal-to-red-noise value (-13.390 compared to -13.564).

5.6.2 Lack of detections

It has been suggested that the lack of transiting multiple planet systems is perhaps surprising given the prevalence of RV multiple systems. Specifically, Fabrycky (2009) notes that 11 companion planets are known to exist in the systems with the 33 shortest period planets. An

apparently similar sample of transiting planets, however, contains no systems with known additional planets. Although Fabrycky (2009) does acknowledge the existence of observational biases which could partly explain this lack of transiting multiple planet systems, I argue that a careful examination of the characteristics of the known RV multiple planet systems reveals that the dearth of such systems is not surprising.

Of the 28 known multiple planet systems, only four have an inner planet which might reasonably have been detected by a wide-field transit survey, i.e. has $P < 5$ d and $M_p \sin i > 0.2\ M_J$, suggesting a radius large enough to be detected. None of these systems contains further planets with periods conducive to detection by means of transits; the second planet from the star orbits with $P > 95$ d in each of the four cases[5]. In other words, there is currently no multiple-planet system known by RV studies that is of the kind that can be detected at present with SuperWASP. This does not, of course, mean that such systems do not exist, or that we should not look for them; especially given the low expenditure and potentially high reward involved.

5.7 Conclusions

A search for additional planets was conducted, with periods between 5 and 25 d, orbiting 24 stars known to harbour a transiting hot Jupiter, using SuperWASP photometry to search for additional transits. No planets were detected, so in order to place upper limits on the existence of such planets, Monte Carlo simulations were performed of planets of various sizes, and with various orbital periods. The results of these simulations suggest that, for objects like WASP-1 with three seasons of SuperWASP photometry, there is a good chance (> 50 per cent) of detecting Saturn-sized ($R_S = 0.843\ R_J$) planets out to about 10 d, and a sporting chance of detecting such planets with longer periods (there is a ~ 20 per cent chance of detecting a Saturn analogue in a 20 d orbit). These detection thresholds improve with increasing planet radius (up to about $1.2\ R_J$), and are lower for stars, like HAT-P-4, with fewer data.

5.7.1 Future prospects

There are three things which would improve the chances of finding a transiting multiple planet system using SuperWASP with the method used here: (i) lightcurves spanning a longer period

[5]The four systems are HIP 14810, Ups And, HD 187123, and HD 217107; the second planets in these systems orbit with periods of 95, 241, 3810, and 4210 d, respectively.

of time, (ii) improved signal-to-noise, and (iii) knowledge of more (single) transiting planet systems.

First, as our simulations (Sec. 5.5.3) demonstrated, the longer the span of the lightcurve, the greater our sensitivity to longer-period planets. As transit surveys continue to observe some of the known planets, our ability to detect additional transits in these systems will increase. Another possibility for increasing the number of available photometric data points is to share data between transit surveys, as suggested by Fleming et al. (2008).

Second, any improvement to the signal-to-noise ratio of the SuperWASP data would allow shallower transits, and therefore smaller planets, to be detected. A significant improvement to the quality of SuperWASP data may arise from the proposed implementation of difference imaging analysis (instead of aperture photometry) in the near future. If such a change were demonstrated to improve the noise characteristics of SuperWASP lightcurves, the search for additional transits described in this paper could be repeated.

Finally, as the number of known transiting planet systems continues to increase, so does the probability that one of them harbours an additional, detectable planet. The space mission *Kepler* has the capability to find small transiting planets in long-period orbits, so any additional such planets orbiting stars in the *Kepler* field are likely to be discovered in the coming years. *Kepler* may also discover a transiting multiple planet system, perhaps TrES-2, which is known to harbour a hot Jupiter and lies within the *Kepler* field-of-view (O'Donovan et al., 2006a).

6

Radio observations of the transiting exoplanet HD 189733 b

This chapter is based on an article published in *Monthly Notices of the Royal Astronomical Society*:
Smith, A. M. S., Collier Cameron, A., Greaves, J., Jardine, M., Langston, G., & Backer, D., '*Secondary radio eclipse of the transiting planet HD 189733 b: an upper limit at 307 – 347 MHz*', 2009, MNRAS, 395, 335.

All the work described here was conducted by the author. The observations were conducted jointly by the author and Jane Greaves, and the code used to generate Fig. 6.1 was written by Glen Langston.

In this chapter, results from the first-ever attempt to observe the secondary eclipse of a transiting extra-solar planet at radio wavelengths are reported. Observations of HD 189733 b

Above: The Robert C. Byrd Green Bank Telescope of the National Radio Astronomy Observatory, Green Bank, West Virginia, USA. Photograph by the author.

were made with the Robert C. Byrd Green Bank Telescope of the NRAO over about 5.5 hours before, during and after secondary eclipse, at frequencies of 307 – 347 MHz. Upper limits to the flux density are calculated and compared to theoretical predictions of the flux density of cyclotron-maser emission from the planet.

6.1 Introduction

In the solar system, all the magnetised planets are known to emit at radio wavelengths. One of the principal mechanisms producing this is electron-cyclotron maser radiation, which produces emission at the local gyrofrequency, f_g, given by

$$f_g(\mathrm{MHz}) = 2.8B(\mathrm{G}), \tag{6.1}$$

where B is the planetary magnetic field strength.

Of the solar system planets, Jupiter has the strongest radio emission, outshining the (quiescent) Sun by several orders of magnitude at frequencies of about 30 MHz. Jupiter was also the first planet discovered to emit at radio wavelengths, detected at 22 MHz by Burke & Franklin (1955), since the other solar system planets (including Earth) emit at frequencies below the Earth's ionospheric cut-off at $\sim 5 - 10$ MHz (Grießmeier et al., 2005).

It has long been suggested that analogous radio emission might arise in an extra-solar planetary system, and that it may be possible to detect this radiation from Earth. Indeed, several attempts have been made to detect radio emission from an extra-solar planetary system, beginning with observations in the 1970s and 80s before any extra-solar planets were known (see Grießmeier et al. 2006 for a list of observational campaigns). More recently, with the discovery of hundreds of extra-solar planets starting with 51 Peg b (Mayor & Queloz, 1995), several further attempts have been made to detect radio emission from these planets, none successfully to date.

Observations of the radio emission from Jupiter have allowed the planet's magnetic field strength to be inferred from the high-frequency cut-off (around 40 MHz). The emission with this highest frequency is generated in the region with the highest magnetic field strength (equation 6.1), close to the planet. Observations of the radio spectrum of hot Jupiters could provide similar information about the planetary magnetic field, composition and rotation (see

Zarka 2007 for a review of what may be expected from exoplanetary radio emission).

Although Jupiter's emission is several orders of magnitude stronger than the (quiescent) Sun's at certain frequencies, the analogous emission from extra-solar systems is expected to be very faint because of the distance involved. Consequently, the planetary systems most favoured by observers tend to be those within a few pc of Earth.

Several theoretical models (Lazio et al. 2004; Grießmeier et al. 2007; Jardine & Cameron 2008) predict the radio flux from a range of exoplanets, and magnetic environments. Reconnection between the stellar and planetary magnetic fields provides the pool of accelerated electrons necessary for the electron-cyclotron maser instability. The model of Jardine & Cameron (2008) reproduces the observed emission from solar-system planets and predicts that the radio flux from exoplanets in close orbits should scale as

$$S_\nu \propto \left[\frac{N}{B_\star^{1/3}} \right]^2 \tag{6.2}$$

where N is the coronal density and $B_\star$ is the surface field strength of the parent star.

In particular, this model predicts the radio flux for HD 189733 b, a hot-Jupiter planet orbiting a K2 dwarf (Bouchy et al., 2005). For the observed field strength of 40 G (Moutou et al., 2007) and a solar coronal density, this gives 15 mJy, at a frequency determined by the planetary magnetic field strength. It is likely, however, that the coronal density will be greater than the solar value, since HD 189733 rotates more rapidly than the Sun. If scalings in the range $N \propto \Omega^{0.6}$ to $N \propto \Omega$ (Unruh & Jardine 1997, Ivanova & Taam 2003) are assumed then for the rotation rate of 11.73 days appropriate for HD 189733, the flux rises to 39 - 72 mJy respectively.

In this work, I make use of the fact that HD 189733 b transits its host star to observe the system during secondary eclipse, when the planet passes behind the star. Detecting the secondary eclipse at radio wavelengths would provide unambiguous evidence that the emission is of planetary, rather than stellar, origin. These observations (described in Section 6.2), conducted on a bandwidth centred at 327 MHz, are used to determine new upper limits to the radio flux from HD 189733 b (Section 6.3). This relatively low frequency was chosen because the planet could emit at this frequency given a plausibly strong magnetic field. The significance of these upper limits and the prospects of future work are discussed in Section

6.4.

6.2 Observations

I observed the HD 189733 system for ∼5.7 hours, encompassing a 1.827 hour (Winn et al., 2007) secondary eclipse on 2007 April 23, when the star was at altitudes between 45° and 74°. The observations were conducted using the Spectral Processor at prime focus 1 of the Robert C. Byrd Green Bank Telescope (GBT) of the National Radio Astronomy Observatory (NRAO)

The dual polarisation observations span the frequency range 307 MHz to 347 MHz and consist of a series of spectra comprising 1024 frequency channels, each with an integration time of one second. Spectra were grouped into scans, of duration 120 s, and scans of the target (ON) were alternated with off-target scans (OFF) of a patch of sky whose centre is 2° South of the target in declination.

The reason for choosing to make spectral-line observations, despite the broad-band nature of the expected signal, is to mitigate against radio frequency interference (RFI). Much RFI is narrow-band in nature, so observing with a large number of frequency channels allows channels affected by RFI to be excluded (see Section 6.3.1).

Because of the large beam size at this frequency, there are expected to be other radio sources within the beam. The Westerbork Northern Sky Survey (WENSS) 300 MHz survey has a sensitivity of 18 mJy, but does not extend below +30° in declination and so does not cover our target star; it can, however, give us an idea of how many objects are expected in a typical GBT beam (FWHM = 36'). I looked in the WENSS catalogue at ten beam pointings spaced between 20 and 21 hours in RA, at +31° in declination. An average of 4.8 objects were found within 20' of the beam centre; these objects have a median integrated flux of 121 mJy. The Texas Survey of discrete radio sources at 365 MHz (Douglas et al., 1996) is less sensitive (90 per cent complete to 400 mJy and 80 per cent to 250 mJy), but it does cover HD 189733. The Texas survey includes an object with a flux density of 550 mJy 18.8' from the centre of our ON beam, and two objects of flux density 581 mJy and 241 mJy, respectively 3.6' and 16.1' from the centre of our OFF beam.

Given that I am searching for a source exhibiting a specific, known variability[1], the other

[1]Using the period and transit duration of Winn et al. (2007), and the time of mid-eclipse from Deming et al.

radio sources in our beam are unlikely to be a problem. This is because in order to mimic the eclipse that is sought, any variable object would not only have to vary, but would have to produce a large ($\sim$ 10 per cent or greater) eclipse-like signal on a specific, relatively short, time-scale.

Each observation was calibrated using a noise tube calibrator, but no corrections are made for atmospheric opacity, since such effects are negligible in the 1 m wavelength regime. Given the beam size and pointing stability of the GBT, there is no need to correct for pointing errors. An increase in raw flux was observed in both our target and off-target beams at around 2454214.0 JD which corresponds to 8 am local time and is probably caused by an increase in radio-frequency interference.

6.3 Analysis

6.3.1 Production of lightcurves

Initially, the data were visually inspected by stacking a number of spectra into a time series. A typical set of stacked spectra are shown in Fig. 6.1, using colour to indicate flux. The most noticeable features in these stacked spectra are (i) the sharp 'spikes' spanning just one or two frequency channels and (ii) an oscillation with a period of around 20 s across all frequencies. Since both these effects are observed in both the ON and OFF scans, I conclude that they are due to radio-frequency interference.

In order to determine which frequency channels suffer from intermittent 'spiky' RFI, the variance of each of the 1024 channels over the whole dataset was calculated (Fig. 6.2(a)). After noticing a small number of pairs of scans suffer from a high level of RFI over a broad range of frequencies, a total of seven pairs of scans were identified and excluded from further analysis. It is believed that the RFI in at least some of these scans was caused by electrical interference in the control room of the GBT. The variance in each frequency channel after the exclusion of these scans (Fig. 6.2(b)) shows only narrow band spikes of RFI, which are easily identified and removed. Note that the same analysis of the raw OFF scans reveals spikes of high flux density in identical frequency channels, confirming that RFI, and not flaring of the target star, is responsible. A total of 177 of the 1024 channels were in this way identified as containing RFI and excluded, resulting in a variance plot without spikes (Fig. 6.2(c)).

(2006), and associated uncertainties, it is concluded that the eclipse time is known to within 200 s.

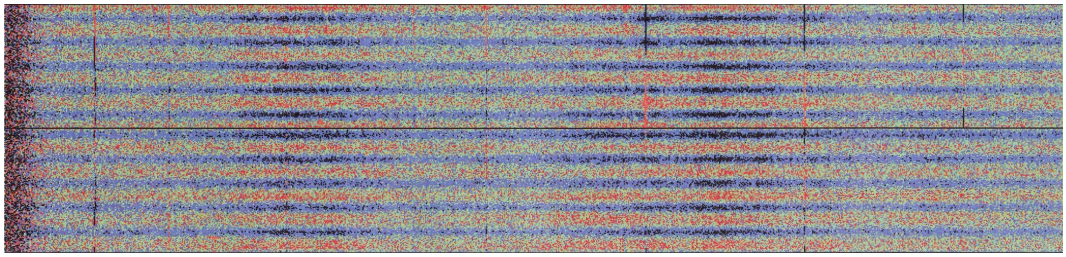

Figure 6.1: Series of time-stacked spectra for a typical pair of scans (ON, *lower* half of figure; OFF, *upper* half), each of duration 120 s. Time increases from bottom to top; frequency from left (307 MHz) to right (347 MHz). Colours are indicative of raw flux counts, red (light) represents high flux and blue (dark) low flux.

In order to determine which parts of the remaining bandpass to use to construct lightcurves and search for an eclipse signal, I calculated the standard deviation of each frequency channel of the raw ON lightcurve, which is normalised by dividing by the mean raw flux (Fig. 6.3). With the aid of this figure, four regions of the bandpass that show less variation than surrounding regions were identified. These four subsets of the bandpass are numbered (i) - (iv) and I construct lightcurves from the frequency channels in each of these bandpasses, as well as one from all of the remaining 847 frequency channels.

In each case, single, uncalibrated ON and OFF lightcurves were created by taking the mean of the relevant channels at 1 s intervals. The periodic RFI identified in Fig. 6.1 earlier is clearly visible in plots of these ON and OFF lightcurves spanning only a few minutes (Fig. 6.4). A rectified sine wave was used to fit this periodic modulation, which is believed to be caused by a distant radar system. The ON and OFF lightcurves for the whole bandpass, after the rectified sine wave has been subtracted, are shown in Fig. 6.5.

After subtracting the rectified sine wave from each scan (ON and OFF), the lightcurves were median-binned on the duration of a scan, and the ON scan was converted to a flux density, S_ν, in Jy, according to

$$S_\nu = \frac{1}{\Gamma} \times \frac{(ON - OFF)}{OFF} \times T_{\rm sys}, \tag{6.3}$$

where ON and OFF are the raw fluxes of the ON and OFF scans respectively, $T_{\rm sys}$ is the system temperature, and $\Gamma = 2.0$ KJy^{-1} is the telescope sensitivity. The resulting binned, calibrated lightcurves are shown in Fig. 6.6. Although the residuals in the fit to the periodic RFI result in errors on individual points of magnitude $\sim$ 100 mJy, this should not affect our ability to detect a signal, given our number of data points.

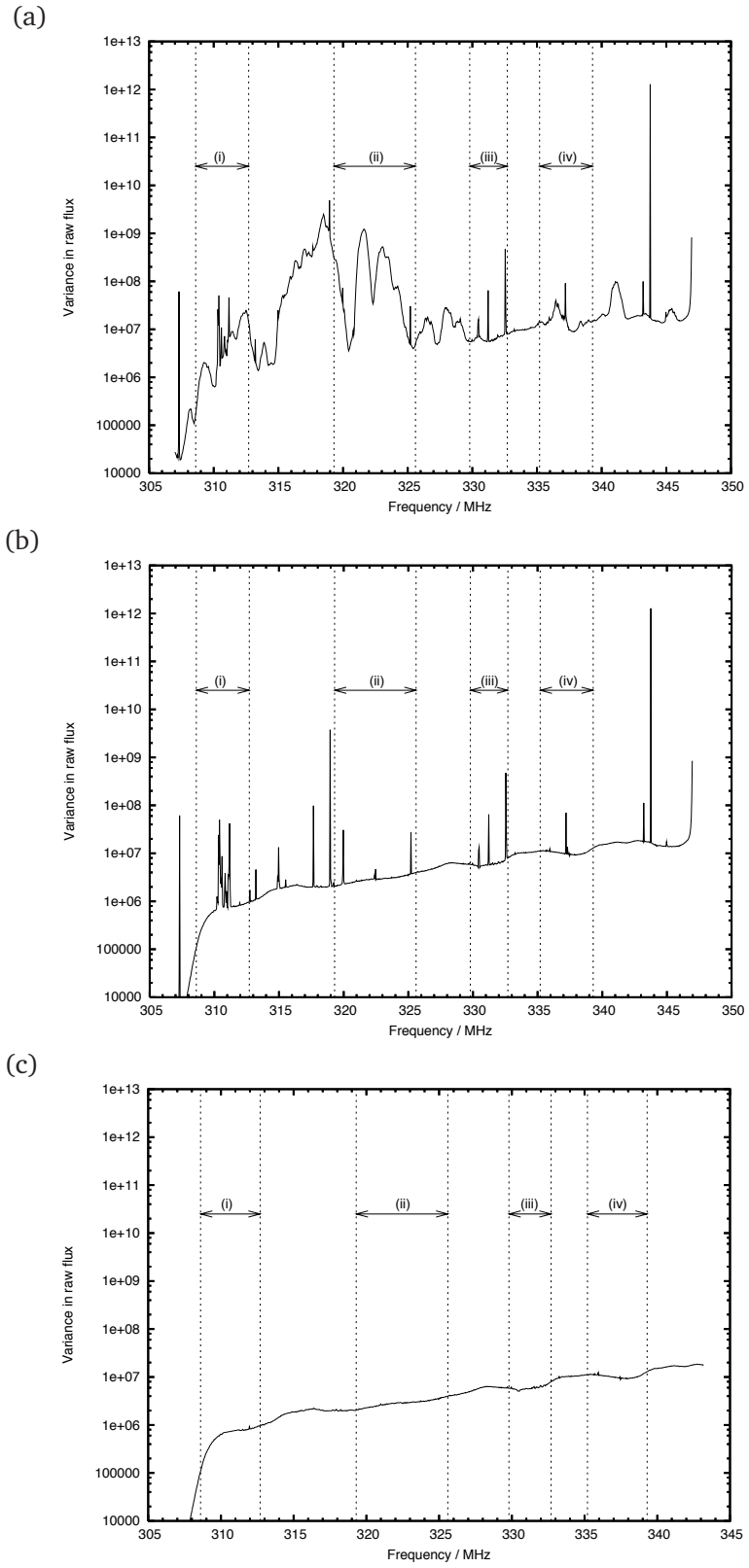

Figure 6.2: Variance in the raw flux for the ON scans taken on 2007 April 23. The top panel includes all 66 ON scans and all frequency channels. The middle panel is the same as the top panel, but 7 noisy scans have been completely excluded. The bottom panel is the same as the middle panel, but with 177 noisy frequency channels removed. The four regions indicated in each panel are those parts of the bandwidth for which lightcurves are generated (see text).

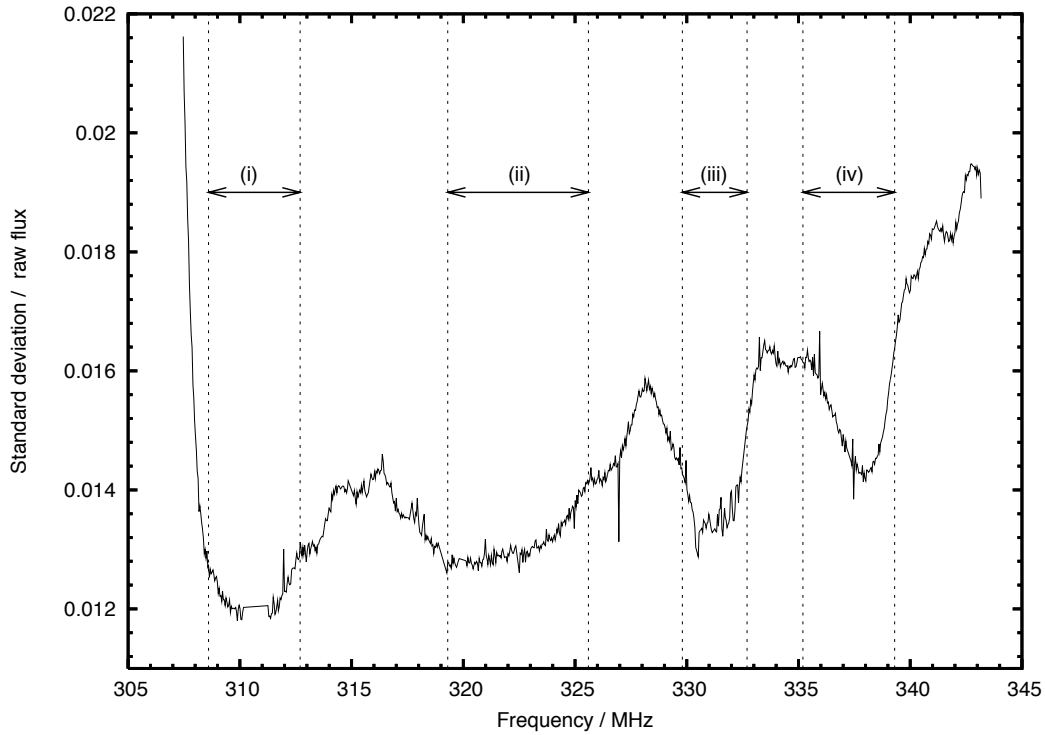

Figure 6.3: Standard deviation of each channel of raw ON data, normalised by the mean flux of each channel as a function of frequency. The four regions indicated are those parts of the bandwidth for which lightcurves are generated (see text).

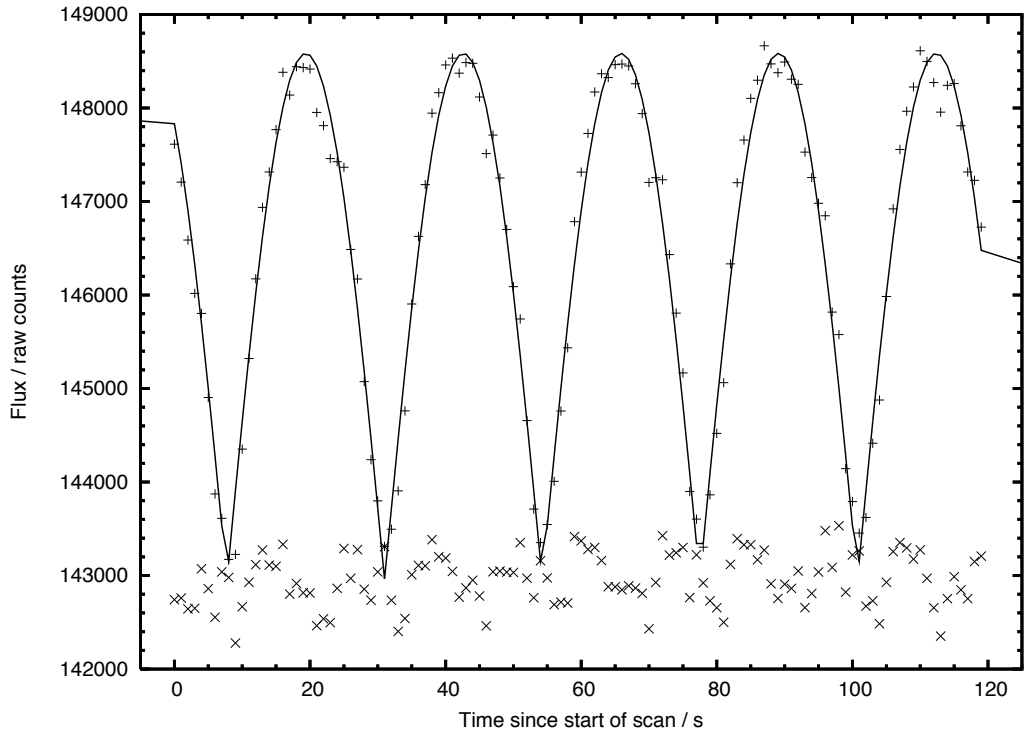

Figure 6.4: A typical ON scan of duration 120 s showing the raw counts (averaged over all frequency channels) as a function of time (+). Also plotted are the rectified sine wave fitted to this scan (solid line) and the residuals of this fit (x).

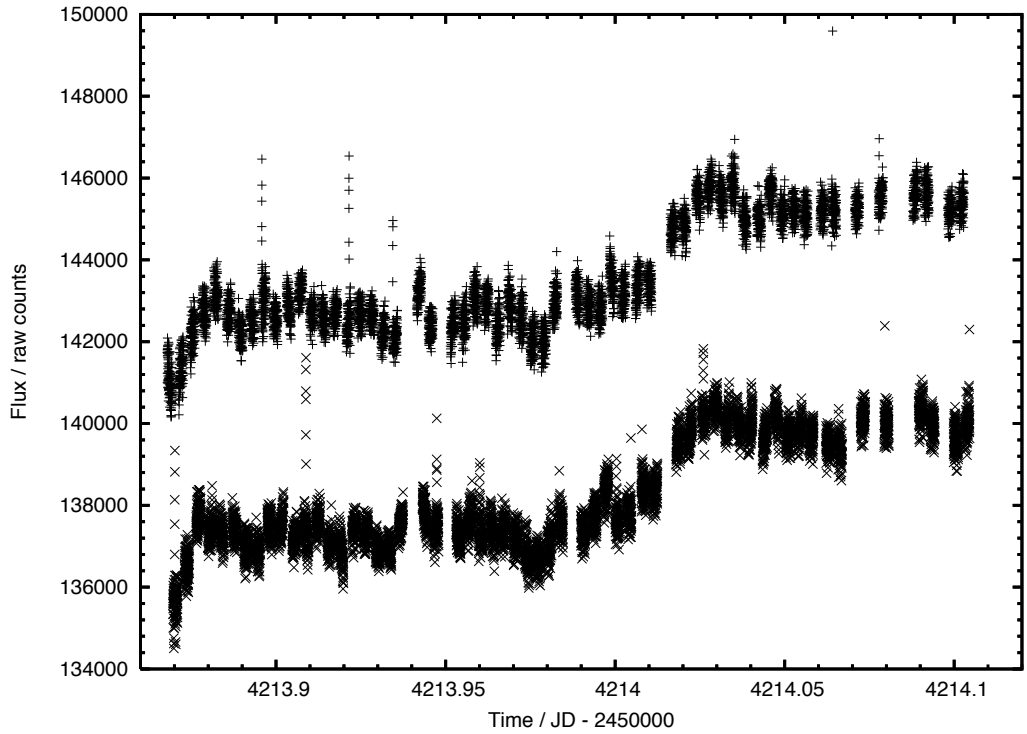

Figure 6.5: Uncalibrated lightcurves ON (upper curve; denoted by +) and OFF (lower; x) target, after subtraction of periodic (rectified sine wave) RFI.

6.3.2 Measuring the eclipse depth

I use the period ($P = 2.2185733$ days), epoch of transit ($t_0 = 2453988.80336$ (HJD)), and transit duration ($t_{IV} - t_I = 1.827$ hours) determined by Winn et al. (2007) and the fact that the orbit of HD 189733 b is circular to identify the 'low' points, ℓ, observed during secondary eclipse. I then follow the method of Collier Cameron et al. (2006) to calculate the depth of transit and the associated uncertainty. The weighted mean of the lightcurve is subtracted from all lightcurve points, x_i, and the inverse-variance weights, w_i, are scaled to give $\chi^2 = 1$ for a constant-flux model fitted to the out-of-eclipse data. The transit depth, δ, and its variance, Var(δ) are then calculated according to,

$$\delta = \frac{\sum_{i\in\ell} x_i w_i \sum_i w_i}{\sum_{i\in\ell} w_i \left[\sum_i w_i - \sum_{i\in\ell} w_i\right]} \tag{6.4}$$

and

$$\mathrm{Var}(\delta) = \frac{\sum_i w_i}{\sum_{i\in\ell} w_i \left[\sum_i w_i - \sum_{i\in\ell} w_i\right]} \tag{6.5}$$

respectively. With the null hypothesis that there is no eclipse, the n-σ upper limit to the flux density is given by $n\sqrt{\mathrm{Var}(\delta)}$.

Table 6.1: Measured eclipse depths and upper limits to the radio flux density from HD 189733 b in several parts of the bandwidth.

Bandpass	Frequency range (MHz)	Eclipse depth (mJy)	Standard deviation of depth (mJy)	Significance	3-σ upper limit to flux density (mJy)
all	307.0 - 347.0	-21.6	27.1	-0.8 σ	81
(i)	308.6 - 312.7	+15.6	31.4	+0.5 σ	94
(ii)	319.3 - 325.6	+6.8	26.5	+0.3 σ	80
(iii)	329.8 - 332.7	-50.3	33.9	-1.5 σ	102
(iv)	335.2 - 339.3	-56.5	28.0	-2.0 σ	84

The depth of transit, associated uncertainty and the 3-σ upper limit to the flux density for each of the five lightcurves of Fig. 6.6 are displayed in table 6.1.

Over the whole bandwidth, a significant eclipse is not detected, but it is possible to place a 3-σ upper limit of 81 mJy to the flux density from the planet. Of the four selected subsets of the bandpass, insignificant brightening (consistent with a constant flux model) is found at the predicted time of secondary eclipse in regions (i) and (ii). Eclipses with significances of 1.5-σ and 2.0-σ are found in regions (iii) and (iv), respectively.

It is possible that these 'detections' of the radio eclipse are caused by scatter in the lightcurve, and are not real; it is not understood why it should be any easier to detect the eclipse signal in these particular narrow frequency ranges than in any other. It is not possible to conclude with any confidence that the eclipse has been detected, although these offer the possibility that I am tantalisingly close to detecting the first radio emission from an extra-solar planet.

6.4 Discussion

6.4.1 Interpretation of results

There are four aspects of planetary cyclotron maser emission that might lead to a non-detection: (i) the planet does not radiate at the observed frequencies, (ii) any emission is insufficiently strong for us to detect, (iii) the emission is beamed out of the line of sight and (iv) the emission is absorbed or trapped (Grießmeier et al., 2007).

I consider first the case where the magnetic field strength of the planet does not allow radiation to be generated at the observed frequency range. It seems unlikely that the magnetic field is too strong, since it is expected that the low-frequency tail of the spectrum will be fairly flat (Grießmeier et al., 2005). The fact that our higher frequency observations produce more

(a)

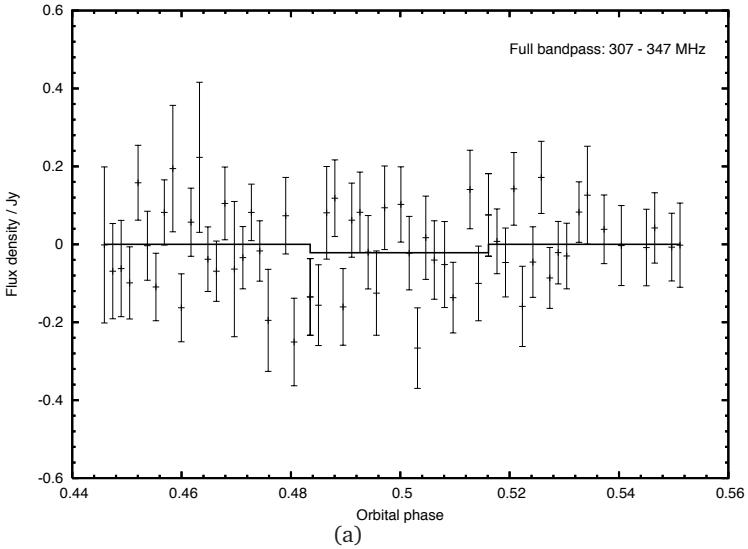

(a)

(b)

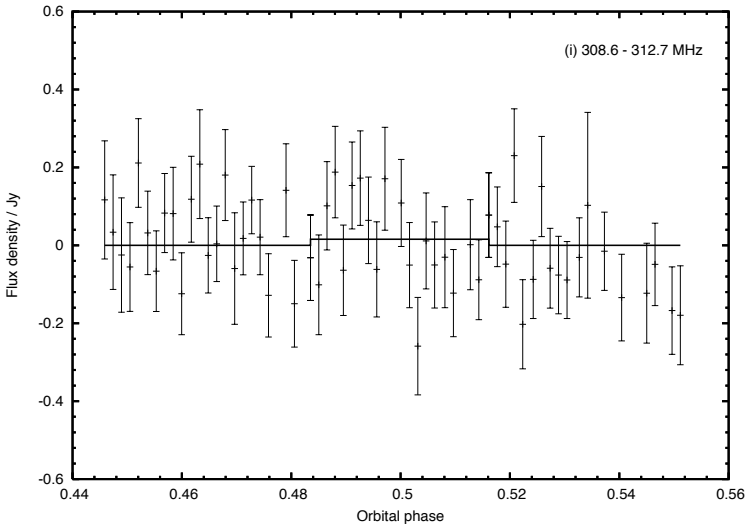

(c)

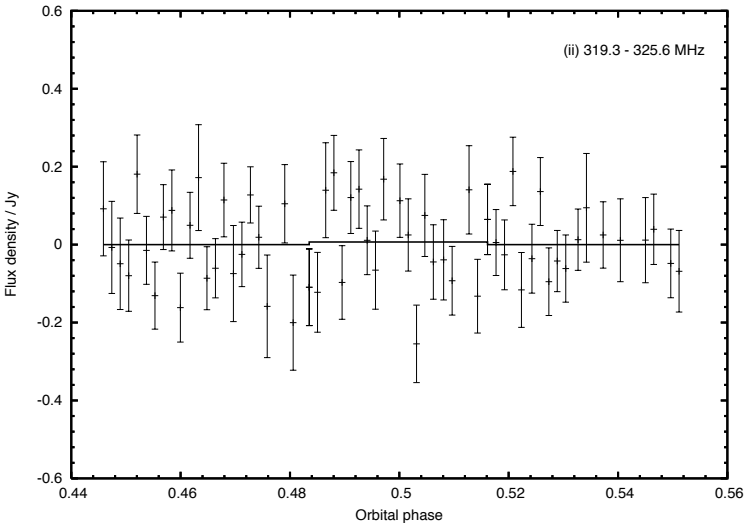

Figure 6.6: (continued on next page)

(d)

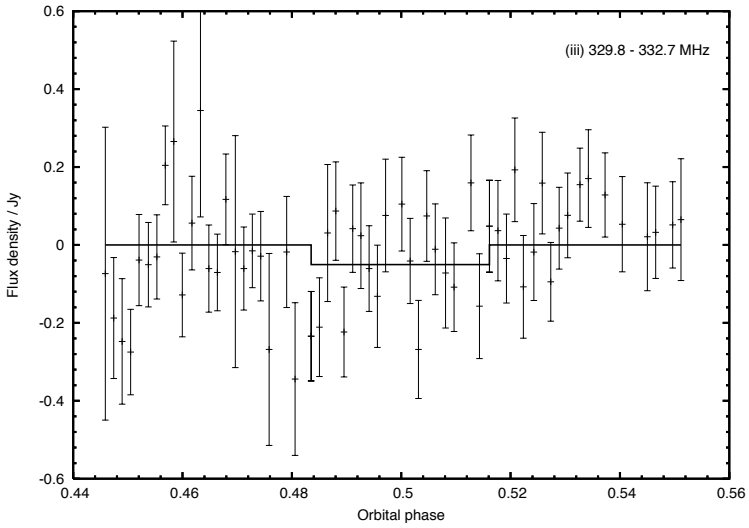

(e)

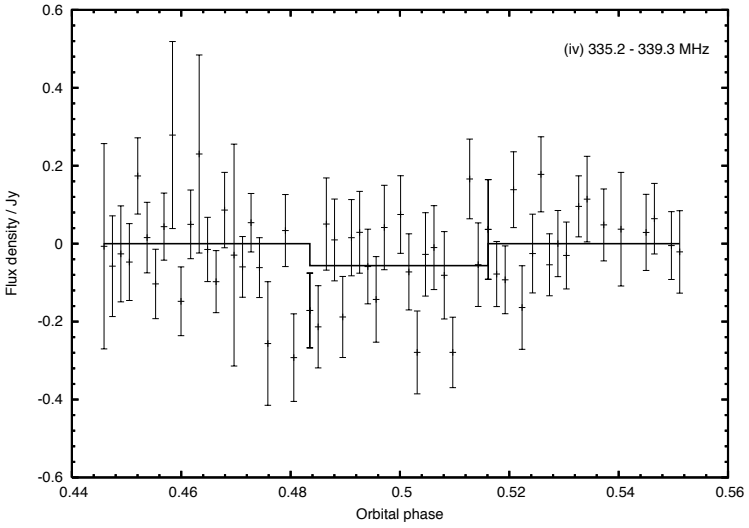

Figure 6.6: Calibrated lightcurves of HD 189733 in different frequency ranges, (a) the whole bandpass, and (b), (c), (d) and (e), the four bandpasses (i), (ii), (iii) and (iv) respectively (see Fig. 6.3). Also plotted in each panel is the best fit to the data (see text for details).

encouraging results, however, hints at the possibility that the magnetic field is too strong to produce emission at the low-frequency end of the observed bandwidth.

Jupiter's cyclotron maser emission is observed from about 0.3 to 40 MHz, corresponding to a highest local value of the magnetic field strength of about 14 G. In order for us to detect emission at 307 – 347 MHz, the emission would have to be generated in a region where the local field strength is ∼110 G. Since Jupiter's emission originates well above the cloud deck, it is possible that emission from an extra-solar planet could be produced closer to the planetary surface, where the local field strength would be greater. However, if no emission is generated in regions where the magnetic field strength is about 110 G or stronger, all of the emission would occur at frequencies below our observing bandwidth and no signal would be detected.

The second case is that in which the planet produces emission in the observed frequency range, but at an insufficient intensity to be detectable in our data. According to the theoretical model of Jardine & Cameron (2008), a stellar coronal density between 2.0 and 2.5 times greater than the solar value implies the existence of a population of electrons sufficient to generate radiation that would be detected at our 3-σ confidence level. Therefore, the stellar coronal density must be at least twice solar in order for us to have been able to detect the emission, even if our observations were conducted at the optimum frequency.

Third, the emission may be beamed in a hollow cone, in a manner similar to Jupiter's Io-controlled radiation. If this is the case it may be that the beam does not cross our line of sight during our observations and no radio emission would be observed. Predicting this possible beaming effect is beyond the scope of the current model, however.

Additionally, there exist potential observational reasons for the lack of detection. One possibility is that the integration time of individual spectra was too long, at 1 s, given that Jupiter's emission displays variability on very short time-scales. The emission from Jupiter that varies on the shortest (millisecond) time-scales, however, is that controlled by the moon Io, whereas the emission not associated with Io varies on time-scales of order 1s or greater (Carr et al., 1983). Furthermore, even if there is short period variability of the emission from HD 189733 b, it should still be possible to observe the mean level of this flux drop as the planet goes into eclipse.

Another possibility is that the eclipse was masked by the variability of another radio source in either the ON or the OFF beam. This is discussed in Section 6.2, where it is suggested that

it is unlikely that the eclipse signal is mimicked or masked by the variability of other objects, given the nature and timing of the expected signal.

6.4.2 Comparison with previous observations

The upper limits calculated in this work compare favourably with those derived in previous work on different systems. Bastian et al. (2000) observed seven extra-solar planetary systems with the Very Large Array (VLA), with typical 1 σ sensitivities of around 50 mJy at 74 MHz and 1 – 10 mJy at 333 MHz. More recently, Lazio et al. (2004) observed five systems with the VLA at 74 MHz and derived 2.5 σ upper limits of 218 to 325 mJy. A further limit of 150 - 300 mJy using the VLA at 74 MHz was placed on the radio flux from the extra-solar planet τ Boo (Lazio & Farrell, 2007). Tighter (2.5-σ) upper limits of 7.9 and 15.5 mJy were placed on the emission from ϵ Eri b and HD 128311b respectively by George & Stevens (2007) at 150 MHz using the Giant Metrewave Radio Telescope. Ours are the first eclipse observations, and they produce upper limits comparable with previous observations.

6.5 Conclusions and future prospects

I have determined new upper limits to the radio flux density from the transiting planet HD 189733 b; the 3-σ limit to the flux density over 307 – 347 MHz is 81 mJy. Of the four subsets of this bandpass selected for their noise properties, no eclipse is detected in two of them, but marginal eclipses are detected in the other two, the strongest of which is a 2-σ detection. Further observations at the time of secondary eclipse in the future may enable us to improve the signal-to-noise further in order to determine whether the signal apparently detected is real or not.

Since the publication of the work described in this chapter in Smith et al. (2009a), I have been awarded further telescope time to observe HD 189733 b (NRAO proposal GBT09B_044). The intention is to observe five further secondary eclipses in the same manner as in 2007, and combine the data in order to increase the signal-to-noise. It is anticipated that this will increase the 3-σ sensitivity by a factor of 2 or more. It is also hoped that the question of whether the tentative eclipse detections at certain wavelengths are real will be resolved by these observations.

Secondary eclipse observations of HD 189733 b at radio wavelengths have also recently

been attempted by Ingrosso et al. (2009b). Using the array of dishes that comprise the Giant Metrewave Radio Telescope (GMRT) at Pune, India, Ingrosso et al. (2009b) establish deep upper limits at two frequencies. The upper limits to the flux density established are 2 mJy at 244 MHz and 160 μJy at 614 MHz. Although these upper limits are deeper than those it is anticipated will be set by new GBT observations, any cyclotron emission may be intermittent in nature, so a detection may still be made.

Ultimately, it may be that a more sensitive, low frequency instrument such as the forthcoming Low Frequency Array (LOFAR) is required to make the first detection of radio emission from the magnetosphere of an extra-solar planet. Not only will LOFAR be more sensitive than existing instruments, but it will be able to observe at frequencies of 10 – 240 MHz (Farrell et al., 2004), enabling the detection of emission from planets with weaker magnetic fields than at present.

7

Conclusions and possible future work

In this chapter, I briefly review the major conclusions of this thesis and present some thoughts on possible future research that may follow on from the work presented in this thesis.

7.1 Summary of the major findings

The number of known transiting planets, which are vital for the understanding of planet properties and formation, has increased rapidly over the past few years. This has been due in large part to the successes of the ground-based, wide-field transit surveys, HAT, TrES, XO, and SuperWASP. Fully understanding the properties of noise in the photometry from these instruments has been vital to reconciling early predictions of the planet yield from such surveys, with the actual numbers of planets discovered to date.

In chapter 2, the level of red (correlated) noise in SuperWASP photometry was quantified,

Above: The setting Sun above the island of La Palma, viewed from Tenerife, Spain. Photograph by the author.

and the impact of this noise on planet detection explored. As predicted by Pont et al. (2006), SuperWASP suffers from levels of red noise which significantly impact its ability to detect the ~ 1 per cent reductions in brightness caused by transiting hot Jupiter planets. It is determined through the use of Monte Carlo simulations that the number of detectable planets may be increased by simply observing the same fields for longer, thus boosting the signal-to-noise ratio.

Identifying transiting planet candidates from wide-field photometry, such as that obtained by SuperWASP is by no means the end of the planet-discovery process. As well as false positives as a result of artefacts in the data, there are many astrophysical objects which may mimic a transiting planetary system. These may be identified with a combination of photometry of higher precision and spatial resolution than that from SuperWASP, and spectroscopy.

In chapter 3, the importance of photometric follow-up observations is discussed, and several examples of these observations are presented. As well as a candidate that was confirmed to be an extra-solar planet, candidates that were determined to be eclipsing stellar binary systems are included. Two of these candidates were revealed to be non-planetary in nature solely by photometry with a modestly-sized telescope (< 1 m), illustrating the ability of such photometry to reduce the need for expensive spectroscopic follow-up with larger telescopes.

In recent years, the secondary eclipses and transits of transiting extra-solar planets have allowed various different methods of planetary characterisation, such as the detection of molecules in planetary atmospheres, and measurements of temperature and albedo. In chapter 4, I present an MCMC code designed to measure the transit depth, and thus apparent planetary radius, as a function of wavelength. It is hoped that in the near future, such techniques can be employed to test theoretical atmospheric models. For instance it may be possible to distinguish between the two classes of hot Jupiter proposed by Fortney et al. (2008).

The discovery of more than 350 extra-solar planets since 1995 has included the detection of several multiple planet systems, although none of these systems contains a planet known to transit. The discovery of a multiple planet system in which one or more of the planets exhibit transits would prove valuable for studies of planetary dynamics and formation. The obvious way to find such a system is to search the currently known transiting systems for further planets; one way to do this is to use long-term photometric monitoring to hunt for additional transits. Such observations of twenty-four transiting planetary systems were made with the

SuperWASP instruments, revealing no evidence for any new planets. Monte Carlo simulations were used to quantify the ability of SuperWASP to detect additional planets. Stellar rotation was confirmed in the case of WASP-10, at a period of 11.91 ± 0.05 d.

In chapter 6, I return to the theme of exoplanet characterisation, presenting results from the first-ever attempt to detect the secondary eclipse of an exoplanet at radio wavelengths. It is thought, by analogy to Jupiter, that some exoplanets may emit low-frequency radio waves as a result of a stellar wind interacting with a planetary magnetic field. This interaction is thought to result in the production of electron-cyclotron maser emission; several theoretical models predict the flux of such emission. An upper limit of 81 mJy to the flux density of emission from HD 189733 b was established over a 307 – 347 MHz bandpass.

7.2 Possible future work

There are a number of potential avenues for future research leading on from the work presented in this thesis; a number of these are briefly outlined below.

The approach used to model the SuperWASP planet catch in chapter 2 could be used in future to help uncover the underlying distribution of planet properties, necessary to provide constraints for models of planet formation. In order to do this, the selection effects present in wide-field surveys such as SuperWASP must be understood fully. Understanding the noise properties of the data, and comparing the planets discovered by SuperWASP to a model stellar catalogue populated with exoplanets could enable this. It is hoped that this sort of modelling will allow, for instance, the frequency of hot Jupiters as a function of stellar spectral type, and the distribution of planetary radii to be determined.

As already discussed, high-precision transit photometry (for instance from the VLT) in numerous passbands in conjunction with the code described in chapter 4 may allow confrontation with theoretical models and further characterisation of planetary atmospheres. The search for a transiting multiple planet system is ongoing, and the first discovery of such a system may come from a similar search to the one I presented in chapter 5. Alternatively, this may come through long-term radial velocity monitoring of known transiting systems, which has the potential to be more sensitive to longer-period planets. The transit-timing technique offers the advantage of extreme sensitivity to low-mass planets in orbits that are resonant with the transiting planet.

Further observations of exoplanets at radio wavelengths are expected eventually to yield a detection of cyclotron-maser emission, offering the opportunity to measure the magnetic field strength of an extra-solar planet for the first time. Such a detection may come from observations using existing single-dish (e.g. GBT) or multi-dish (e.g. VLA, GMRT) telescopes or from future instruments with increased sensitivity at low frequencies. The technique of attempting to observe the radio secondary eclipse, pioneered in chapter 6, gives the ability to unambiguously identify the provenance of any signal as the target planet, and not another object in the beam. This is particularly important in the case of single-dish observations at low frequency, where the beam size is very large.

References

Adams, F. C., Bodenheimer, P., & Laughlin, G. 2005, Astronomische Nachrichten, 326, 913

Adams, J. C. 1846, MNRAS, 7, 149

Agol, E., Steffen, J., Sari, R., & Clarkson, W. 2005, MNRAS, 359, 567

Anderson, D. R., Gillon, M., Hellier, C., Maxted, P. F. L., Pepe, F., Queloz, D., Wilson, D. M., Collier Cameron, A., Smalley, B., Lister, T. A., Bentley, S. J., Blecha, A., Christian, D. J., Enoch, B., Hebb, L., Horne, K., Irwin, J., Joshi, Y. C., Kane, S. R., Marmier, M., Mayor, M., Parley, N. R., Pollacco, D. L., Pont, F., Ryans, R., Ségransan, D., Skillen, I., Street, R. A., Udry, S., West, R. G., & Wheatley, P. J. 2008, MNRAS, 387, L4

Bakos, G. Á., Lázár, J., Papp, I., Sári, P., & Green, E. M. 2002, PASP, 114, 974

Bakos, G. Á., Pál, A., Torres, G., Sipőcz, B., Latham, D. W., Noyes, R. W., Kovács, G., Hartman, J., Esquerdo, G. A., Fischer, D. A., Johnson, J. A., Marcy, G. W., Butler, R. P., Howard, A. W., Sasselov, D. D., Kovács, G., Stefanik, R. P., Lázár, J., Papp, I., & Sári, P. 2009, ApJ, 696, 1950

Bakos, G. Á., Shporer, A., Pál, A., Torres, G., Kovács, G., Latham, D. W., Mazeh, T., Ofir, A., Noyes, R. W., Sasselov, D. D., Bouchy, F., Pont, F., Queloz, D., Udry, S., Esquerdo, G., Sipőcz, B., Kovács, G., Stefanik, R., Lázár, J., Papp, I., & Sári, P. 2007, ApJ, 671, L173

Barge, P., Baglin, A., Auvergne, M., Rauer, H., Léger, A., Schneider, J., Pont, F., Aigrain, S., Almenara, J.-M., Alonso, R., Barbieri, M., Bordé, P., Bouchy, F., Deeg, H. J., La Reza, D., Deleuil, M., Dvorak, R., Erikson, A., Fridlund, M., Gillon, M., Gondoin, P., Guillot, T., Hatzes, A., Hebrard, G., Jorda, L., Kabath, P., Lammer, H., Llebaria, A., Loeillet, B., Magain, P., Mazeh, T., Moutou, C., Ollivier, M., Pätzold, M., Queloz, D., Rouan, D., Shporer, A., & Wuchterl, G. 2008, A&A, 482, L17

Bastian, T. S., Dulk, G. A., & Leblanc, Y. 2000, ApJ, 545, 1058

Benedict, G. F., McArthur, B. E., Forveille, T., Delfosse, X., Nelan, E., Butler, R. P., Spiesman, W., Marcy, G., Goldman, B., Perrier, C., Jefferys, W. H., & Mayor, M. 2002, ApJ, 581, L115

Beuzit, J.-L., Feldt, M., Dohlen, K., Mouillet, D., Puget, P., Wildi, F., Abe, L., Antichi, J., Baruffolo, A., Baudoz, P., Boccaletti, A., Carbillet, M., Charton, J., Claudi, R., Downing, M., Fabron, C., Feautrier, P., Fedrigo, E., Fusco, T., Gach, J.-L., Gratton, R., Henning, T., Hubin, N., Joos, F., Kasper, M., Langlois, M., Lenzen, R., Moutou, C., Pavlov, A., Petit, C., Pragt, J., Rabou, P., Rigal, F., Roelfsema, R., Rousset, G., Saisse, M., Schmid, H.-M., Stadler, E., Thalmann, C., Turatto, M., Udry, S., Vakili, F., & Waters, R. 2008, in Society of Photo-Optical Instrumentation Engineers (SPIE) Conference Series, Vol. 7014

Beuzit, J.-L., Mouillet, D., Oppenheimer, B. R., & Monnier, J. D. 2007, in Protostars and Planets V, ed. B. Reipurth, D. Jewitt, & K. Keil, 717–732

Bond, I. A., Udalski, A., Jaroszyński, M., Rattenbury, N. J., Paczyński, B., Soszyński, I., Wyrzykowski, L., Szymański, M. K., Kubiak, M., Szewczyk, O., Żebruń, K., Pietrzyński, G., Abe, F., Bennett, D. P., Eguchi, S., Furuta, Y., Hearnshaw, J. B., Kamiya, K., Kilmartin, P. M., Kurata, Y., Masuda, K., Matsubara, Y., Muraki, Y., Noda, S., Okajima, K., Sako, T., Sekiguchi, T., Sullivan, D. J., Sumi, T., Tristram, P. J., Yanagisawa, T., & Yock, P. C. M. 2004, ApJ, 606, L155

Borucki, W., Koch, D., Batalha, N., Caldwell, D., Christensen-Dalsgaard, J., Cochran, W. D., Dunham, E., Gautier, T. N., Geary, J., Gilliland, R., Jenkins, J., Kjeldsen, H., Lissauer, J. J., & Rowe, J. 2009, in IAU Symposium, Vol. 253, Proceedings of IAU Symposium 253, eds. Pont, Sasselov & Holman, Cambridge University Press, 289–299

Boss, A. P. 2003, in Reports on Astronomy, Transactions of the International Astronomical Union, Vol. XXVA, Astronomical Society of the Pacific, San Fransisco, 144–146

Bouchy, F., & The Sophie Team. 2006, in Tenth Anniversary of 51 Peg-b: Status of and prospects for hot Jupiter studies, Frontier Group, Paris, ed. L. Arnold, F. Bouchy, & C. Moutou, 319–325

Bouchy, F., Udry, S., Mayor, M., Moutou, C., Pont, F., Iribarne, N., da Silva, R., Ilovaisky, S., Queloz, D., Santos, N. C., Ségransan, D., & Zucker, S. 2005, A&A, 444, L15

Bouwman, J., Meyer, M. R., Kim, J. S., Silverstone, M. D., Carpenter, J. M., & Hines, D. C. 2006, The formation and evolution of planetary systems: placing our solar system in context., eds. H. Klahr & W. Brandner, ed. H. Klahr & W. Brandner (Cambridge University Press), 14–+

Brown, T. M. 2003, ApJ, 593, L125

Brown, T. M., Charbonneau, D., Gilliland, R. L., Noyes, R. W., & Burrows, A. 2001, ApJ, 552, 699

Burke, B. F., & Franklin, K. L. 1955, J. Geophys. Res., 60, 213

Cameron, A. C., Bouchy, F., Hébrard, G., Maxted, P., Pollacco, D., Pont, F., Skillen, I., Smalley, B., Street, R. A., West, R. G., Wilson, D. M., Aigrain, S., Christian, D. J., Clarkson, W. I., Enoch, B., Evans, A., Fitzsimmons, A., Fleenor, M., Gillon, M., Haswell, C. A., Hebb, L., Hellier, C., Hodgkin, S. T., Horne, K., Irwin, J., Kane, S. R., Keenan, F. P., Loeillet, B., Lister, T. A., Mayor, M., Moutou, C., Norton, A. J., Osborne, J., Parley, N., Queloz, D., Ryans, R., Triaud, A. H. M. J., Udry, S., & Wheatley, P. J. 2007, MNRAS, 375, 951

Carr, T. D., Desch, M. D., & Alexander, J. K. 1983, Phenomenology of magnetospheric radio emissions (Physics of the Jovian Magnetosphere), 226–284

Charbonneau, D. 2009, in IAU Symposium, Vol. 253, Proceedings of IAU Symposium 253, eds. Pont, Sasselov & Holman, Cambridge University Press, 1–8

Charbonneau, D., Allen, L. E., Megeath, S. T., Torres, G., Alonso, R., Brown, T. M., Gilliland, R. L., Latham, D. W., Mandushev, G., O'Donovan, F. T., & Sozzetti, A. 2005, ApJ, 626, 523

Charbonneau, D., Brown, T. M., Latham, D. W., & Mayor, M. 2000, ApJ, 529, L45

Charbonneau, D., Brown, T. M., Noyes, R. W., & Gilliland, R. L. 2002, ApJ, 568, 377

Chauvin, G., Lagrange, A.-M., Dumas, C., Zuckerman, B., Mouillet, D., Song, I., Beuzit, J.-L., & Lowrance, P. 2004, A&A, 425, L29

——. 2005, A&A, 438, L25

Christian, D., Pollacco, D. L., Clarkson, W. I., Collier-Cameron, A., Evans, N., Fitzsimmons, A., Haswell, C. A., Hellier, C., Hodgkin, S. T., Horne, K. D., Kane, S. R., Keenan, F. P., Lister, T. A., Norton, A. J., Ryans, R., Skillen, I., Street, R. A., West, R. G., & Wheatley, P. J. 2005, in

13th Cambridge Workshop on Cool Stars, Stellar Systems and the Sun, ed. F. Favata, G. A. J. Hussain, & B. Battrick (ESA SP-560), 475–477

Christian, D. J., Gibson, N. P., Simpson, E. K., Street, R. A., Skillen, I., Pollacco, D., Collier Cameron, A., Joshi, Y. C., Keenan, F. P., Stempels, H. C., Haswell, C. A., Horne, K., Anderson, D. R., Bentley, S., Bouchy, F., Clarkson, W. I., Enoch, B., Hebb, L., Hébrard, G., Hellier, C., Irwin, J., Kane, S. R., Lister, T. A., Loeillet, B., Maxted, P., Mayor, M., McDonald, I., Moutou, C., Norton, A. J., Parley, N., Pont, F., Queloz, D., Ryans, R., Smalley, B., Smith, A. M. S., Todd, I., Udry, S., West, R. G., Wheatley, P. J., & Wilson, D. M. 2009, MNRAS, 392, 1585

Christian, D. J., Pollacco, D. L., Skillen, I., Street, R. A., Keenan, F. P., Clarkson, W. I., Collier Cameron, A., Kane, S. R., Lister, T. A., West, R. G., Enoch, B., Evans, A., Fitzsimmons, A., Haswell, C. A., Hellier, C., Hodgkin, S. T., Horne, K., Irwin, J., Norton, A. J., Osborne, J., Ryans, R., Wheatley, P. J., & Wilson, D. M. 2006, MNRAS, 372, 1117

Claret, A. 2000, A&A, 363, 1081

Collier Cameron, A., Pollacco, D., Street, R. A., Lister, T. A., West, R. G., Wilson, D. M., Pont, F., Christian, D. J., Clarkson, W. I., Enoch, B., Evans, A., Fitzsimmons, A., Haswell, C. A., Hellier, C., Hodgkin, S. T., Horne, K., Irwin, J., Kane, S. R., Keenan, F. P., Norton, A. J., Parley, N. R., Osborne, J., Ryans, R., Skillen, I., & Wheatley, P. J. 2006, MNRAS, 373, 799

Collier Cameron, A., Wilson, D. M., West, R. G., Hebb, L., Wang, X.-B., Aigrain, S., Bouchy, F., Christian, D. J., Clarkson, W. I., Enoch, B., Esposito, M., Guenther, E., Haswell, C. A., Hébrard, G., Hellier, C., Horne, K., Irwin, J., Kane, S. R., Loeillet, B., Lister, T. A., Maxted, P., Mayor, M., Moutou, C., Parley, N., Pollacco, D., Pont, F., Queloz, D., Ryans, R., Skillen, I., Street, R. A., Udry, S., & Wheatley, P. J. 2007, MNRAS, 380, 1230

Coughlin, J. L., Stringfellow, G. S., Becker, A. C., López-Morales, M., Mezzalira, F., & Krajci, T. 2008, ApJ, 689, L149

Croll, B., Matthews, J. M., Rowe, J. F., Gladman, B., Miller-Ricci, E., Sasselov, D., Walker, G. A. H., Kuschnig, R., Lin, D. N. C., Guenther, D. B., Moffat, A. F. J., Rucinski, S. M., & Weiss, W. W. 2007a, ApJ, 671, 2129

Croll, B., Matthews, J. M., Rowe, J. F., Kuschnig, R., Walker, A., Gladman, B., Sasselov, D., Cameron, C., Walker, G. A. H., Lin, D. N. C., Guenther, D. B., Moffat, A. F. J., Rucinski, S. M., & Weiss, W. W. 2007b, ApJ, 658, 1328

Cumming, A. 2004, MNRAS, 354, 1165

de Pater, I., & Lissauer, J. J. 2001, Planetary Sciences, Cambridge University Press

Deming, D., Harrington, J., Seager, S., & Richardson, L. J. 2006, ApJ, 644, 560

Douglas, J. N., Bash, F. N., Bozyan, F. A., Torrence, G. W., & Wolfe, C. 1996, AJ, 111, 1945

Edelson, R. A., & Krolik, J. H. 1988, ApJ, 333, 646

Einstein, A. 1936, Science, 84, 506

Fabrycky, D. C. 2009, in Proceedings of IAU Symposium 253, eds. Pont, Sasselov & Holman, Cambridge University Press, 173–179

Farrell, W. M., Lazio, T. J. W., Zarka, P., Bastian, T. J., Desch, M. D., & Ryabov, B. P. 2004, Planetary and Space Science, 52, 1469

Fischer, D. A., & Valenti, J. 2005, ApJ, 622, 1102

Fleming, S. W., Kane, S. R., McCullough, P. R., & Chromey, F. R. 2008, MNRAS, 386, 1503

Fortney, J. J., Lodders, K., Marley, M. S., & Freedman, R. S. 2008, ApJ, 678, 1419

George, S. J., & Stevens, I. R. 2007, MNRAS, 382, 455

Gilks, W. R., Richardson, S., & Spiegelhalter, D. J. 1996, Markov chain Monte Carlo in practice, Chapman & Hall

Gillon, M., Anderson, D. R., Triaud, A. H. M. J., Hellier, C., Maxted, P. F. L., Pollaco, D., Queloz, D., Smalley, B., West, R. G., Wilson, D. M., Bentley, S. J., Collier Cameron, A., Enoch, B., Hebb, L., Horne, K., Irwin, J., Joshi, Y. C., Lister, T. A., Mayor, M., Pepe, F., Parley, N., Segransan, D., Udry, S., & Wheatley, P. J. 2009a, A&A, 501, 785

Gillon, M., Demory, B. ., Triaud, A. H. M. J., Barman, T., Hebb, L., Montalban, J., Maxted, P. F. L., Queloz, D., Deleuil, M., & Magain, P. 2009b, A&A, in press

Graham, J. R., Macintosh, B., Doyon, R., Gavel, D., Larkin, J., Levin, M., Oppenheimer, B., Palmer, D., Saddlemyer, L., Sivaramakrishnan, A., Veran, J., Wallace, K., & Gemini Planet Imager Science Team. 2007, in Bulletin of the American Astronomical Society, Vol. 38, 968–+

Gregory, P. C. 2007, MNRAS, 381, 1607

Grießmeier, J.-M., Motschmann, U., Glassmeier, K. H., Mann, G., & Rucker, H. O. 2006, in Tenth Anniversary of 51 Peg-b: Status of and prospects for hot Jupiter studies, Frontier Group, Paris, ed. L. Arnold, F. Bouchy, & C. Moutou, 259–266

Grießmeier, J.-M., Motschmann, U., Mann, G., & Rucker, H. O. 2005, A&A, 437, 717

Grießmeier, J.-M., Zarka, P., & Spreeuw, H. 2007, A&A, 475, 359

Hastings, W. K. 1970, Biometrika, 57, 97

Hebb, L., Collier-Cameron, A., Loeillet, B., Pollacco, D., Hébrard, G., Street, R. A., Bouchy, F., Stempels, H. C., Moutou, C., Simpson, E., Udry, S., Joshi, Y. C., West, R. G., Skillen, I., Wilson, D. M., McDonald, I., Gibson, N. P., Aigrain, S., Anderson, D. R., Benn, C. R., Christian, D. J., Enoch, B., Haswell, C. A., Hellier, C., Horne, K., Irwin, J., Lister, T. A., Maxted, P., Mayor, M., Norton, A. J., Parley, N., Pont, F., Queloz, D., Smalley, B., & Wheatley, P. J. 2009, ApJ, 693, 1920

Hellier, C., Anderson, D. R., Cameron, A. C., Gillon, M., Hebb, L., Maxted, P. F. L., Queloz, D., Smalley, B., Triaud, A. H. M. J., West, R. G., Wilson, D. M., Bentley, S. J., Enoch, B., Horne, K., Irwin, J., Lister, T. A., Mayor, M., Parley, N., Pepe, F., Pollacco, D. L., Segransan, D., Udry, S., & Wheatley, P. J. 2009a, Nat, 460, 1098

Hellier, C., Anderson, D. R., Gillon, M., Lister, T. A., Maxted, P. F. L., Queloz, D., Smalley, B., Triaud, A. H. M. J., West, R. G., Wilson, D. M., Alsubai, K., Bentley, S. J., Cameron, A. C., Hebb, L., Horne, K., Irwin, J., Kane, S. R., Mayor, M., Pepe, F., Pollacco, D., Skillen, I., Udry, S., Wheatley, P. J., Christian, D. J., Enoch, R., Haswell, C. A., Joshi, Y. C., Norton, A. J., Parley, N., Ryans, R., Street, R. A., & Todd, I. 2009b, ApJ, 690, L89

Henry, G. W., Marcy, G. W., Butler, R. P., & Vogt, S. S. 2000, ApJ, 529, L41

Herschel, M., & Watson, D. 1781, Royal Society of London Philosophical Transactions Series I, 71, 492

Holman, M. J., & Murray, N. W. 2005, Science, 307, 1288

Horne, K. 2001, in Techniques for the detection of planets and life beyond the solar system, 4th Annual ROE Workshop, held at Royal Observatory Edinburgh, Scotland, Nov 7-8, 2001. Edited by W.R.F. Dent. Edinburgh, Scotland: Royal Observatory, 2001, p.5, ed. W. R. F. Dent

Ingrosso, G., Novati, S. C., de Paolis, F., Jetzer, P., Nucita, A. A., & Zakharov, A. F. 2009a, MNRAS, 399, 219

——. 2009b, MNRAS, 399, 219

Irwin, J., Charbonneau, D., Nutzman, P., & Falco, E. 2009, in IAU Symposium, Vol. 253, Proceedings of IAU Symposium 253, eds. Pont, Sasselov & Holman, Cambridge University Press, 37–43

Ivanova, N., & Taam, R. E. 2003, ApJ, 599, 516

Jardine, M., & Cameron, A. C. 2008, A&A, 490, 843

JBAA. 2005, Journal of the British Astronomical Association, 115, 159

Joshi, Y. C., Pollacco, D., Cameron, A. C., Skillen, I., Simpson, E., Steele, I., Street, R. A., Stempels, H. C., Christian, D. J., Hebb, L., Bouchy, F., Gibson, N. P., Hébrard, G., Keenan, F. P., Loeillet, B., Meaburn, J., Moutou, C., Smalley, B., Todd, I., West, R. G., Anderson, D. R., Bentley, S., Enoch, B., Haswell, C. A., Hellier, C., Horne, K., Irwin, J., Lister, T. A., McDonald, I., Maxted, P., Mayor, M., Norton, A. J., Parley, N., Perrier, C., Pont, F., Queloz, D., Ryans, R., Smith, A. M. S., Udry, S., Wheatley, P. J., & Wilson, D. M. 2009, MNRAS, 392, 1532

Kalas, P., Graham, J. R., Chiang, E., Fitzgerald, M. P., Clampin, M., Kite, E. S., Stapelfeldt, K., Marois, C., & Krist, J. 2008, Science, 322, 1345

Kasting, J. F., Whitmire, D. P., & Reynolds, R. T. 1993, Icarus, 101, 108

Knutson, H. A., Charbonneau, D., Allen, L. E., Fortney, J. J., Agol, E., Cowan, N. B., Showman, A. P., Cooper, C. S., & Megeath, S. T. 2007, Nat, 447, 183

Koch, D., & Borucki, W. 1996, in Circumstellar Habitable Zones, ed. L. R. Doyle

Konacki, M., Torres, G., Jha, S., & Sasselov, D. D. 2003, Nat, 421, 507

Kovács, G., Bakos, G. Á., Torres, G., Sozzetti, A., Latham, D. W., Noyes, R. W., Butler, R. P., Marcy, G. W., Fischer, D. A., Fernández, J. M., Esquerdo, G., Sasselov, D. D., Stefanik, R. P., Pál, A., Lázár, J., Papp, I., & Sári, P. 2007, ApJ, 670, L41

Kovács, G., Zucker, S., & Mazeh, T. 2002, A&A, 391, 369

Lazio, T. J. W., & Farrell, W. M. 2007, ApJ, 668, 1182

Lazio, T. J. W., Farrell, W. M., Dietrick, J., Greenlees, E., Hogan, E., Jones, C., & Hennig, L. A. 2004, ApJ, 612, 511

Le Verrier, U. J. 1847, Astronomische Nachrichten, 25, 81

Lister, T. A., Anderson, D. R., Gillon, M., Hebb, L., Smalley, B. S., Triaud, A. H. M. J., Collier Cameron, A., Wilson, D. M., West, R. G., Bentley, S. J., Christian, D. J., Enoch, R., Haswell, C. A., Hellier, C., Horne, K., Irwin, J., Joshi, Y. C., Kane, S. R., Mayor, M., Maxted, P. F. L., Norton, A. J., Parley, N., Pepe, F., Pollacco, D., Queloz, D., Ryans, R., Segransan, D., Skillen, I., Street, R. A., Todd, I., Udry, S., & Wheatley, P. J. 2009, ApJ, 703, 752

Lowell Putnam, R., & Slipher, V. M. 1932, The Scientific Monthly, 34, 5

Mandel, K., & Agol, E. 2002, ApJ, 580, L171

Mandushev, G., O'Donovan, F. T., Charbonneau, D., Torres, G., Latham, D. W., Bakos, G. Á., Dunham, E. W., Sozzetti, A., Fernández, J. M., Esquerdo, G. A., Everett, M. E., Brown, T. M., Rabus, M., Belmonte, J. A., & Hillenbrand, L. A. 2007, ApJ, 667, L195

Mao, S., & Paczynski, B. 1991, ApJ, 374, L37

Marois, C., Macintosh, B., Barman, T., Zuckerman, B., Song, I., Patience, J., Lafrenière, D., & Doyon, R. 2008, Science, 322, 1348

Mayor, M., & Queloz, D. 1995, Nat, 378, 355

McCullough, P. R., Burke, C. J., Valenti, J. A., Long, D., Johns-Krull, C. M., Machalek, P., Janes, K. A., Taylor, B., Gregorio, J., Foote, C. N., Gary, B. L., Fleenor, M., García-Melendo, E., & Vanmunster, T. 2008, arXiv:0805.2921

McCullough, P. R., Stys, J. E., Valenti, J. A., Fleming, S. W., Janes, K. A., & Heasley, J. N. 2005, PASP, 117, 783

Metropolis, N., Rosenbluth, A. W., Rosenbluth, M. N., Teller, A. H., & Teller, E. 1953, The Journal of Chemical Physics, 21, 1087

Moutou, C., Donati, J.-F., Savalle, R., Hussain, G., Alecian, E., Bouchy, F., Catala, C., Collier Cameron, A., Udry, S., & Vidal-Madjar, A. 2007, A&A, 473, 651

Noyes, R. W., Bakos, G. Á., Torres, G., Pál, A., Kovács, G., Latham, D. W., Fernández, J. M., Fischer, D. A., Butler, R. P., Marcy, G. W., Sipőcz, B., Esquerdo, G. A., Kovács, G., Sasselov, D. D., Sato, B., Stefanik, R., Holman, M., Lázár, J., Papp, I., & Sári, P. 2008, ApJ, 673, L79

O'Donovan, F. T., Charbonneau, D., Mandushev, G., Dunham, E. W., Latham, D. W., Torres, G., Sozzetti, A., Brown, T. M., Trauger, J. T., Belmonte, J. A., Rabus, M., Almenara, J. M., Alonso, R., Deeg, H. J., Esquerdo, G. A., Falco, E. E., Hillenbrand, L. A., Roussanova, A., Stefanik, R. P., & Winn, J. N. 2006a, ApJ, 651, L61

O'Donovan, F. T., Charbonneau, D., Torres, G., Mandushev, G., Dunham, E. W., Latham, D. W., Alonso, R., Brown, T. M., Esquerdo, G. A., Everett, M. E., & Creevey, O. L. 2006b, ApJ, 644, 1237

Pál, A., Bakos, G. Á., Torres, G., Noyes, R. W., Latham, D. W., Kovács, G., Marcy, G. W., Fischer, D. A., Butler, R. P., Sasselov, D. D., Sipőcz, B., Esquerdo, G. A., Kovács, G., Stefanik, R., Lázár, J., Papp, I., & Sári, P. 2008, ApJ, 680, 1450

Pollacco, D., Skillen, I., Collier Cameron, A., Loeillet, B., Stempels, H. C., Bouchy, F., Gibson, N. P., Hebb, L., Hébrard, G., Joshi, Y. C., McDonald, I., Smalley, B., Smith, A. M. S., Street, R. A., Udry, S., West, R. G., Wilson, D. M., Wheatley, P. J., Aigrain, S., Alsubai, K., Benn, C. R., Bruce, V. A., Christian, D. J., Clarkson, W. I., Enoch, B., Evans, A., Fitzsimmons, A., Haswell, C. A., Hellier, C., Hickey, S., Hodgkin, S. T., Horne, K., Hrudková, M., Irwin, J., Kane, S. R., Keenan, F. P., Lister, T. A., Maxted, P., Mayor, M., Moutou, C., Norton, A. J., Osborne, J. P., Parley, N., Pont, F., Queloz, D., Ryans, R., & Simpson, E. 2008, MNRAS, 385, 1576

Pollacco, D. L., Skillen, I., Cameron, A. C., Christian, D. J., Hellier, C., Irwin, J., Lister, T. A., Street, R. A., West, R. G., Anderson, D., Clarkson, W. I., Deeg, H., Enoch, B., Evans, A., Fitzsimmons, A., Haswell, C. A., Hodgkin, S., Horne, K., Kane, S. R., Keenan, F. P., Maxted, P. F. L., Norton, A. J., Osborne, J., Parley, N. R., Ryans, R. S. I., Smalley, B., Wheatley, P. J., & Wilson, D. M. 2006, PASP, 118, 1407

Pont, F. 2006, in Tenth Anniversary of 51 Peg-b: Status of and prospects for hot Jupiter studies, Frontier Group, Paris, ed. L. Arnold, F. Bouchy, & C. Moutou, 153–164

Pont, F., Zucker, S., & Queloz, D. 2006, MNRAS, 373, 231

Pravdo, S. H., & Shaklan, S. B. 2009, ApJ, 700, 623

Press, W. H., Teukolsky, S. A., Vetterling, W. T., & Flannery, B. P. 1992, Numerical recipes in FORTRAN. The art of scientific computing, Cambridge University Press, 2nd ed.

Robin, A. C., Reylé, C., Derrière, S., & Picaud, S. 2003, A&A, 409, 523

Sackett, P. D. 1999, in NATO ASIC Proc. 532: Planets Outside the Solar System: Theory and Observations, ed. J.-M. Mariotti & D. Alloin

Shkolnik, E., Aigrain, S., Cranmer, S., Fares, R., Fridlund, M., Pont, F., Schmitt, J., Smith, A., & Suzuki, T. 2009, in American Institute of Physics Conference Series, Vol. 1094, American Institute of Physics Conference Series, ed. E. Stempels, 275–282

Singer, D. W. 1950, Giordan Bruno: His Life and Thought, with annotated translation of his work On the Infinite Universe and Worlds (Henry Schuman, New York), 304

Skillen, I., Pollacco, D., Collier Cameron, A., Hebb, L., Simpson, E., Bouchy, F., Christian, D. J., Gibson, N. P., Hébrard, G., Joshi, Y. C., Loeillet, B., Smalley, B., Stempels, H. C., Street, R. A., Udry, S., West, R. G., Anderson, D. R., Barros, S. C. C., Enoch, B., Haswell, C. A., Hellier, C., Horne, K., Irwin, J., Keenan, F. P., Lister, T. A., Maxted, P., Mayor, M., Moutou, C., Norton, A. J., Parley, N., Queloz, D., Ryans, R., Todd, I., Wheatley, P. J., & Wilson, D. M. 2009, A&A, 502, 391

Smith, A. M. S., Cameron, A. C., Greaves, J., Jardine, M., Langston, G., & Backer, D. 2009a, MNRAS, 395, 335

Smith, A. M. S., Collier Cameron, A., Christian, D. J., Clarkson, W. I., Enoch, B., Evans, A., Haswell, C. A., Hellier, C., Horne, K., Irwin, J., Kane, S. R., Lister, T. A., Norton, A. J., Parley, N., Pollacco, D. L., Ryans, R., Skillen, I., Street, R. A., Triaud, A. H. M. J., West, R. G., Wheatley, P. J., & Wilson, D. M. 2006, MNRAS, 373, 1151

Smith, A. M. S., Hebb, L., Collier Cameron, A., Anderson, D. R., Lister, T. A., Hellier, C., Pollacco, D., Queloz, D., Skillen, I., & West, R. G. 2009b, MNRAS, 398, 1827

Sozzetti, A. 2005, PASP, 117, 1021

Struve, O. 1952, The Observatory, 72, 199

Swain, M. R., Vasisht, G., & Tinetti, G. 2008, Nat, 452, 329

Tamuz, O., Mazeh, T., & Zucker, S. 2005, MNRAS, 356, 1466

Tegmark, M., Strauss, M. A., Blanton, M. R., Abazajian, K., Dodelson, S., Sandvik, H., Wang, X., Weinberg, D. H., Zehavi, I., Bahcall, N. A., Hoyle, F., Schlegel, D., Scoccimarro, R., Vogeley, M. S., Berlind, A., Budavari, T., Connolly, A., Eisenstein, D. J., Finkbeiner, D., Frieman, J. A., Gunn, J. E., Hui, L., Jain, B., Johnston, D., Kent, S., Lin, H., Nakajima, R., Nichol, R. C., Ostriker, J. P., Pope, A., Scranton, R., Seljak, U., Sheth, R. K., Stebbins, A., Szalay, A. S., Szapudi, I., Xu, Y., Annis, J., Brinkmann, J., Burles, S., Castander, F. J., Csabai, I., Loveday, J., Doi, M., Fukugita, M., Gillespie, B., Hennessy, G., Hogg, D. W., Ivezić, Ž., Knapp, G. R., Lamb, D. Q., Lee, B. C., Lupton, R. H., McKay, T. A., Kunszt, P., Munn, J. A., O'Connell, L., Peoples, J., Pier, J. R., Richmond, M., Rockosi, C., Schneider, D. P., Stoughton, C., Tucker, D. L., vanden Berk, D. E., Yanny, B., & York, D. G. 2004, Phys. Rev. D, 69, 103501

Tinetti, G., Vidal-Madjar, A., Liang, M.-C., Beaulieu, J.-P., Yung, Y., Carey, S., Barber, R. J., Tennyson, J., Ribas, I., Allard, N., Ballester, G. E., Sing, D. K., & Selsis, F. 2007, Nat, 448, 169

Tingley, B., & Sackett, P. D. 2005, ApJ, 627, 1011

Tuomi, M., Kotiranta, S., & Kaasalainen, M. 2009, A&A, 494, 769

Unruh, Y. C., & Jardine, M. 1997, A&A, 321, 177

van de Kamp, P. 1969, AJ, 74, 757

West, R. G., Anderson, D. R., Gillon, M., Hebb, L., Hellier, C., Maxted, P. F. L., Queloz, D., Smalley, B., Triaud, A. H. M. J., Wilson, D. M., Bentley, S. J., Collier Cameron, A., Enoch, B., Horne, K., Irwin, J., Lister, T. A., Mayor, M., Parley, N., Pepe, F., Pollacco, D., Segransan, D., Spano, M., Udry, S., & Wheatley, P. J. 2009a, AJ, 137, 4834

West, R. G., Collier Cameron, A., Hebb, L., Joshi, Y. C., Pollacco, D., Simpson, E., Skillen, I., Stempels, H. C., Wheatley, P. J., Wilson, D., Anderson, D., Bentley, S., Bouchy, F., Christian, D., Enoch, B., Gibson, N., Hébrard, G., Hellier, C., Loeillet, B., Mayor, M., Maxted, P., McDonald, I., Moutou, C., Pont, F., Queloz, D., Smith, A. M. S., Smalley, B., Street, R. A., & Udry, S. 2009b, A&A, 502, 395

Wilson, D. M., Gillon, M., Hellier, C., Maxted, P. F. L., Pepe, F., Queloz, D., Anderson, D. R., Collier Cameron, A., Smalley, B., Lister, T. A., Bentley, S. J., Blecha, A., Christian, D. J.,

Enoch, B., Haswell, C. A., Hebb, L., Horne, K., Irwin, J., Joshi, Y. C., Kane, S. R., Marmier, M., Mayor, M., Parley, N., Pollacco, D., Pont, F., Ryans, R., Segransan, D., Skillen, I., Street, R. A., Udry, S., West, R. G., & Wheatley, P. J. 2008, ApJ, 675, L113

Winn, J. N., Holman, M. J., Henry, G. W., Roussanova, A., Enya, K., Yoshii, Y., Shporer, A., Mazeh, T., Johnson, J. A., Narita, N., & Suto, Y. 2007, AJ, 133, 1828

Wolszczan, A., & Frail, D. A. 1992, Nat, 355, 145

Zarka, P. 2007, Planet Space Sci, 55, 598

Zechmeister, M., & Kürster, M. 2009, A&A, 496, 577